Lab on a Chip

TUTORIAL REVIEW

View Article Online
View Journal | View Issue



Cite this: *Lab Chip*, 2024, **24**, 1441

# Microfluidic systems for infectious disease diagnostics

Thomas Lehnert * and Martin A. M. Gijs

Microorganisms, encompassing both uni- and multicellular entities, exhibit remarkable diversity as omnipresent life forms in nature. They play a pivotal role by supplying essential components for sustaining biological processes across diverse ecosystems, including higher host organisms. The complex interactions within the human gut microbiota are crucial for metabolic functions, immune responses, and biochemical signalling, particularly through the gut–brain axis. Viruses also play important roles in biological processes, for example by increasing genetic diversity through horizontal gene transfer when replicating inside living cells. On the other hand, infection of the human body by microbiological agents may lead to severe physiological disorders and diseases. Infectious diseases pose a significant burden on global healthcare systems, characterized by substantial variations in the epidemiological landscape. Fast spreading antibiotic resistance or uncontrolled outbreaks of communicable diseases are major challenges at present. Furthermore, delivering field-proven point-of-care diagnostic tools to the most severely affected populations in low-resource settings is particularly important and challenging. New paradigms and technological approaches enabling rapid and informed disease management need to be implemented. In this respect, infectious disease diagnostics taking advantage of microfluidic systems combined with integrated biosensor-based pathogen detection offers a host of innovative and promising solutions. In this review, we aim to outline recent activities and progress in the development of microfluidic diagnostic tools. Our literature research mainly covers the last 5 years. We will follow a classification scheme based on the human body systems primarily involved at the clinical level or on specific pathogen transmission modes. Important diseases, such as tuberculosis and malaria, will be addressed more extensively.

Received 9th January 2023,
Accepted 6th February 2024

DOI: 10.1039/d4lc00117f

rsc.li/loc



## 1 Introduction

### The burden of infectious diseases

Infectious diseases are undeniably linked to the fate of human society, be it on a regional or global scale. Even before the era of globalization, spreading of infectious pathogens by human migration caused substantial morbidity and mortality.[1] Large parts of the native population of the Americas were devastated by smallpox and measles during the European conquest.[2] More recently, the Spanish flu (1918–1920), one of the most severe pandemics in history, infected up to one third of the global population at that time with at least 50 million deaths.[3,4] Over the last decades, a rise in human infectious disease outbreaks was observed on a global scale (time frame 1980–2013).[5] An analysis based on disability-adjusted life years (DALY) indicated that in Europe (2009–2013) seasonal influenza burden was the highest, followed by tuberculosis, human immunodeficiency virus (HIV), and invasive pneumococcal disease (IPD).[6] Another extensive study on the global burden of disease (1990–2019) also listed different infectious diseases, depending on the age category, among the top-ranked causes of DALYs.[7] Increasing densification of populations in urban areas and global mobility fosters outbreaks of communicable diseases. This was dramatically demonstrated by the latest COVID-19 pandemic related to the air-borne SARS-CoV-2 coronavirus.[8] Infectious diseases of poverty (including, among others, malaria, tuberculosis, AIDS and neglected tropical infections) disproportionately affect populations in developing countries.[9–12] Endemic or epidemic outbreaks of tropical vector-borne diseases (*e.g.* dengue,[13] Zika or chikungunya) or hemorrhagic fevers (*e.g.* Ebola[14]), as well as infections due to food- or water-borne pathogens (*e.g.* Salmonella infections[15] or cholera) are recurring.[16,17] Moreover, climate change affects regional vector and pathogen distributions, thereby playing an increasingly important role in the evolving global landscape of infectious diseases.[18,19]

The current health system is facing growing challenges due to the fast and dynamic evolution of societal and environmental parameters that impact pathogen transmission, distribution and biological adaptation

*Laboratory of Microsystems, École Polytechnique Fédérale de Lausanne, Lausanne, CH-1015, Switzerland. E-mail: lehnert77@gmail.com*

strategies.[1] Precise epidemiological approaches to infectious diseases are needed to be prepared for future outbreaks, for instance by implementing technological advances enabling a broader application of pathogen genome sequencing.[20] Vaccines are probably among one of the most important achievements of humanity, enabling the eradication (smallpox, poliomyelitis) or at least control (*e.g.* measles/mumps/rubella, hepatitis, influenza *etc.*) of several severe infectious diseases.[21] For others, vaccines are currently under development or undergoing the WHO evaluation process.[22] A prominent example is the recent approval of malaria vaccines, and the launch of large-scale vaccination campaigns.[23,24] However, such protection does not yet exist against some major pathogens, such as AIDS/HIV, for instance. The importance of the development and fast implementation of new vaccine concepts in a context of emerging viral diseases and constantly arising genetic mutations became evident during the COVID-19 pandemic.[25,26] Artificial intelligence is expected to facilitate vaccine or drug design and significantly support progress in the fight against infectious diseases in general.[27]

### Emerging challenges of the global health system

One of the major upcoming threats to global health is antimicrobial resistance (AMR) to drugs, in particular for the ESKAPE pathogen species.[28] Methicillin-resistant *Staphylococcus aureus* (MRSA) is only one example for a globally disseminated superbug.[29] AMR is a leading cause of death around the world, with the highest burden in the developing world.[30] Following the current trend, AMR is expected to cause more deaths than cancer in a few decades. New resistance mechanisms are emerging and spreading rapidly on a global scale, challenging our ability to treat common infectious diseases, due an increasingly limited availability of still efficient or new antibiotics. For instance, multidrug-resistant tuberculosis does not respond to the first-line drugs isoniazid and rifampicin, thus requiring extensive second-line treatments.[31] Among major reasons for this situation are the empirical and often unnecessary prescription of (broad-spectrum) antibiotics in human disease management,[32] but also abusive use in the agriculture/veterinary sector.[33] New surveillance and antimicrobial stewardship strategies are therefore urgently needed.[34,35] One of the keys is the development of rapid antimicrobial susceptibility testing (AST), including microfluidic and biosensor-based methods, for the appropriate choice of prescription at the point-of-care (POC).[36–43]

Today diagnostics still relies on time-consuming pathogen culture-based methods and/or on techniques that are limited to central laboratory facilities. This is a particular problem for primary health care in low-resource settings, most likely facing severe constraints, due to a lack of infrastructure and related technical issues (*e.g.* hazardous electricity supply and refrigeration), health workers with insufficient qualification and limited accessibility in rural areas.[44] As a consequence, the benefit and outcome of individual healthcare and disease management on a larger scale is very limited. To address these challenges, new paradigms for fast POC pathogen detection and identification, possibly combined with rapid AST, are required.[45,46] Advanced microfluidic approaches demonstrate high potential in this regard.

### Motivation and scope of the review

Our review offers an opportunity to explore recent research trends and emerging technologies in the field of microfluidic systems enabling rapid and sensitive detection of pathogens or biomarkers associated with infectious diseases. This topic

**Thomas Lehnert**

*Thomas Lehnert is a senior scientist at the Swiss Federal Institute of Technology in Lausanne (Switzerland), specializing in advanced microfabrication and microfluidic devices with bioanalytical/biomedical applications (BioMEMS). He has experience in the management of European projects, as well as teaching and mentoring PhD students. At EPFL his previous research and development activities focused on materials science (shape memory alloys). At IRAM in Grenoble (France) he developed superconducting electronic sensors for radio telescopes. Thomas Lehnert received his PhD degree in Physics in 1992 from the University of Würzburg (Germany).*

**Martin Gijs**

*Martin Gijs received his degree in physics in 1981 from the Katholieke Universiteit Leuven, Belgium, and his PhD degree in physics at the same university in 1986. He joined the Philips Research Laboratories in Eindhoven, The Netherlands, in 1987, and, subsequently, the Ecole Polytechnique Fédérale de Lausanne (EPFL) in 1997, where he presently is a full professor in the Institute of Electrical and Microengineering. His main interests are in developing technologies for microsystems fabrication in general and the development and use of microfluidics for biomedical applications in particular.*

encompasses various disciplines such as micro- and molecular biology, engineering, healthcare delivery, and public health. While existing reviews often focus on specific applications, pathogen types, or technologies, our aim is to provide a comprehensive resource for researchers and stakeholders seeking to advance infectious disease diagnostics. Throughout this review, we will highlight the latest advancements in sensitive biosensor technologies, innovative assay strategies, and advanced microfluidic integration, all of which show great promise in facilitating near-patient testing and enabling real POC diagnosis of infectious diseases. Furthermore, in a broader context, we aim to underscore the potential of microfluidics-based technology in addressing the increasing burden of infectious diseases on global healthcare.

Our review begins by briefly introducing the scope and background of microfluidics and biosensors, along with a non-exhaustive summary of available review articles related to infectious disease diagnostics (section 2). Following this, we will elaborate on our discussion of recent microfluidic devices and platforms. We adopt a classification scheme primarily based on the human body systems involved at the clinical level. This classification includes infections of the respiratory tract (section 3), the urinary tract (section 4), the gastrointestinal tract (section 5) and the bloodstream (section 6). For other pathogens or diseases, categorization by specific transmission mode was more convenient, in particular for sexually transmitted infections (section 7) and vector-based infections (section 8). Additionally, based on the availability of recent developments in microfluidic systems, we will provide more in-depth discussions of key diseases, namely tuberculosis and malaria.

Our approach in this review is as follows: (i) in sections 3 to 8, we aim to provide a comprehensive overview of the state-of-the-art of microfluidic biosensor-based systems for infectious disease diagnostics, with an emphasis on microtechnological or microfluidic aspects. Recent devices for rapid AST will also be included. The timeframe covers the last 5 years (2018–2023, with a few exceptions). Corresponding tables outline the most relevant work, ordered by pathogens or analytical targets. (ii) Each section introduces the scope of the infection category, emphasizing microbiological, biomedical, or societal aspects. We believe this approach is crucial for our review, as it provides a concise insight into the complexity of each topic, especially for microfluidic system developers. This not only sets the framework that motivates advanced technological developments but may also help bridge the gap between research and clinical practice in this interdisciplinary field. To this end, we have included highly relevant articles related to each specific topic of our classification scheme. These articles do not focus on microfluidics but cover essential background information and may therefore have been published before 2018. (iii) Each section of our tutorial review also includes an overview of corresponding existing reviews, some of which were published before 2018. In general, these articles focus on specific applications, types of pathogens, or technologies. This approach allows the reader to explore a topic of particular interest more thoroughly.

# 2 Lab-on-a-chip devices for infectious disease diagnostics

## 2.1 Microfluidics and microfluidic devices

**Fluid properties at the microscale.** Fluidic dynamics is governed by the Navier–Stokes equations that accounts in principle for any kind of complex fluidic phenomena on the macroscale, including turbulent flow patterns.[47] By reducing dimensions to the microscale the balance of forces changes. Inertial forces generally become irrelevant with respect to viscous forces (Stokes flow) or forces related to interfaces, such capillary forces or surface tension.[48] This gives rise to particular fluid properties that oppose our intuition, but may have significant impact on life on the microscale and on the design of microfluidic devices. For example, bacteria need flagella instead of fins for propulsion because of the reversibility of Stokes flow.[49] Microfluidic system design needs to take into account that efficient and fast mixing at the microscale is challenging due to laminar flow properties.[50] On the other hand, capillary forces enable self-propelled continuous-flow fluidic circuits.[51] In two-phase liquid systems non-equilibrium effects may be used to generate monodisperse droplets in microchannels.[52] Fluidic properties can be conveniently described by dimensionless numbers. In particular, the microfluidic domain is characterized by small Reynolds numbers Re (Re $\sim 10^{-6}$ to $\sim 1$), corresponding to the ratio of inertial to viscous forces in the fluid. If operated at intermediate Re numbers ($\sim 1 <$ Re $< \sim 100$), microfluidic applications may also make use of inertial effects.[53] Other examples of relevant numbers that describe flow dynamics and molecular transport in microfluidics are the Péclet number (convective/diffusive transport) or the capillary number (viscous/interfacial forces).[54] These numbers play an important role in the design of microfluidic devices and assay integration.

**Microfluidic device categories.** Microfluidic systems enable precise spatio-temporal control of small liquid sample volumes and the accurate manipulation of biomolecules, cells or particles. A major breakthrough in microfluidic device or lab-on-a-chip (LOC) design was brought about by the elastomeric polymer (poly)dimethylsiloxane (PDMS).[55] Microfluidic systems with on-chip monolithic PDMS valves and peristaltic pumps can be readily fabricated by multilayer soft lithography,[56] enabling ultimately microfluidic large-scale integration of biomolecular assays.[57,58] As PDMS is an oxygen permeable and transparent material, advanced cell-based assays were implemented on-chip, for instance rapid AST with single-cell resolution, the study of microbial consortia or larger model organisms (*e.g. Caenorhabditis elegans*).[59–62] Moreover, biomolecules can be captured and transported on-chip by means of functionalized magnetic beads for instance.[63] Droplet microfluidics is a powerful and

versatile format, enabling high-throughput bioassays with digital readout.[64–68] Compartmentalization in nL-sized droplets and simultaneous coding provides high multiplexing capabilities. Other properties, such as fast chaotic mixing in droplets may also be exploited.[69] A host of applications has been adapted to digital microfluidics, in particular for single-cell analysis,[68] including rapid high-throughput AST with single-cell resolution, or for molecular biology.[70,71] Centrifugal microfluidics or lab-on-a-disc (LoaD) devices, *i.e.* the implementation of bioassays on polymer disc cartridges featuring custom-designed fluidic circuits, are platforms that can potentially be used for POC applications.[72] Operations like aliquoting, valving and mixing,[73] *e.g.* for purification and amplification of nuclei acids, can be carried out directly on the disc with minimal user intervention, also thanks to reagent storage on the disc.[74,75] As an example, one lab-on-a-disc platform was designed for automated POC differential diagnosis of acute febrile illness.[76] Paper is an attractive substrate material for microfluidic applications, as it is cheap, disposable and does not require external fluidic control due self-driven capillary flow. Lateral flow assays (LFA) or rapid diagnostic test (RDT) are commonly used simple paper devices for qualitative diagnosis, mainly with immunochromatographic detection. Implementation for more sensitive and quantitative assays seeks to overcome current limitations of LFAs,[77–79] and to extend the range of possible applications.[80] Microfluidic paper analytical devices (μPADs) feature patterned hydrophobic boundaries on the paper substrate to create microfluidic fluidic structures and possible other fluidic control tools.[81] μPADs are capable of analyzing complex (*e.g.* blood) and small amounts of biochemical samples.[82] 3D paper stacks or foldable origami designs extend the complexity and multiplexing capabilities of μPADs, enabling the integration of more advanced antibody or nucleic acid assays.[83–86] μPADs are electricity-free and instrument-free devices thus are promising diagnostic tools for POC applications in low resource settings.

### 2.2 Biosensor technologies and analytical nucleic acid-based assays

Actual laboratory procedures, POC devices and commercial systems for clinical diagnosis of infectious diseases cannot necessarily meet the emerging needs of the global health system, such as the capability to respond rapidly and on a population-wide scale to the increasing risk of viral disease outbreaks, or to perform accurate informed diagnosis and screening campaigns of antimicrobial-resistant bacterial strains.[87,88] Emerging diagnostic methods, based on microfluidic and biosensor integration are therefore being developed, aiming POC pathogen detection/identification with high sensitivity and specificity at early stages of infection.[89,90]

**Biosensor principles.** A biosensor comprises mainly two functional parts, namely (i) the biomolecular recognition element immobilized on the sensor surface, and (ii) the transducer that transforms the biomolecular binding event into a measurable physical signal.[90–92] Antibodies with high affinity and specificity are widely used recognition elements. Nucleic acid aptamers also show high specificity but low stability. Other possible sensing entities include bacteriophages or antimicrobial peptides. Molecularly imprinted polymers are synthetic polymers that can be tuned for specific capture of a selected analyte. Transducers make use of a range of physical properties for monitoring pathogen detection. Optical detection of colorimetric or fluorescence signals is commonly used. Surface plasmon resonance (SPR) sensors take advantage of a refractive index change in a functionalized glass/metal film upon binding of biomolecules. For surface-enhanced Raman spectroscopy (SERS) sensor surfaces with plasmonic nanostructures (*e.g.* gold islands) for signal enhancement are fabricated.[93] Electrochemical detection methods are convenient for sensor applications as label-free pathogen detection can be carried out.[94–96] Mass-based detection or detection of magnetically-labelled targets are other options.

**Nucleic acid amplification in analytical tools.** In addition to immunoassay-based approaches, different types of nucleic acid amplification tests/technologies (NAAT), enabling highly specific and sensitive pathogen detection, are currently integrated with emerging microfluidic/biosensor diagnostic technologies.[83,97,98] A key method is polymerase chain reaction (PCR) requiring multiple temperature cycles to amplify DNA strands. Reverse transcription-PCR (RT-PCR) is utilized for amplification of viral RNA. Real-time quantitative PCR (qPCR) measures the concentration of (fluorescently) labelled target amplicons throughout the reaction.[99] The advantage of loop-mediated isothermal amplification (LAMP) is that constraints of thermal assay control are relieved (typically performed at 60–65 °C), leading to a shorter time-to-result than PCR.[100,101] Recombinase polymerase amplification (RPA) makes use of two proteins (a recombinase and a single-stranded DNA binding protein) for repeated cycling operated at constant temperature (normally 37–42 °C).[102] DNA-helicase unwinds double stranded DNA in the process of helicase-dependent amplification (HDA).[103] In rolling circle amplification (RCA), circular DNA sequences are amplified.[104] Technologies leveraged by clustered regularly interspaced short palindromic based methods (CRISPR-Cas) are rapidly expanding in the field of diagnostics.[105,106]

### 2.3 Microfluidic cartridge-based commercial systems

Commercial benchtop systems for infectious disease diagnostics aim to implement sample-to-answer strategies, often designed for fully integrated and automated NAAT methods for pathogen detection, requiring only minimal hands-on steps for sample preparation and assay protocol operations. Nevertheless, constraints like system or assays cost or the requirement of external power supplies may still limit the use in low resource settings. Wang *et al.* provide a comprehensive tabular comparison of microfluidic POC

 

platforms for molecular diagnostics arranged by approval time.[107] In a review on diagnostic tools for tackling febrile illness, Mitsakakis *et al.* proposed detailed descriptions of relevant microfluidic cartridge-based commercial platforms.[108] Other authors focus on more specific applications, such as Nelson *et al.*, who presented available POC tests and systems for respiratory viruses.[109] Commercial assays for specific types of infections will be addressed in the corresponding sections of this review.

The GeneXpert® (Cepheid, USA) is an example for a microfluidic cartridge-based RT-PCR system that returns test results in about an hour, including minimum sample preparation. Individual assay cartridges are generally designed for one or two pathogens.[110] The BioFire® FilmArray® (BioFire Diagnostics/bioMérieux, USA) is a nested multiplex PCR system for panels of more than 20 targets and a throughput of up to 175 samples per day (unprocessed samples, results in about an hour). Reagents are stored in a pouch in freeze-dried format.[111] Another chip-based approach is the VerePLEX™ Biosystem platform (Veredus Laboratories, Singapore) that offers chip panels for multiplex (more than 10) molecular testing of different pathogen families, including custom-designed applications (VereChip™). The cartridge comprises a microfluidic PCR unit and microarray modules for multiplexed DNA amplification and detection, respectively. Time to result is approximately 3.5 h.[112] The Bosch Vivalytic Analyser (Bosch Healthcare Solutions, Germany) is an automated cartridge-based molecular diagnostics POC platform for rapid detection of multiple pathogens.[113] The microfluidic cartridges have been developed by means of a rapid prototyping approach using generic polymer parts.[114] A PCR test portfolio covering a wide range of pathogens is available.[115] The LabDisk centrifugal microfluidic platform from Hahn-Schickard[116] (Germany) and IMTEK (University of Freiburg, Germany) is a versatile technology that has been used for a variety of applications.[108] The Rhonda player, a component of an *in vitro* diagnostic system based on the LabDisk technology, was successfully introduced to the market in 2020, in particular in combination with a SARS-CoV-2 RT-PCR test (Spindiag). The Rhonda player is now manufactured by Dialunox (Germany).[117]

### 2.4 Microfluidic-based diagnostics for infectious diseases – relevant review articles

Some review articles addressing the field of microfluidic-based infectious disease diagnostics form a broader perspective will be cited in the following (non-exhaustive list). X. Wang *et al.* discussed microfluidic strategies for molecular diagnostics of infectious diseases.[107] Flores-Contreras *et al.* summarized microfluidic biosensing platforms for POC testing SARS-CoV-2 and seroprevalence.[118] C. Wang *et al.* presented an extensive review on POC diagnostics for infectious diseases from the device/application perspective.[119] Basiri *et al.* introduced microfluidic devices for detection of RNA viruses.[120] Rezvani Jalal *et al.* was interested in magnetic nanomaterials in microfluidic sensors for virus detection, and applications were classified by the type of virus.[121] Mitsakakis *et al.* approached the topic of infectious/tropical diseases by investigating diagnostic tools for febrile illness and enhancing patient management.[108] Earlier relevant reviews have been proposed by Magro *et al.*, who focused on NAAT combined with paper microfluidics for infectious diseases diagnosis,[83] or Tay *et al.*, who reviewed advances in microfluidics in combating infectious diseases.[122] Damhorst *et al.* explored microfluidics and nanotechnology for detection of global infectious diseases, in particular for detection of HIV, malaria, and tuberculosis.[123] A host of other review articles focusing on specific types of infections or diseases exists. We will summarize these articles in the corresponding sections of the present review. A large number of microfluidic biosensing platforms has also been designed for the detection of foodborne pathogens.[124,125]

## 3 Respiratory tract infections

### 3.1 Scope and common pathogens

Respiratory tract infections (RTI) may be conveniently categorized as upper respiratory tract infection (URI) (nasal cavity, pharynx and larynx) or lower respiratory tract infection (LRI) affecting trachea, bronchi and the lung. Nevertheless, several pathogens, such as influenza viruses, may progressively infect the upper and lower parts likewise.[126] Typically, respiratory pathogens may be detected in saliva, nasopharyngeal swabs or blood. Most of URIs (common cold, pharyngitis, sinusitis, *etc.*) are caused by viruses and are far less severe than LRIs, causing for instance whooping cough (pertussis) and or potentially life-threatening pneumonia.[127,128] LRIs are among the leading causes of death, even before the COVID-19 pandemic outbreak. According to a WHO factsheet (2020), LRIs claimed 2.6 million lives in 2019, thus being the world's most deadly communicable disease category at that time.[129] Superinfections, *e.g.* influenza virus-associated bacterial pneumonia, increase disease severity and mortality.[130] Annual seasonal epidemics generated by influenza viruses type A or B are estimated to result in about 3 to 5 million cases of severe illness worldwide and hundreds of thousands respiratory deaths.[131] A strain of the H1N1 influenza virus caused the extremely deadly Spanish flu pandemic outbreak in 1918.[4] Among the multiple pathogenic conditions related to infections with coronaviruses, in particular the Middle East respiratory syndrome coronavirus (MERS-CoV) and the severe acute respiratory syndrome coronavirus (SARS-CoV), pneumonia-associated respiratory disorders are common.[132] An ongoing WHO update indicated that the SARS-CoV-2/COVID-19 pandemic caused a cumulative number of nearly 7 million deaths until the end of 2023 worldwide.[8] Other common viral pathogens possibly leading to serious respiratory illnesses include the respiratory syncytial virus (RSV), human parainfluenza viruses (HPIV), human adenoviruses (HAdV), human metapneumovirus (HMPV), human rhinovirus (HRV) or

the human bocavirus (HBoV).[109,133] *Streptococcus pneumoniae* is the most prevalent bacterial microorganism pathogen in community-acquired pneumonia (CAP), with an increasing global burden related to drug-resistant strains.[134,135] Among other CAP-causative pathogens are *Klebsiella pneumoniae*, *Haemophilus influenzae*, and *Pseudomonas aeruginosa*.[136,137] *Mycoplasma pneumoniae* generally causes mild infections, but which may evolve in more severe respiratory illness.[138] Nosocomial pneumonia is the leading cause of mortality attributed to hospital-acquired infections and is significantly challenged by drug-resistance bacterial strains.[139]

Tuberculosis, usually affecting the lungs, is caused by the bacillus *Mycobacterium tuberculosis* that spreads from person to person through the air. On a global scale, tuberculosis is still one of the leading causes of death due to an infectious agent and the second leading infectious killer after COVID-19 (2021).[140] The scope of the disease and microfluidics-based tuberculosis diagnostics will be extensively discussed in a separate section.

### 3.2 Commercial platforms and reviews in the field

Nelson *et al.* analysed the landscape of current and future POC tests for common, emerging and novel respiratory viruses. In particular, this review provides extensive tabular overviews on available commercial devices for nucleic acid and antigen POC or near-POC tests, as well as links to corresponding datasheets, company websites or device evaluation studies. We refer to this review for more details on actual commercial systems.[109] Huang *et al.* also evaluated the diagnostic accuracies of three multiplex PCR systems for the detection of viral respiratory infections.[141]

**Table 1** Selection of recent approaches for RTI pathogen detection

| Pathogens | Device and assay principle | Performance indications | Ref. |
|---|---|---|---|
| ***Microfluidic platforms or devices based on NAAT assays*** | | | |
| Up to 21 RTI viruses, SARS-CoV-2 variants | Multiplexed CRISPR-based droplet/microwell platform | 300–550 patient specimens in an 8 h working day | 155 |
| HAdV, HBoV, *S. pneumonia* | Hybridization chain reaction in an encoded particle platform | High multiplexing capability, low fM LOD values | 157 |
| SARS-CoV-2, RSV, influenza | Multiplexed chip-powered CRISPR/Cas12a system | Detection of co-infection in clinical swab samples | 159 |
| Up to 19 RTI pathogens | RT-PCR assays on a LoaD platform | Multiplex detection of pathogen panels in a single run within 200 min | 158 |
| RTI pathogens panels | Various (isothermal) NAAT-based LoaD systems | Simultaneous detection of several pathogens, typically within less than 1–2 h | 160–163 |
| Up to 21 RTI pathogens | Fully integrated RT-PCR array system | Process completed within 1.5 h. Tested with clinical samples. LOD $\sim 1 \times 10^3$ viral copies per mL | 164 |
| SARS-CoV-2 | Multifunctional micro-PCR droplet/microwell platform | Fast screening (running time 15 min). LOD of 10 nucleic acid copies per test | 165 |
| 11 RTI pathogens | Digital microfluidic RT-qPCR platform | LOD 12 to 150 copies per test, using positive plasmids samples | 166 |
| SARS-CoV-2, influenza, HPV | RT-PCR system with a gravity-driven microfluidic cartridge | qPCR in <30 min, up to 12 cartridges per test | 167 |
| 5 RTI pathogens | Quantitative multiplex digital PCR on a self-partitioning SlipChip | Melting curve analysis with a resolution of 1.5 K enabled amplicon classification | 179 |
| *M. pneumoniae* | qPCR on a 3D-printed device | Macrolide-resistant genes detection in PCR tubes fitted to the chip | 180 |
| *B. pertussis* | Paper/polymer hybrid microfluidic biochip integrated with LAMP | Tested with clinical samples. LOD 5 DNA copies, within 45 min | 182, 183 |
| ***Other microfluidic approaches*** | | | |
| SARS-CoV-2 and H1N1 | Nanotemplating fluidic impedimetric assay with multiplexed readout | Parallel detection of viral load and specific antibodies in saliva or blood within 11 min | 168 |
| SARS-CoV-2 | 3D-printed LOC with multiplexed electrochemical outputs | Concurrent detection of SARS-CoV-2 RNA and anti-SARS-CoV-2 antibodies in saliva | 169 |
| SARS-CoV-2, influenza, HAdV, RSV | Immunoassays in microarray-format on a LoaD | Semi-automated analysis of 6 samples in 30 min (serum and nasopharyngeal samples) | 170 |
| SARS-CoV-2 | ELISA chip with a coil microreactor | Custom-developed antibodies and colorimetric read-out | 171 |
| ***Specific biosensing methods*** | | | |
| SARS-CoV-2 and H1N1 | Aptamer-based detection on a rotational paper-based device | Aptamer attachment on a tetrahedral DNA framework improved assay performance | 174 |
| SARS-CoV-2 | Viral RNA sensing on ssDNA coated $SiO_2$ slides | LOD 10 aM for viral RNA in saliva. Detection in <10 min | 175 |
| SARS-CoV-2 | Nucleic acid hybridization on a plasmonic biosensors | Thermoplasmonic heat generated on gold nanoislands improved performance | 172 |
| SARS-CoV-2 | Field-effect transistor based immunological assay | Graphene coating enhanced sensitivity. LOD $2.4 \times 10^2$ copies per mL with clinical samples | 173 |

 

Examples among commercially available microfluidic molecular diagnostic systems are the GeneXpert® (Cepheid, USA) or the BioFire® FilmArray® (bioMérieux) which, for instance, a pneumonia panel test for 33 bacterial and viral clinically relevant RTI pathogens is available. The Rhonda system was used to screen the international biathlon season during the COVID-19 pandemic and a total of 22 182 tests were made during a 4 month period (2020–2021).[142] The assay portfolio of the Bosch Vivalytic® also includes RTI tests, in particular a rapid SARS-CoV-2 test that can be performed within 39 min.[143]

Recent more general discussions on LOC-based methods for virus detection also include examples of respiratory pathogens.[120,144] Fostered by the recent SARS-CoV-2 pandemic, a host of authors focused more specially on microfluidic and biosensor POC tools for respiratory virus detection. The non-exhaustive list of most recent articles includes a review by Breshears *et al.* on biosensor technology with a discussion on the background of airborne virus transmission,[145] a contribution by Zhang *et al.* on advanced POC technologies for eight typical acute human respiratory viruses,[146] a review by Tarim *et al.* on microfluidic virus detection methods for respiratory diseases,[147] and discussions by Qin *et al.* of integrated micro- and nanosystems for COVID-19/viral infection diagnostics,[148] or by Ribeiro *et al.* of RTI-related biosensor technologies, respectively.[149] Flores-Contreras *et al.* explored emerging frontiers in POC testing SARS-CoV-2 and seroprevalence.[118] In the review by Goud *et al.* on electrochemical diagnostics of infectious viral diseases, biosensors specifically designed for COVID-19/SARS-CoV-2 have been included.[96] Zenhausern *et al.* explored microfluidic sample preparation for respiratory virus detection,[150] whereas Krokhine *et al.*, as well as Lee *et al.*, discussed microfluidic sampling methods for airborne virus isolation and bioaerosol, respectively.[151,152] Shabani *et al.* focused on laboratory detection methods for human coronaviruses, including RT-PCR, RT-LAMP, electrochemical and optical biosensors for RNA detection, and whole virus or viral proteins detection assays.[153] Chen *et al.* also reviewed emerging detection technologies and auxiliary analysis for COVID-19.[154] In the following, we discuss a selection of microfluidic/biosensor systems for respiratory virus and bacteria detection. Table 1 provides an overview of recent approaches for RTI pathogen detection.

### 3.3 Microfluidic systems for respiratory virus detection

**Integrated microfluidic platforms.** Welch *et al.* presented a CRISPR-based microfluidic diagnostic platform for multiplex nucleic acid detection of respiratory viruses and variants (Fig. 1a).[155] The system builds on a previously developed workflow (CARMEN) as described by Ackerman *et al.*[156] Two distinct nL-droplet emulsions, containing the amplified sample and a Cas13 protein mix, respectively, are prepared on conventional microtiter plates and combined with a distinct fluorescent colour code for optical identification. Subsequently, the pool of droplets was loaded into a PDMS microwell array, creating all possible pairwise combinations in replicate. Confined droplet pairs were then merged by electric field exposure, enabling digital fluorescence monitoring of more than 4500 CRISPR RNA (crRNA)/target pairs on a single array. The first version of this device could differentiate 169 human-associated viruses in 8 samples simultaneously.[156] Welch *et al.* modified and implemented the assay on commercially available integrated fluidic circuits on an automated system (Fluidigm Biomark) in order to meet the high-throughput and multiplexed requirements of a clinically relevant surveillance technology. The platform was validated by testing up to 21 human respiratory viruses (including SARS-CoV-2, other coronaviruses and both influenza strains) and SARS-CoV-2 variant mutations with high concordance to comparator assays. 300 to 550 patient specimens could be tested in parallel in an 8 hour working day.[155] Rutten *et al.* used a microfluidic platform (Evalution™, MyCartis NV, Belgium) providing a high-throughput microfluidic system combined with high-level multiplex capacity due to encoded microparticles (Fig. 1b). Functionalized microparticles serve as substrates for hybridization chain reaction (HCR), an enzyme-free isothermal amplification technique, for simultaneous detection of several disease-related biomarkers. Virus strains (HAdV and HBoV), virus subtypes (HAdV type B and D) and antibiotic-resistant bacteria (*S. pneumonia*) could be discriminated. Experiments revealed a LOD of ~400 fM for HAdV spiked in a clinically sample matrix (HCR for 60 min).[157]

Rombach *et al.* introduced a LabDisk-format POC system named RespiDisk. This system enables multiplex RT-PCR detection of up to 19 viral and bacterial RTI pathogens from a single sample. Respiratory samples mimicking clinical conditions were loaded onto the disc for automated nucleic acid extraction (50 min), elution and target amplification (150 min).[158] Liu *et al.* developed a multiplex analysis platform based on nested RPA and CRISPR/Cas12a-assisted virus identification for diagnosis of co-infections in the microfluidic format. The assays were designed for simultaneously detection of eight respiratory viral pathogen targets in nasopharyngeal samples, including SARS-CoV-2, RSV and influenza viruses/subtypes. The microfluidic chip was inserted in a centrifugal platform for running the assay steps, namely multiplex RT-RPA, subsequent RPA for separate amplification of each target gene and transfer into CRISPR/Cas12a detection chambers. LODs were 50–200 copies per mL depending on the assay with an on-chip protocol duration of 40 min.[159] Other recent centrifugal microfluidic systems for RTI diagnostics (SARS-CoV-2, influenza A/B) implemented RT-LAMP/Cas12a detection or RT-qPCR,[160,161] rapid differential diagnosis of seven human respiratory coronaviruses,[162] or isothermal amplification for detection of 19 types of respiratory viruses.[163]

A fully automated microfluidic PCR-array platform, developed by Huang *et al.*, could complete detection of 21

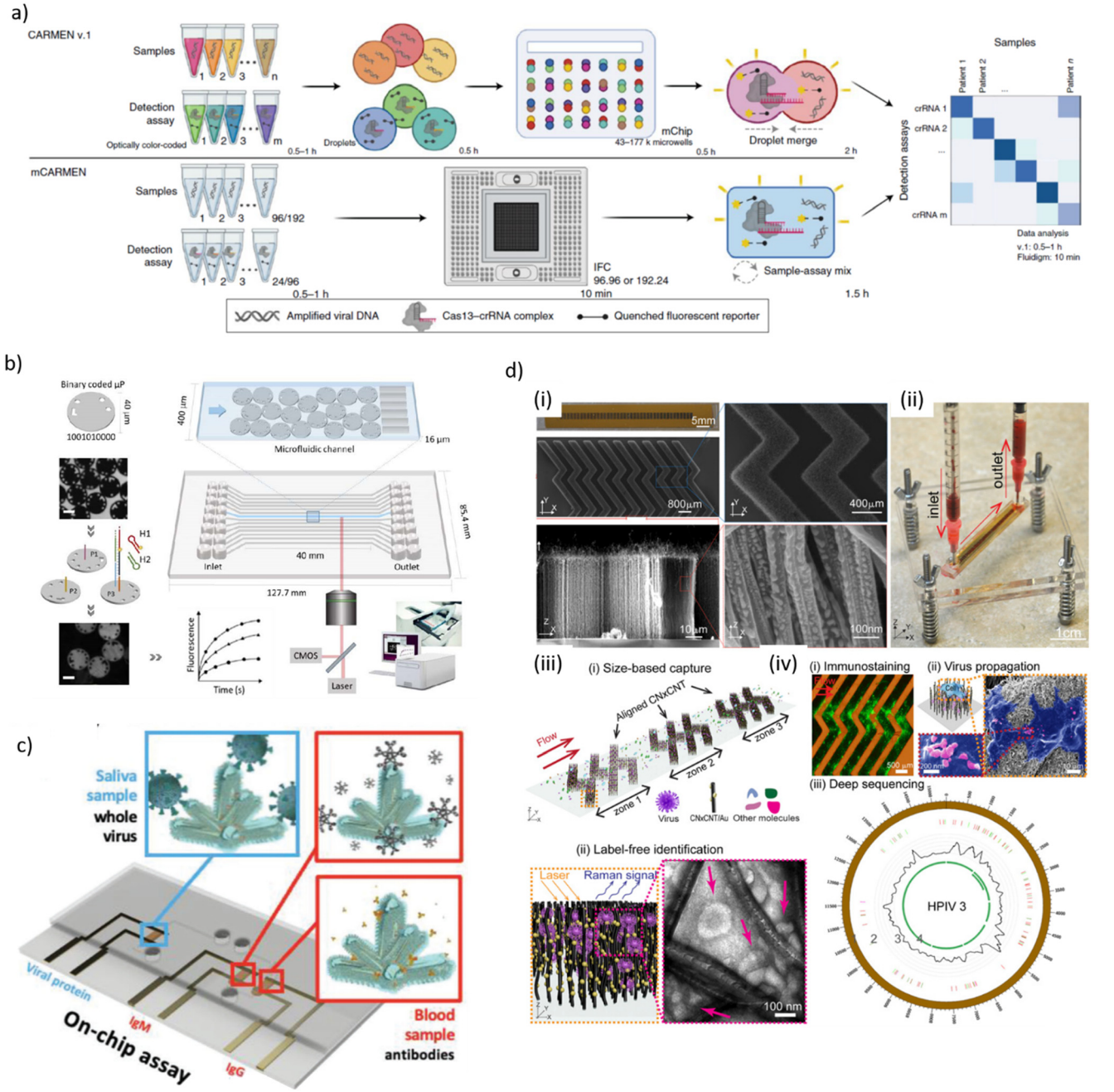


**Fig. 1** a) Schematic process flow of two virus and variant detection platforms, called combinatorial arrayed reactions for multiplexed evaluation of nucleic acids (CARMEN v.1, top) and its microfluidic version (mCARMEN, bottom), the latter combining CRISPR-based diagnostics and microfluidics. A mCARMEN respiratory virus panel allows testing for up to 21 viruses, including SARS-CoV-2, other coronaviruses and both influenza strains. b) Schematic representation of the processing of digitally barcoded microparticles using a microfluidic cartridge and an integrated instrument. Each microfluidic channel is embedded with encoded microparticles (P1, P2 and P3) that each serve as the substrate for the detection of a specific target. In presence of target, the hybridization chain reaction is initiated and the microparticles are identified during signal read-out. Scale bar is 20 μm. c) Schematic of an electrochemical microfluidic device for use with on-chip assays for the specific detection of whole viral particles in saliva and antibodies in blood using nanostructure-gold electrodes. d) Design and working principle of a microfluidic platform for effective virus capture and identification. (i) Photograph and SEM images of aligned carbon nanotubes (CNTs) exhibiting herringbone patterns decorated with gold nanoparticles for virus capture. (ii) Picture showing assembled device and processing of a blood sample. (iii) Illustration of size-based capture and *in situ* Raman spectroscopy for label-free optical virus identification. (iv) On-chip virus analysis and enrichment for next generation sequencing of human para-influenza virus type 3 (HPIV 3) [a) reproduced from ref. 155, ©2022, Creative Commons license, CC BY 4.0 (**http://creativecommons.org/licenses/by/4.0/**); b) reproduced from ref. 157, ©2023, CC BY 4.0; c) reproduced from ref. 168, ©2022, CC BY 4.0; d) reproduced from ref. 177, CC BY 4.0].

RTI pathogens (mainly viral and some bacterial) within 1.5 h with a LOD of $1.0 \times 10^3$ nucleic acid target copies per mL.[164] Yin *et al.* designed a multifunctional rapid RT-PCR system for two different microfluidic chips, namely a microwell array chip of qualitative screening assays, or a droplet microfluidic chip for rapid quantification. Detection of SARS-CoV-2 virus sequences in serially diluted reference RNA samples was achieved within 15 min with a LOD of 10 copies per test.[165] Another approach was a digital microfluidic (DMF) RT-qPCR platform for simultaneous detection of 11 viral and bacterial pathogens.[166] Zai *et al.* operated a microfluidic test cartridge for multiplex RT-qPCR respiratory virus detection with passive gravity-driven fluid flow control. Assays were completed in 30 min with a LOD in the range of 200 RNA copies per mL (SARS-CoV-2, influenza A/B).[167]

**Combining viral antigen and serological tests.** Siavash Moakhar *et al.* proposed a microfluidic multiplexed home-test device for automated diagnosis of viral respiratory infection. In order to provide a complete profile of the patient's clinical status following infection, three electrochemical assays were implemented in a cartridge for simultaneous quantification of the viral load in saliva and for IgG/IgM antibody detection in blood for monitoring immune response, respectively (Fig. 1c). The system took advantage of nano-roughness gold sensors with a biomimetic receptor based on thin-film molecularly imprinted polymers featuring tuneable target-specific recognition sites. Influenza A H1N1 and different SARS-CoV-2 variants were detected with clinically relevant sensitivity and specificity within 11 min.[168] Following the same motivation, Najjar *et al.* designed a 3D-printed LOC with multiplexed electrochemical outputs that concurrently detected SARS-CoV-2 RNA by LAMP and a CRISPR-based assay from unprocessed saliva, as well as SARS-CoV-2 antibodies using polystreptavidin-HRP/TMB reaction chemistry for readout. Detection was accomplished within 2 h and a LOD of RNA 0.8 copies per μL was reported for SARS-CoV-2.[169] Teixeira *et al.* presented a multiplexed disc device, comprising target-specific bioreceptor microarrays, for quantification of viral antigens or antibodies against the respiratory viruses from human serum and nasopharyngeal samples simultaneously (SARS-CoV-2, Influenza A/B, HAdV and RSV). Analysis of 6 samples could be performed within 30 min with high diagnostic sensitivity.[170] In another assay, custom-generated monoclonal antibodies against the SARS-CoV-2 nucleocapsid protein were evaluated on a microfluidic ELISA chip with a coil microreactor for colorimetric COVID19 on-chip detection from clinical samples.[171]

**Alternative biosensing methods.** Plasmonic biosensors are sensitive tools for real-time and label-free analyte detection that are readily amendable for microfluidic integration, although a host of currently published work focuses more on sensor characterisation. For instance, Qiu *et al.* developed a dual-functional sensing approach that combined localized SPR and the plasmonic photothermal effect for sensitive SARS-CoV-2 viral nucleic acid detection. The sensor surface consisted of Au nano-islands functionalized with complementary DNA receptors for hybridisation with specific SARS-CoV-2 nucleic acid sequences. Thermoplasmonic heat generated near the Au nano-absorbers elevated the temperature locally and improved hybridization kinetics, enabling accurate discrimination of similar viral gene sequences. The biosensor exhibited high sensitivity with a LOD of 0.22 pM for SARS-CoV-2 (RdRp sequence).[172] A field-effect transistor (FET) microfluidic device was developed by Seo *et al.* for sensitive immunological COVID-19 diagnostics. The FET chip was coated with graphene as sensing material conjugated with antibody against SARS-CoV-2 spike protein. This technique enabled rapid detection of SARS-CoV-2 from clinical nasopharyngeal swabs with a LOD of $2.42 \times 10^2$ copies per mL and 100 fg $mL^{-1}$ for SARS-CoV-2 spike protein in clinical transport medium.[173] Li *et al.* implemented a detection scheme based on a tetrahedral DNA framework for attaching recognition aptamers in well-defined manner on a paper device for simultaneous detection of SARS-CoV-2 and influenza A H1N1 virus. The rotational design of the devices allowed performing subsequent fluidic protocol steps.[174] A biosensor with ssDNA-coated sensing $SiO_2$ slides for SARS-CoV-2 RNA hybridization and fluorescence readout reached a LOD of 6 RNA copies per μL (equal to 10 aM) within 10 min.[175]

Hydrophilic droplet surface energy traps served as virtual reaction chambers on a structure-free super-hydrophobic chip. Aptamer-coated magnetic microbeads provided the mobile substrates for the ELISA-like on-chip assay. A LOD of 0.032 hemagglutination units/reaction was reported for influenza A H1N1 detection.[176] Yeh *et al.* used carbon nanotube (CNT) arrays with differential filtration porosity for virus enrichment combined with SERS identification in a microfluidic format (Fig. 1d). Au nanoparticle-decorated CNTs have been arranged in herringbone patterns for size-based capture and label-free detection. The device was validated with clinical samples from patients with rhinovirus, influenza A virus or HPIV infection. Viral detection was done in a few minutes with a 70-fold enrichment.[177] Ramachandran *et al.* proposed a microfluidic assay for automated SARS-CoV-2 RNA detection using on-chip isotachophoresis (ITP) extraction of nucleic acids form clinical samples (5 min), followed by off-chip RT-LAMP preamplification (20–30 min) and on-chip ITP/CRISPR-based fluorescent target detection (SARS-CoV-2 N gene and E gene) (5 min). Electrokinetic protocols for ITP extraction and CRISPR/Cas12 enzymatic reactions were performed on a glass chip comprising two distinct cross-geometry channels. The LOD of the ITP/CRISPR method was found to be 10 copies per μL of viral RNA spiked into pooled nucleic acid extracts from negative clinical samples.[178]

### 3.4 Microfluidic systems for bacterial RTI pathogen panels

Yu *et al.* used the SlipChip technology to perform digital PCR for the detection of a panel of bacterial RTI-causative pathogens. As a proof of concept, the assay was designed for

multiplex quantification of *S. aureus*, *A. baumannii*, *S. pneumoniae*, *H. influenzae*, and *K. pneumoniae* in a single test. The chip comprised two silanized glass microfluidic plates. The solution containing target nucleic acid templates and reactants was introduced into the chain-of-pearl channels of the top plate, which was subsequently slipped over the microwell array in the bottom plate. This operation resulted in surface tension-driven compartmentalization into a large number of reaction droplet partitions (2240 droplets with a volume of 4.5 nL). The chip was then placed on a thermal cycler for the PCR process. Differentiation of the target templates was performed by melting curve analysis of amplicons designed with different melting temperature $T_m$ signatures and fluorescence detection by means of EvaGreen intercalation dye. Amplicons with $T_m$ differences of 1.5 °C could be clearly separated.[179]

A 3D-printed microfluidic device was developed for qPCR-based identification of *M. pneumoniae* mutant types with resistance to macrolide antibiotics. On-chip reservoirs contained sample solutions and PCR reactants, respectively, which were mixed and dispensed *via* pneumatic fluidic control into separately attached PCR tubes. The system was tested with plasmids containing a specific mutation, indicating a sensitivity 100 copies per reaction and a processing time of 80 min.[180] Another device for POC detection of *S. pneumoniae* and *M. pneumoniae* took advantage of a polymer/paper microfluidic chip for genomic DNA extraction, performing LAMP in microchambers hosting chromatography paper substrates with pathogen-specific LAMP primers and calcein-mediated fluorescence detection. The analytical sensitivity of the LAMP microchamber reaction was 20 fg of target DNA.[181] Dou *et al.* also proposed a hybrid microfluidic portable LAMP platform applied to the diagnosis of whooping cough (pertussis) in this case. The chip comprises six LAMP zones with paper disks for storage of DNA primers specific to *B. pertussis*. The assay reached a LOD of 5 DNA copies per LAMP zone (purified DNA samples) within 45 min. The clinical performance of the system, evaluated with lysates from *B. pertussis* spiked nasopharyngeal swabs and clinical samples from pediatric patients with signs of whooping cough, was comparable to real-time PCR tests.[182,183] In an earlier approach, Huang *et al.* used a disc device with 24 test cells and pre-stored LAMP primers for multiplex identification of pathogens related to clinical pneumonia, in particular *M. pneumoniae*, *S. aureus*, and methicillin-resistant *S. aureus*. DNA samples and reactants were mixed off-chip prior to injection on the disc. The device had an analytical sensitivity of 10 nucleic acid copies. Assessment of with clinical samples demonstrated very good agreement with commercial real-time PCR systems.[184]

### 3.5 Tuberculosis

**Scope of the disease and reviews.** Tuberculosis (TB) is a communicable disease mainly affecting the lungs (pulmonary TB) but also serious extrapulmonary forms, such as tuberculous meningitis, exist.[185] TB is one of the leading causes of death due to an infectious agent, usually caused by the rod-shaped *Mycobacterium tuberculosis* (*Mtb*), which belongs to the *Mycobacterium tuberculosis* complex (MTBC).[186] *Mtb* is a very slow-growing (dividing every 18–24 h), non-motile and highly aerobic pathogen that is spread through aerosol particles.[187] Distinctive cell biology, in particular asymmetric growth giving rise to daughter cells of unequal sizes and growth rates, may impact susceptibility to antibiotics.[188] According to the WHO Global TB Report 2023 approximately 10.6 million people fell ill with TB in 2022.[140] Multidrug-resistant (MDR) and extensive drug resistance (XDR) represents an increasing global health threat, requiring prolonged and complex antimicrobial treatments.[189,190]

Acid-fast bacillus (AFB) smear microscopy performed from sputum is still widely used for initial TB diagnosis, even if this simple manual technique suffers from a lack of sensitivity (LOD $\sim 10^4$ CFU $mL^{-1}$).[191] *Mtb* culture is the gold standard for laboratory TB diagnosis and drug susceptibility testing, however, due to the slow *Mtb* growth rate, time-to-result may extend to several weeks.[190,192] NAAT methods enable early detection and identification of mutations related to drug resistance. An update of WHO guidelines (2021) on rapid TB diagnostics outlines currently recommended technologies and products.[193] WHO-endorsed TB diagnostics has been reviewed recently by Nandlal *et al.* and Hong *et al.*, respectively.[194,195]

Commercial microfluidic PCR assays include Xpert® MTB/RIF (GeneXpert®, Cepheid, USA), a landmark development in TB diagnostics that detects MTBC bacteria and rifampicin (RIF) resistance within 2 h.[196] Xpert® MTB/RIF Ultra has improved sensitivity (LOD 15.6 CFU $mL^{-1}$ for MTBC) and Xpert® MTB/XDR was designed for detection of mutations resistant to 6 anti-TB drugs within 90 min.[195] The VereMTB™ assay (VerePLEX™ Biosystem, Veredus Laboratories, Singapore) detects MTBC, several nontuberculous mycobacteria, as well as RIF and isoniazid (INH) resistance. Other WHO-endorsed on-chip RT-PCR assays are the Truenat® MTB, MTB Plus and MTB-RIF Dx assays (Molbio Diagnostics, India).[197] Recently, Schlanderer *et al.* implemented a TB diagnostic workflow on the Rhonda player. MTBC detection including antibiotic resistance testing against the first-line antibiotics INH and RIF is performed on the disc from a single sputum sample. If the qPCR on-chip data indicates drug resistance, a detachable sample tube containing enriched MTBC DNA is available for subsequent comprehensive resistance profiling *via* targeted next generation sequencing (tNGS) in a centralized lab facility. This two-stage TB diagnostic can be completed within three days.[198]

Serological TB tests have insufficient diagnostic value.[199] As a consequence, there is more focus on TB antigen detection, for instance lipoarabinomannan (LAM), a structural component of the outer cell wall of mycobacteria that may be released into urine.[200] The LAM antigen can be

 

detected on LFAs within minutes using unprocessed urine samples.[201,202] Assays have also been developed for clinically relevant other TB antigens (such as MPT64, CPF-10 or ESAT-6).[203–205] In a recent review on LFAs for detection of pathogenic bacteria, Sohrabi *et al.* also addressed assays specifically designed for TB diagnosis.[80]

Hong *et al.* discussed challenges in the development of rapid POC TB diagnosis and drug susceptibility testing, including some selected microfluidic and nanophotonic systems.[194] Paul *et al.* discussed advanced integrative sensing technologies for detection of drug-resistant TB.[190] Gupta *et al.* focused on developments in nano-biosensing technologies.[206] Srivastava *et al.* also analysed biosensor-based detection.[207] Earlier reviews on POC TB diagnosis, also discussing to some extend the potential of microfluidics, have been proposed by Mani *et al.*, Wang *et al.*, Dheda *et al.* and Niemz *et al.*[208–211] In the following, we discuss a selection of microfluidic/biosensor systems for TB diagnostics. Table 2 provides an overview of recent approaches, including AST tools.

**Recent microfluidic nucleic acid-based technologies for TB diagnostics.** Minero *et al.* developed a lab-on-a-disc assay for mutation-specific ligation of padlock probes (PLP) and RCA combined with optomagnetic read-out for highly specific detection of a single-nucleotide mutation in the *Mtb katG* catalase peroxidase gene responsible for INH resistance. In one of the proposed assay strategies, PLP ligation is performed in on-disc chambers, while RCA reagents are stored separately. Subsequent mixing by centrifugal actuation enabled RCA amplification and real-time detection. A DNA target LOD of 2–5 pM was obtained within an assay time of 2 h.[212] Previously a similar molecular assay was implemented on a multi-chamber polymer chip using magnetic transportation and optomagnetic detection.[213] Homann *et al.* adapted the lab-on-a-disc technology to automated DNA sample preparation for TB diagnosis (Fig. 2a).[214] The fluidic network was designed to provide two separate DNA aliquots for subsequent off-chip analysis from the same initial sample. DNA extracts from liquified sputum were collected in two PCR tubes attached to the disc cartridge. Composite foil pouches (stickpacks) served as reservoirs for buffer solutions. A LOD of 10 CFU $mL^{-1}$ in *M. bovis* BCG spiked sputum samples was demonstrated with a workflow using cartridge-based DNA extraction and a benchtop PCR cycler.[214] Moreover, Beutler *et al.* presented an extended study with bacteriologically confirmed TB sputum samples to evaluate the performance of this TB-disk for clinical TB diagnosis and resistance testing against first- and second-line drugs. The availability of two identical DNA extracts significantly increased the versatility of the diagnostic workflow.[215] Kaur *et al.* proposed a low-cost hybrid paper/plastic device for LAMP-based TB assays on 12 test zones. The chip features an array of sealed paper pads as amplification sites with dry-stored reagents and fluorescence smartphone read-out. The analytical sensitivity was 10 copies of *Mtb* DNA and good clinical performance with sputum samples was demonstrated.[216]

Droplet digital PCR (ddPCR) has been used in clinical applications thanks to its high accuracy and sensitivity for low-abundance DNA, and for absolute quantification of nucleic acid target sequences.[217,218] Nyaruaba *et al.* recently reviewed the application of ddPCR as TB diagnostic tool.[219] Several TB-related studies took advantage of the Bio-Rad QX200 droplet generator system (Bio-Rad Laboratories, USA)

Table 2 Selected microfluidic approaches for TB diagnostics and AST

| Target | Device and assay principle | Performance indications | Ref. |
|---|---|---|---|
| ***Microfluidic devices based on NAAT assays*** | | | |
| *Mtb katG* gene | LoaD for analysis of TB drug-resistance by mutation-specific PLP ligation and RCA | Mixing on-disc and real-time optomagnetic readout. Assay time of 2 h, LOD 5 pM | 212 |
| *M. bovis* BCG and *Mtb* (drug resistant strains) | LoaD for automated PCR analysis. Two separate DNA extracts are obtained | LOD of 10 CFU $mL^{-1}$ in spiked sputum. Drug resistance testing with clinical samples | 214, 215 |
| *Mtb* gDNA | Modular LAMP paper-and-plastic POC device with dry-stored reagents | High analytical (10 copies of *Mtb* gDNA) and clinical sensitivity | 216 |
| Circulating cell-free *Mtb*-specific DNA | Droplet digital PCR using a commercial droplet generator | Absolute quantification of nucleic acid target sequences | 220, 221 |
| *M. bovis* BCG | Distinction of live/dead bacteria *via* PMA binding and on-chip PCR | Automated detection within 90 min | 223 |
| *Mtb* H37Ra bacilli | Modular sputum-to-genotype system with a lab-on-a-film gel element array | Multiplex detection of mutations. LOD 43 CFU $mL^{-1}$ in raw sputum | 224, 225 |
| RIF-resistant *Mtb* (*rpoB* gene) | RT-PCR in on-chip reactors and high-resolution DNA melting-based TB test | Drug-resistance mutations were detected in clinical isolates. 20 PCR reactions per chip | 226 |
| ***Microfluidics for antimicrobial testing*** | | | |
| *M. smegmatis* | Microfluidic chip for voltammetric detection of nucleic acid sequences | Antibiotic susceptibility apparent after 24 h through measuring *16SrRNA* levels | 232 |
| *M. smegmatis* | On-chip cell trapping for visualization of growth and phenotypic alterations | Drug response assessed by real-time tracking for over 48 h at single-cell level | 233 |
| *M. smegmatis* (*msm2570::Tn* mutant) | Microfluidic-microscopy method to reveal antibiotic tolerance mechanisms | Antibiotic exposure of the *msm2570::Tn* mutant showed low number of lysed cells | 234 |
| *M. smegmatis* | Microfluidic acoustic trapping of live *Mtb* and Raman spectroscopy | Raman fingerprints change substantially upon INH exposure. Trapping for up to 8 h | 235 |

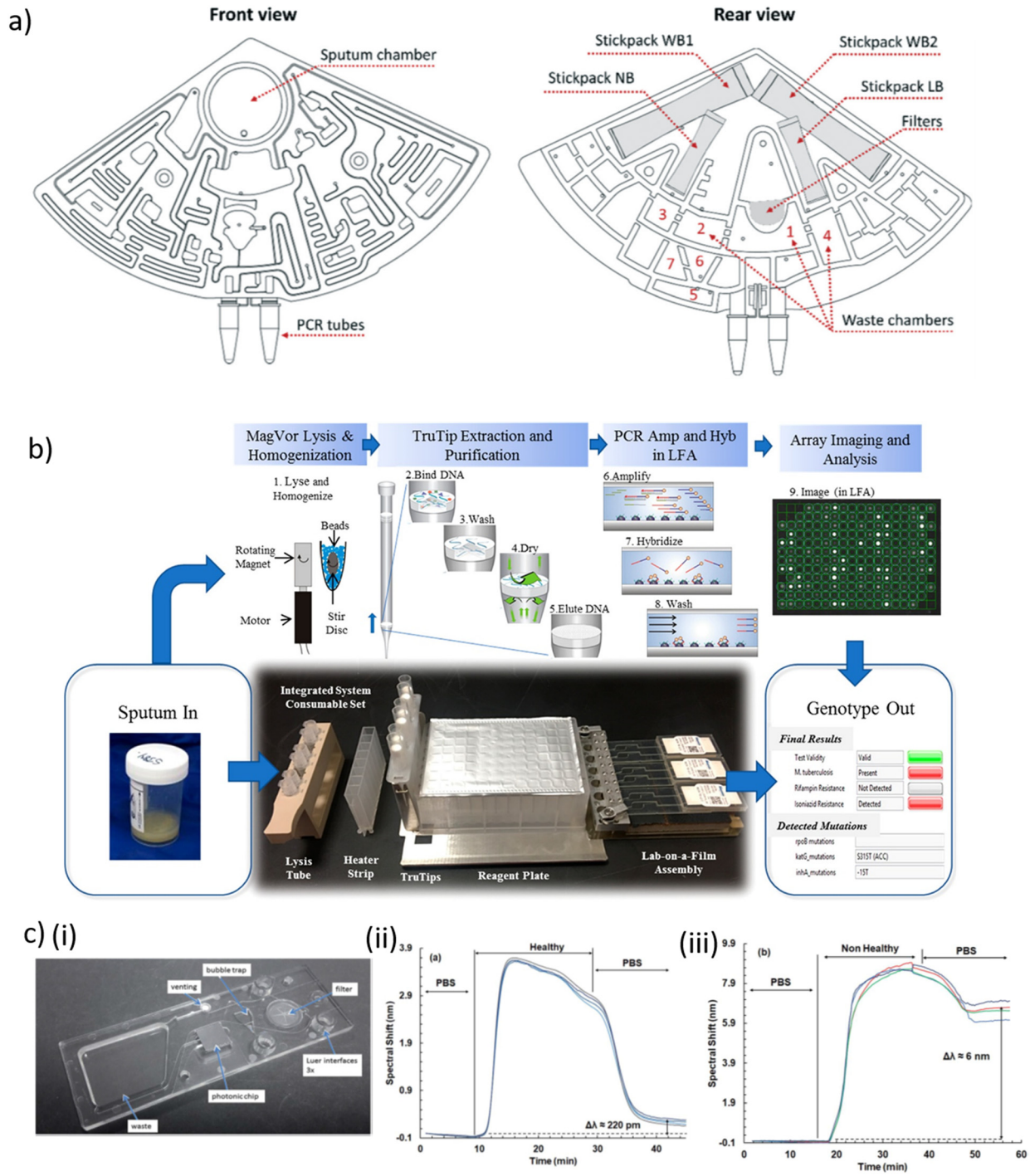


**Fig. 2** a) Design of a cartridge for *Mtb* diagnosis, three of which can be placed in a laboratory centrifuge in front view (left) and rear view (right), indicating the fluidic network with chambers and channels, the interfaces for sample input (sputum chamber) and product collection (PCR tubes), the filters, the waste collection chambers and 4 stickpacks for pre-storage of the reagents. Abbreviations: washing buffer 1 + 2 (WB1+2); lysis buffer (LB); neutralisation buffer (NB). b) Layout of the consumable in an automated *Mtb* sputum-to-genotype system for processing of six samples, in which the following steps occur. (1) Lysis and homogenization occur in lysis tubes, which include a magnetized stir disc and glass beads. (2) TruTip aspirates the sample mixed with a binding buffer, so that it flows through the pores of the matrix in the tip resulting in DNA bound to the matrix. (3) Porous matrix is washed to remove the impurities. (4) Matrix is dried with air. (5) Bound DNA is eluted into an elution buffer. (6) Purified DNA is amplified with an asymmetric PCR reaction. (7) Product (with fluorescent labels) hybridize to the gel elements. (8) Gel elements are washed to remove unbound product. (9) Image of the array is captured and analyzed. c) (i) Picture of a waveguide-based SiN nanophotonic chip with anti-LAM molecules covalently coupled to the SiN surface and assembled in a polymer cartridge. Spectral shift observed in the interferometric signal upon exposure of a waveguide to LAM, a biomarker for TB, in urine of (ii) a healthy and (iii) a non-healthy person. Presence of LAM in the sample leads to a long-term spectral shift [a) reproduced from ref. 214 with permission from the Royal Society of Chemistry; b) reprinted with permission from ref. 225, ©2020 American Chemical Society; c) reproduced from ref. 227 with permission from the Royal Society of Chemistry].

and ddPCR for detecting low levels of circulating *Mtb*-specific DNA, drug susceptibility testing and other applications.[220–222] Based on a different approach, Wang *et al.* proposed a microfluidic system featuring 12 PCR reaction chambers enabling distinction of live/dead bacteria *via* photo-reactive propidium monoazide (PMA) binding. Selective covalent binding of PMA to DNA from dead bacteria inhibited PCR amplification. Heparin-binding haemagglutinin (HBHA) antibody-conjugated magnetic beads were used as capture probe against *M. bovis* Bacille Calmette–Guérin (BCG) and *Mtb* clinical isolates. Bacteria capture, thermolysis and DNA release, PMA treatment and rpoB gene PCR amplification was performed on-chip within 90 min and a reported LOD of 100 CFU.[223] Kukhtin *et al.* developed a disposable lab-on-a-film that detects MDR-TB from sputum extracts.[224] The device comprises a gel-based microarray printed onto a flexible polyester film. Target amplification and hybridization on the microarray was carried out within a single closed microfluidic flow-cell. Nucleic acid was purified off-chip using a pipet tip with an embedded matrix for nucleic acid isolation (TruTip, Akonni Biosystems). Initially a LOD of 32 CFU $mL^{-1}$ for *Mtb*-spiked sputum was obtained. In a follow-up development improved sample homogenization and cell lysis was implemented in the workflow and a *Mtb* LOD of 43 CFU $mL^{-1}$ in raw sputum was reported (Fig. 2b).[225] Mbano *et al.* performed real-time PCR and subsequent high-resolution melting curve analysis on a microfluidic PDMS chip with 20 independent PCR chambers and fluorescence readout. RIF-resistant strains of *Mtb* were used to assess the performance of this method.[226]

**Microfluidic immunodetection of TB antigens.** A biosensing platform comprising a photonic sensor chip based on Mach–Zehnder interferometer transducers and readout with an on-chip optical spectral analyser was adapted for non-invasive detection of the TB LAM antigen (Fig. 2c). The sensor was integrated in a microfluidic cartridge. Anti-LAM IgG was immobilized on the surface of the photonic sensor chip for direct immunodetection from urine samples with in a LOD of 475 pg $mL^{-1}$ (27.1 pM) achieved less than 15 min. Validation of the device with clinical samples showed excellent correlation with standard techniques.[227,228] ESAT-6 (early secretory antigenic target of 6-kDa) is suitable for diagnosing TB in human blood at early stages. For instance, a magnetic bead-coupled gold nanoparticle immuno-PCR assay or a giant magnetic resistance biosensor for detection in pg $mL^{-1}$ range was developed for ESAT-6 detection,[229,230] however, these assays have not been integrated in microfluidic format for the time being. In another study, a LFA detects the CFP-10 (culture filtrate protein 10)/ESAT-6 antigen complex for increased the diagnostic performance as compared to assays based on single antigens.[231]

**Microfluidics for antimicrobial testing with the model organism *Mycobacterium smegmatis*.** *M. smegmatis* is a faster growing and non-pathogenic model organism for research related to *Mycobacteria* species. A multilayer device enabled integrated rapid on-chip AST with *M. smegmatis* by direct electrochemical detection. The chip had two incubation chambers for bacterial suspensions with and without antibiotics, respectively. After thermal lysis, the samples were transferred into adjacent chambers where the resulting nucleic acid levels in response to the specific incubation conditions were measured *via* integrated Au microelectrodes.[232] A microfluidic PDMS chip for real-time monitoring of the growth dynamics and phenotypic alterations of *M. smegmatis* has been proposed as a tool for investigating drug-induced stress with single cell resolution. The device was composed of arrays of 0.9 μm high chambers for bacteria trapping and culture under different conditions, including drug exposure.[233] In another study, the antibiotic tolerance of wild-type *M. smegmatis* and *msm2570::Tn* mutant cells was investigated by single-cell timelapse microscopy. Cells were trapped by means of a semipermeable membrane in PDMS microfluidic channels, enabling stable flow conditions for on-chip culture and rapid medium exchange.[234] The response of live mycobacteria to antibiotic stress could also be monitored dynamically by wavelength modulated Raman spectroscopy.[235] For this purpose, *M. smegmantis* was acoustically trapped in a microfluidic glass chamber. Levitation and formation of a thin bacterial layer by acoustic force provided good conditions for sensitive Raman spectroscopy. Raman spectra for no-stress and antibiotic-stress conditions showed distinct alterations of peaks related to the cell lipid concentration in real-time. It was suggested that lipid-rich bacteria are prone to higher antibiotic tolerance persistence, a phenomenon that may play a role in patients' relapse.[236]

# 4 Urinary tract infections

## 4.1 Scope and common uropathogens

The urinary tract system comprises the kidneys, the bladder, the ureters and the urethra. Measuring the abundance of specific biomarkers in urine is frequently used for non-invasive health monitoring.[237,238] Paper-based devices, either conventional LFAs or more advanced designs, are well-suited for biochemical urine analysis in general.[239–241] Urinary tract infection (UTI) occurs when uropathogens, such as bacteria from the vaginal area, the rectum or the skin, get into the urinary tract and move upwards into the bladder and eventually into the kidney.[242–244] UTIs are among the most widespread community and hospital-acquired bacterial infections with hundreds of millions of people being affected annually worldwide, entailing a major global clinical and economic burden. Bladder infection (cystitis) is the most common type of UTI, whereas kidney infections (pyelonephritis) are less frequent but may have severe and even life-threatening consequences if pathogens spread into the bloodstream (urosepsis).[245] Significant bacteriuria can be defined as a count of over $10^5$ CFU of the same organism per mL of urine, but the threshold for UTI diagnosis may be set much lower in some cases (100–1000 CFU $mL^{-1}$).[246,247] By far

the most common causative agent for both uncomplicated and complicated UTIs is uropathogenic *E. coli* (UPEC).[248] Other bacterial species, with much lower prevalence and depending on the specific conditions, include *K. pneumoniae*, *P. mirabilis*, *E. faecalis*, *P. aeruginosa*, *S. aureus* and other species.[246,247,249] Catheter-associated UTIs are strongly associated with complicated UTIs and are a common cause of secondary bloodstream infections.[242,246,249] Also the prevalence of fungal *Candida* ssp UTIs is increasing.[250]

At a first stage, UTI diagnosis is based on specific symptoms and prescription of broad-spectrum antibiotics is often the immediate choice for treatment. Urinalysis may include microscopic inspection to detect red or white blood cells in urine samples. Urinary dipsticks testing for nitrites and leukocyte esterase can be used, mainly to exclude the presence of infection.[251] Urine culture remains the gold standard to confirm the presence of infection and for pathogen identification. This process usually takes 24 to 48 h.[252] Subsequently, a second culture step may be necessary to determine the antibiotic resistance profile. The introduction of MALDI-TOF mass spectrometry has enabled fast identification of uropathogens, from cultures and possibly also directly from urine samples.[253]

### 4.2 Antimicrobial resistance of uropathogens and relevant reviews

Uncomplicate UTI occurring in healthy subjects normally can be easily treated with short-term antibiotic administration, however recurring UTIs due to persisting uropathogens and biofilm formation is an important health issue. Complicated UTI or kidney infections are associated with high AMR rates that require long-course antibiotic treatments, resulting in severe alteration of the normal microbiota and proliferation of resistant pathogen strains.[242,249] UPEC bacteria have developed resistance against common antibiotics (*e.g.* ciprofloxacin, nitrofurantoin, ampicillin) with extremely high prevalence in some regions. Moreover, the emergence of UPEC strains possessing extendedspectrum βlactamases that confer resistance against thirdgeneration cephalosporins and monobactams, is observed in community-acquired UTIs.[246,254,255] New technologies enabling early UTI diagnosis and fast POC pathogen identification combined with AST are

Table 3 Selection of recent approaches for UTI pathogen detection and AST

| Pathogen | Device and assay principle | Performance indications | Ref. |
|---|---|---|---|
| ***Microfluidic devices for UTI diagnostics*** | | | |
| *E. coli* (β-lactam antibiotics resistant) | Nanoelectrokinetic PAD with chromo-genic detection of β-lactamases | Label-free detection of drug-resistant bacteria within 7 min by cell phone. LOD $10^4$ CFU $mL^{-1}$ | 264 |
| *E. coli* | Pump-free immunomagnetic separation with colorimetric detection | Laminar flow control by paper pads. LOD $4.7 \times 10^2$ CFU $mL^{-1}$ in urine | 265 |
| *E. coli* | Paper-based device for cultivating bacteria *in situ* and testing for nitrite | $10^4$–$10^7$ CFU $mL^{-1}$ quantified on a β-glucuronidase-specific substrate, within 6 h in urine | 266 |
| UTI bacterial pathogens | Enrichment on a herringbone chip and MALDI-TOF MS identification | Chaotic mixing enhanced bead/bacteria complex formation. Process takes 1.5 h | 267 |
| *C. tropicalis* | PNA-FISH protocol applied to pathogens in a microfluidic trap | Visual detection ($1 \times 10^5$ cells per mL, within 6 h). Tested with spiked synthetic urine | 271 |
| *E. coli* | Bacteria enrichment on Si nanowires and MALDI-TOF MS identification | Detection of ~$10^3$ CFU $mL^{-1}$ in urine (after pre-culture for 4–6 h) | 272 |
| *E. coli*, *P. putida*, *S. epidermidis* | Plasmonic-assisted impedimetric detection on nanostructured surfaces | Hybrid 3D gold/graphene nanostructures enhanced sensitivity (LOD 20 CFU $mL^{-1}$, 10 min) | 273 |
| ***Microfluidic chip-based devices for fast AST of uropathogens*** | | | |
| *E. coli* (ATCC 25922) and UTI-positive urine | Bacteria growth monitoring on a droplet microfluidic platform | Single-cell AST in 90 min (first antibiotic) + 2 min for subsequent antibiotic conditions | 280 |
| UTI bacteria (*16S rRNA* gene) | Fluorogenic PNA probe-based hybridization assay on a droplet chip | Identification and single-cell AST from urine samples within 30 min. Clinical comparison study | 282, 283 |
| *P. mirabilis*, *S. aureus*, *K. pneumoniae*, *E. coli* | Pheno-molecular AST using PCR and digital high-resolution melt | Multiple bacterial species and susceptibility profiles identified in spiked urine within of ~4 h | 284 |
| *S. aureus*, *E. faecalis*, *E. coli*, *K. pneumoniae* | Phenotypic analysis on parallelized droplet microfluidic platform | Simultaneous screening of 4 antibiotics per pathogens within 15–30 min | 285 |
| *E. coli*, other UTI pathogens | DMF for bacterial classification and AST using metabolic markers | Real-time bacterial metabolic monitoring. AST in <18 h, performed with resazurin dye | 287 |
| *E. coli* (ATCC 25922) and resistant strains | Combinatorial antibiotic screening with a nL-sized droplet SlipChip approach | MIC of *E. coli* against 4 antibiotics measured within 3 h on one chip | 288 |
| *E. coli* (ATCC 25922) | Multiplexed AST on a nL chamber array (resazurin indicator) | Antibiotic dilution on-chip. AST in 8–9 h. MIC determination required ~2000 bacteria | 289 |
| *S. epidermidis*, *M. bacteremicum*, uropathogenic *E. coli* | Single-cell pathogen classification and AST in adaptable channels | Bacteria classification based on size and shape in urine. Single-cell AST within 30 min | 292 |
| *E. coli*, *K. pneumoniae*, *S. saprophyticus* | All-electrical AST of bacteria trapped/incubated in channel constrictions | Robust and sensitive resistance measurement of bacterial growth and AST within 2 h | 293 |
| *E. coli*, *K. pneumoniae*, *P. aeruginosa*, *E. faecalis* | Pneumatically-driven microfluidic chip for colorimetric AST assays | AST completed in 4.5–9 h in automated manner | 297 |

 

required to improve therapeutic approaches. Due to the high prevalence of drug-resistant uropathogenic *E. coli* strains, but probably also because urine does not have a complicate sample matrix (as compared to blood for instance), a wide range of microfluidic fast AST methods, in particular enabled by single-cell analysis, has been developed with focus on UTI.

UTI diagnostic methods for laboratory and hospital facilities have been recently reviewed by Santos *et al.* or Harris *et al.*, for instance (including culture-based methods, microscopic urinalysis, flow cytometry, MALDI-TOF, PCR or FISH, *etc.*).[256,257] Santos *et al.* also showed examples of innovative (culture-based) single-use POC tests that are currently available in the market for UTI diagnosis, as well as a summary of POC tests on paper for *E. coli* from various samples.[256] Harris *et al.* more specifically focused on a discussion of currently available automated commercial UIT diagnostic systems.[257] A host of recent and earlier reviews provided overviews on emerging technologies for POC urine analysis and/or UTI diagnosis, including discussions on AST methods and some microfluidic approaches.[240,241,256–262] Paper devices with potential for UTI diagnosis have been recently reviewed by Hasandka *et al.* or Tai *et al.*, for instance.[241,262] Previously mentioned reviews discussing recent and emerging AST methods from a broader perspective are certainly also relevant for UTIs.[42,43,59,263] In the following, we will first discuss innovative microfluidic and/or biosensor devices that have been specifically designed for UTI diagnostics. Recent LOC systems for fast AST of uropathogens will be presented in the second part of this section. Table 3 approaches for UTI diagnosis and fast AST on uropathogens.

### 4.3 Microfluidics and biosensor for UTI diagnostics

**Assays enabled through specific fluidic design properties.** Kim *et al.* designed a nanoelectrokinetic analytic paper device for rapid detection of uropathogenic drug-resistant bacteria (Fig. 3a–c). The design was based on a constricted paper strip with a perm-selective nanoporous membrane placed perpendicular to the flow direction. The device took advantage of an electrical ion concentration polarization effect for analyte manipulation and more than 100-fold bacteria concentration. Moreover, an alkaline counter stream enabled cell lysis and release of drug-resistant markers. In this case, β-lactamase enzymes were detected on a chromogenic cephalosporin patch *via* cell phone readout. The LOD was $10^4$ CFU mL$^{-1}$ for *E. coli* inoculated in human urine within a total diagnosis time of 7 min.[264] Another approach for *E. coli* detection combined a μPAD with H-filter configuration and magnetophoresis for pump-

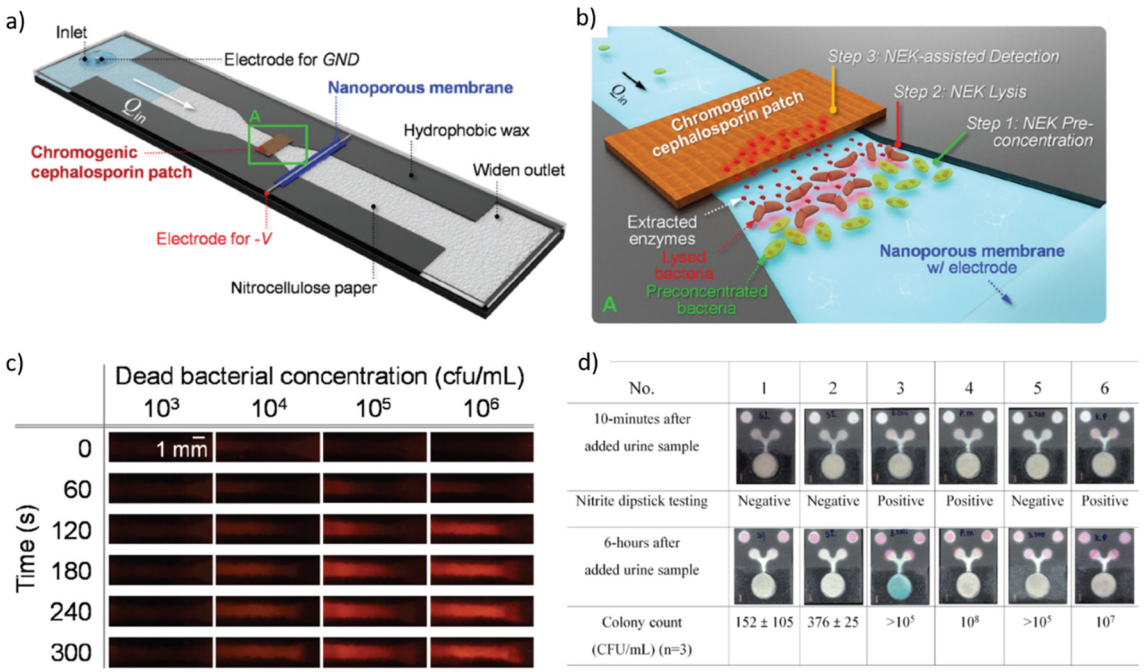


**Fig. 3** a) Schematic diagram of a nanoelectrokinetic (NEK) paper-based analytical device that is based on a constricted paper strip with a perm-selective nanoporous membrane placed perpendicular to the flow direction for inducing ion concentration polarization and inducing bacteria lysis, and with a chromogenic cephalosporin patch for detecting enzymes originating from the lysed bacteria. b) Zoom of rectangle A in a) with indication of the subsequent steps for bacterial detection. c) Color changes of a nitrocefin-coated patch over time for different bacterial concentrations. Color change from orange to red was detected *via* a cell phone-based read-out above bacterial concentrations of $10^4$ CFU mL$^{-1}$. d) *In situ* culture device for *E. coli* and testing for nitrite presence in urine. A colorimetric test for β-glucuronidase, a specific enzyme of *E. coli*, was implemented (blue color), while the pink color indicates presence of nitrite. The two circular zones on the top of the paper-based analytical device serve as a color control for the nitrite detection [a–c reprinted with permission from ref. 264, ©2022 Elsevier; d) reproduced from ref. 266, ©2019, Creative Commons license, CC BY 4.0 (**http://creativecommons.org/licenses/by/4.0/**).

less operation. A colorimetric ELISA assay was performed *via* immunomagnetic separation through the laminar flow pattern, reaching LODs of $2.4 \times 10^2$ CFU $mL^{-1}$ (PBS) and $4.7 \times 10^2$ CFU $mL^{-1}$ (urine), respectively, within 10 min after sample loading.[265] Noiphung *et al.* fabricated a paper device for *in situ* culture of *E. coli* and testing for nitrite, as a biomarker for UTI infection (Fig. 3d). A biochemical test for β-glucuronidase was implemented, enabling specific detection of *E. coli* in urine and colorimetric quantification of bacterial concentrations in the range of $10^4$–$10^7$ CFU $mL^{-1}$ within 6 h.[266]

Shen *et al.* used a microfluidic chip featuring a herringbone mixer structure for pathogen enrichment *via* increased capture efficiency and subsequent detection by MALDI-TOF mass spectrometry. Vancomycin-modified magnetic beads were magnetically retained in the microfluidic channel for capturing the UTI pathogens (*S. aureus*, *S. hominis*, *S. epidermidis* and *E. gallinarum*). The process enabled pathogen identification directly from spiked human samples without bacterial culture (LOD $10^4$–$10^5$ CFU $mL^{-1}$, assay time 1.5 h).[267] Chen *et al.* performed multiplex real-time RPA and pathogen detection (*E. coli*, *S. aureus*, *S. typhimurium*, *P. mirabilis*, and *P. aeruginosa* spiked into urine) on a centrifugal cartridge. Bacteria were concentrated/purified by means of a filter-pipette. Specific RPA primers and probes were preloaded in dedicated reaction chambers on the disc. The entire procedure, from bacterial enrichment to detection, was completed within 40 min (LOD in the range of $10^2$ to $10^3$ CFU $mL^{-1}$).[268] Olanrewaju *et al.* developed a modular system that incorporates an immunoaffinity column for rapid bacteria capture and fluorescence detection, as well as sequential retention burst valves and an on-chip capillary pump for autonomous liquid transport. The fluidic design allowed performing functional assay steps by pre-programmed and self-powered delivery of immunoassay reagents. Detection of *E. coli* was achieved in less than 7 min with a LOD of $1.2 \times 10^2$ CFU $mL^{-1}$ (synthetic urine).[269] Alves *et al.* implemented a quantitative *E. coli* fluorescence sandwich immunoassay in a microcapillary Teflon film strip array through which reagents were successively manually aspirated. By this means, large sample volumes could be passed through the capture antibody coated capillaries, resulting in a LOD of 240 CFU $mL^{-1}$ (synthetic urine) in less than 25 min.[270]

**Other microfluidic approaches.** Barbosa *et al.* proposed a microfluidic platform for detecting the opportunistic uropathogen *Candida* spp. by fluorescence *in situ* hybridization (FISH). The PDMS chip featured arrays of microposts for hydrodynamic separation of target cells, concentration at the backend of the channel and application of FISH reagents. Specific peptide nucleic acid (PNA)-probes targeting Candida 18S rRNA were used to perform the FISH protocol on the trapped pathogens. The method was tested with spiked synthetic urine samples (*C. tropicalis* at $10^5$ cells per mL).[271] Li *et al.* fabricated silicon nanowire surfaces functionalized with concanavalin A and integrated them into a microchannel. The high surface-to-volume ratio of the nanostructured surface enhanced the bacterial capture efficiency. *E. coli* spiked human urine samples was correctly detected by MALDI-TOF for concentrations above $10^6$ CFU $mL^{-1}$ (without culture step), and down to $10^3$ CFU $mL^{-1}$ if a short preculture step was added.[272] Moakhar *et al.* developed a microfluidic device for plasmonic-assisted impedimetric detection of bacteria. Hybrid structures of 3D gold nano/micro-islands and graphene nanosheets enhanced the optoelectrical properties of the sensor. The sample was delivered to the detection site through microfluidic channels. Direct and label-free detection of *E. coli*, *P. putida*, and *S. epidermidis* with LOD as low as 20 CFU $mL^{-1}$ within 10 min was demonstrated.[273]

**Examples of biosensors without microfluidic integration.** Other biosensors and assays that have been designed for POC diagnosis of UTI do not yet benefit from microfluidic integration. For instance, Basak *et al.* used Au nanotwins-coated substrates functionalized with aptamers for specific pathogen capture and optoplasmonic detection. The sensor had a detection range of $5 \times 10^3$ to $10^7$ CFU $mL^{-1}$ for *E. coli* in human urine.[274] Magnetic microgel containing magnetic nanoparticles provided a 3D colloidal support for RNA-cleaving DNAzyme probes with specificity toward *E. coli* protein targets. Electrochemical readout enabled rapid bacterial analysis in unprocessed clinical urine sample (LOD 138 CFU $mL^{-1}$, assay time 1 h).[275] Yang *et al.* used a SERS chip for the identification of three uropathogenic species (LOD of $10^5$ cells per mL).[276] SERS was also implemented on LFAs for *E. coli* detection from urine.[277] Li *et al.* designed a sensitive electrochemical biosensor based on the specific recognition of *E. coli* by T4 phages and signal amplification by means of organic–inorganic hybrid nanoflowers. Live *E. coli* could be quantified over a large linear range (15–$1.5 \times 10^8$ CFU $mL^{-1}$) with a LOD of only 1 CFU $mL^{-1}$. Quantitation was completed within 140 min.[278] A rapid bioluminescence extinction technology (tube or cellphone format) enabled detection of common UTI pathogens (*E. coli*, *Proteus mirabilis*, *S. aureus*, and *C. albicans*). The assays took advantage of signal extinction in standardized suspensions of luminous bacteria in the presence uropathogens. Clinically relevant metrics for positive UTI diagnosis ($\geq 10^5$ CFU $mL^{-1}$) were reached on a time scale of 20 min.[279]

### 4.4 Microfluidic devices for fast AST of uropathogens

**Microfluidic droplet AST platforms.** Zhang *et al.* implemented a cascaded assay for high-throughput flow-through single-cell AST on a microfluidic droplet PDMS platform (Fig. 4a). Fluidic nanoplugs, comprising bacteria, antibiotics and a cell viability indicator (resazurin), were formed in a dedicated on-chip unit and subsequently discretized in a droplet generator. Successive nanoplugs with customized antibiotic conditions generated distinct groups of ~10 000 pico-droplets containing single bacteria. In-line incubation was implemented and oil barrier plugs avoided

 

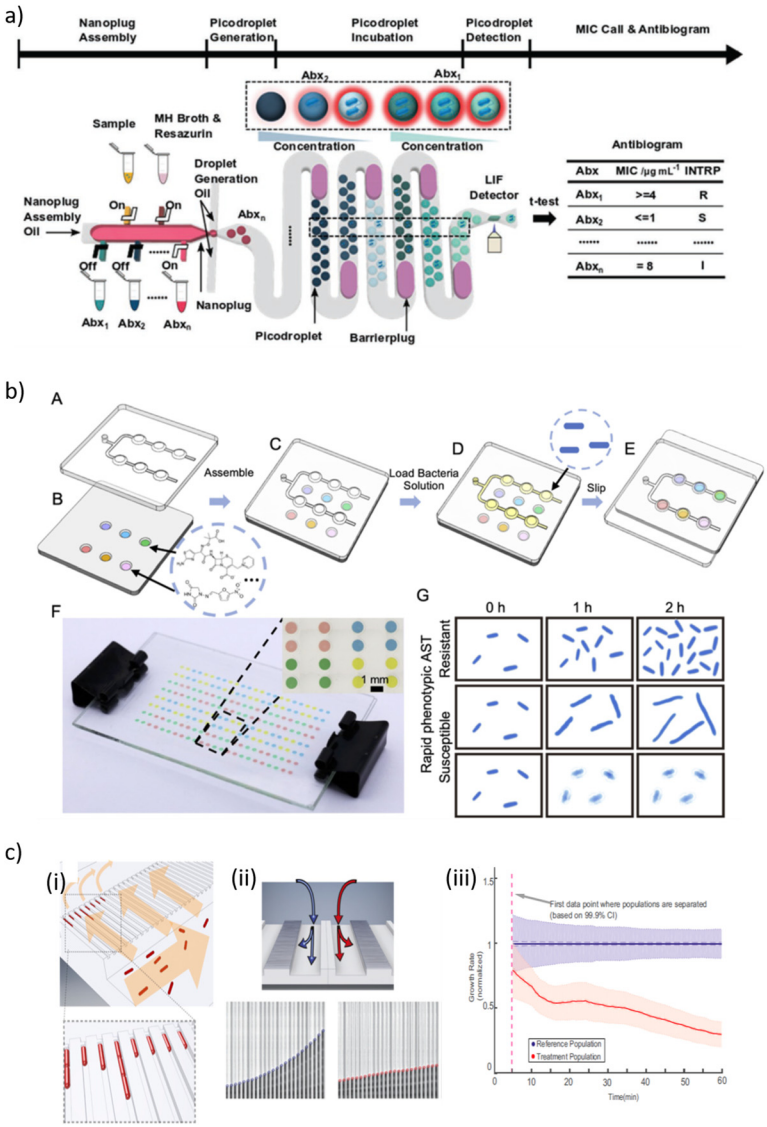


**Fig. 4** a) Overview of a so-called single-cell assembly line antibiotic susceptibility testing (SCALe-AST) device. It is an integrated droplet-based device with programmable microvalves to assemble bacteria sample, Mueller-Hinton II (MHMH) broth, resazurin, and antibiotics (denoted as Abx1, Abx2,…, Abxn) into nanoplugs and subsequently discretize the nanoplugs into groups of picodroplets encapsulating single bacteria. As each group of picodroplets flow through the built-in, 37 °C incubation channel, a barrier plug is introduced behind the picodroplets to keep them separated from adjacent groups of picodroplets, thus preventing cross-talk between different antibiotic conditions. The encapsulated single bacterium stops growing if it is susceptible to the applied antibiotic and the weakly fluorescent resazurin is reduced slowly, resulting in a weak fluorescence signal. In contrast, the bacterium proliferates if it is resistant to the applied antibiotic, and the weakly fluorescent resazurin is reduced to fluorescent resorufin quickly, resulting in a strong fluorescence signal within the picodroplet upon detection *via* a laser-induced-fluorescence (LIF) detector. By comparing picodroplet fluorescence intensity of different antibiotic concentrations, an antibiogram that provides the bacteria susceptibility categorization for multiple antibiotics with measured minimum inhibitor concentrations is constructed. b) Schematic presentations of the combinatorial screening (cs) SlipChip operation principle. (A) The top plate consists of a chain-of-pearls fluidic channel. (B) The bottom plate contains circular expansion microwells preloaded with different antibiotics. (C) The top and bottom plates are assembled in the initial loading position. (D) The bacterial solution (yellow) is introduced into the chain-of-pearls channel by pipetting. (E) The top plate is moved relative to the bottom plate to bring the chain-of-pearls channel into contact with the expansion channel by a manual slipping operation, and the aqueous solution containing the bacteria self-partitions into individual droplets that can be mixed with the preloaded antibiotics. (F) A bright-field photo of a cs-SlipChip loaded with an aqueous solution spiked with blue, red, yellow and green food dyes. (G) Schematic drawing of an antibiotic susceptibility/resistance profile obtained from the cs-SlipChip, as indicated by bacterial growth. c) Design and operation details of a microfluidic chip illustrating (i) the loading of rod-shaped bacterial cells (red) into cell traps. Arrows indicate flow direction during loading. (ii) Detection of growth rate effect of antibiotic. (ii, Top) Media with or without antibiotic are supplied to the two different rows of cell traps to test the effect of the antibiotic on the treatment population compared with the reference population. (ii, Bottom) The status of a single-cell trap from the reference population (left) and another single-cell trap from the treatment population (right) are shown every 2.5 min. The detected front-most cell pole position is given as a blue or red circle. (iii) The overlay of the two population's normalized growth rate distributions. The time of separation of the treatment population from the reference population occurs before the dashed magenta line, which indicates the first time point when different growth rates can be estimated [a) reprinted with permission from ref. 280, ©2021 John Wiley and Sons; b) reproduced from ref. 288 with permission from the Royal Society of Chemistry; c) reprinted with permission from ref. 291, Proceedings of the National Academy of Sciences].

cross-talk between adjacent pL-droplet groups. On-chip single-cell AST for four antibiotics was first characterized with a *E. coli* reference strain, and subsequently with clinical isolates. Clinically useful antibiograms with MIC values could be produced on a time scale of 90 min (mainly due to on-chip incubation) for the first antibiotic condition, plus 2 min for each subsequent condition. Furthermore, breakpoint testing with (filtered) uncomplicated UTI-positive clinical urine samples was performed.[280] Mach *et al.* proposed a droplet microfluidic format for amplification-free detection and identification of single bacterial cells with fluorogenic PNA probes that target bacterial 16S rRNA.[281] Subsequently, Kaushik *et al.* further implemented this approach for UTI diagnosis with single-cell resolution on a droplet platform. The platform was designed for both pathogen identification/classification (in particular *E. coli*) and AST from urine samples within the clinically relevant concentration range. Bacterial cells were encapsulated together with an antibiotic and multiple hybridization probes that target uropathogen-specific 16S rRNA sequences. A fluorescence two-color detection scheme allowed pathogen identification, whereas susceptibility to the antibiotic was revealed by signal intensities, corresponding to the relative amount of 16S rRNA per droplet produced by single cells exposed/not exposed to antibiotics. This pheno-molecular AST method was evaluated with 3 common antibiotics (gentamicin, ciprofloxacin, and ampicillin). The pL-droplet reaction volume enabled very short on-chip incubation times (10 min) and fast subsequent hybridization with the florescent probes (15 min), resulting in an overall assay time to result as short as 30 min. 50 human urine specimens were tested against ciprofloxacin to evaluate the clinical utility of the assay.[282,283] This group also proposed another pheno-molecular AST platform implementing PCR and digital high-resolution melt (HRM) analysis to quantify bacterial DNA molecules. The core of the platform was a digital PCR nanowell array. Multiple bacterial uropathogens and corresponding susceptibility profiles were correctly identified within ~4 h.[284]

Kang *et al.* developed an integrated quadruplex droplet device to screen several combinations of bacteria and/or antibiotics simultaneously. The device comprises four droplet generators and on-chip docking arrays (filled with >8000 droplets, droplet volume ~110 pL) for incubation and observation. The performance of the system was tested with clinically relevant uropathogenic Gram-positive (*S. aureus*, *E. faecalis*) and Gram-negative (*E. coli*, *K. pneumoniae*) bacterial strains. Phenotypic AST was assessed for six concentrations of bactericidal and bacteriostatic antibiotics (oxacillin and tetracycline) at single cell resolution. Optical observation of bacteria proliferation in the droplets enabled MIC quantification for each bacteria/drug combination. Antibiotic susceptibility could be evaluated as fast as 15–30 min.[285] Likewise, Sabhachandani *et al.* co-incapsulated bacteria and antibiotics on a droplet chip for phenotypic AST assessment (*E. coli* spiked human urine). Due to single-cell tracking, discriminatory readouts could be achieved within one 1 h of incubation in the on-chip droplet-docking array.[286] Sklavounos *et al.* performed bacterial classification, breakpoint testing and phenotypic AST on a digital microfluidics platform (DMF). For on-chip AST, dilution series of antibiotics at different concentrations were generated by on-demand manipulation of μL-size droplets and mixed with bacteria-containing droplets (final concentration $5 \times 10^5$ CFU $mL^{-1}$). For bacterial classification, droplets were mixed with different metabolic indicator droplets. The final droplet array was incubated for at least 16 h, resulting in a total of time-to-result of 18 h. AST was validated with two uropathogenic *E. coli* strains. Bacterial classification was performed independently or simultaneously with ciprofloxacin AST for *E. coli*, *K. pneumoniae*, *P. mirabilis* and *S. aureus*. As a proof-of-concept, multiplexed breakpoint testing was carried out with a multidrug resistant *E. coli* strain.[287]

**AST based on sample compartmentalization in on-chip microchambers.** Li *et al.* implemented a microfluidic SlipChip design for combinatorial-screening and high-throughput phenotypic AST (Fig. 4b). The chip consists of two glass plates that are in close contact, *i.e.* (i) a bottom plate with microwells (192 in this case) containing preloaded antibiotics, and (ii) a top plate featuring a chain-of-pearls fluidic channel where the bacterial suspension was confined by self-partition in individual 50 nL droplets (containing 25–50 CFU). Relative displacement of the two plates brings bacteria and antibiotics in contact, enabling diffusive mixing and incubation. Multiplex AST was performed by observation of the bacteria abundance and morphology changes. MIC values for an *E. coli* reference strain were obtained in 3 h against a panel of antibiotics commonly used for UTI. Furthermore, susceptibility/resistance profiles of *E. coli* clinical isolates from patients with UTI were tested against 4 antibiotics and 11 antibiotic combinations simultaneously.[288] Osaid *et al.* designed a multiplexed microfluidic platform with a parallel arrangement of seven microchamber-array lines that hold nL-aliquots of bacterial suspension (40 microchambers per line). Each line was independently flushed with different antibiotic concentrations allowing diffusive mixing with bacteria populations the lateral microchambers. Subsequently the chambers were isolated by air for on-chip incubation and AST. The automated platform comprises a second microfluidic chip for antibiotic dilution and transfer to the AST chip. A short pre-culture step (target ~2000 bacteria) was required to reduce the MIC determination time to 8–9 h.[289] Avesar *et al.* also took advantage of bacteria suspension compartmentalization for rapid AST. Freeze-dried antibiotics were incorporated within the bacterial culture chambers of the PDMS chip, which was loaded with a two-plug formulation (bacterial suspension/oil) for confining bacteria in the nL-wells. An off-chip filter-based bacteria isolation protocol was used for clinical urine samples to perform same-day AST.[290]

 

**Bacterial analysis and AST in constrained microchannels.** Baltekin *et al.* used direct single-cell imaging on a microfluidic channel array (2 × 2000 traps) for AST of *E. coli* (Fig. 4c). Due to the small channel dimensions, the growth dynamics of trapped bacteria could be monitored directly by the increasing number of well-aligned single rod-shaped cells. Comparing the growth rate distribution for reference populations and for antibiotic-treated populations allowed AST in less than 10 min in urine samples (*i.e.* in less than 30 min including array loading). The antibiotic response of *E. coli* to nine different antibiotics used for UTI treatment was tested. Furthermore, 50 uropathogenic clinical *E. coli* isolates could be rapidly classified as ciprofloxacin susceptible or resistance strains.[291] Li *et al.* proposed an adaptable fluidic channel array for pathogen classification and AST. Pneumatic controls for tuning the effective channel cross section enabled size-based pathogen classification. Furthermore, AST could be performed within 30 min by measuring individual cell growth (length) in the presence of antibiotics. A study with clinical urine samples enabled rapid indication of infection, as well as on-chip AST of five groups of most common UTI pathogens (*Staphylococcus*-like, *Enterococcus*-like, *Pseudomonas*-like, *Klebsiella*-like, and *E. coli*-like groups).[292] Yang *et al.* presented a microfluidic device for electrical AST monitoring. The central microfluidic part of the chip is a parallel arrangement 10 microchannels (2 μm high and 2 μm wide). Owing to the small channel size, growth and morphological changes of trapped bacteria could be detected by electrical resistance measurements. The approach allowed for AST in about 2 h (*E. coli*, *K. pneumoniae*, and *S. saprophyticus* against ampicillin and nalidixic acid).[293] Kara *et al.* measured electrical impedance fluctuations for analysing nanomechanical movements of planktonic bacteria in a single-channel constriction and applied this method to AST of two different *E. coli* strains in human urine.[294]

**Other recent AST approaches.** Shumeiko *et al.* performed rapid UTI diagnosis and AST on fluidic cartridges installed on a centrifugal system. The cartridges could be directly fixed on urine sample tubes for bacteria collection. The main functions included (i) bacteria detection within 5 min at concentration down to $5 \times 10^3$ cells per mL (*E. coli* cells spiked into urine), and (ii) AST in less than 2 h on a valve-less multi-channel chip with dried antibiotic (*E. coli* and *K. pneumoniae* clinical isolates).[295] Needs *et al.* emphasized the potential of miniaturised broth microdilution for simplified AST and developed a fluoropolymer microcapillary film approach. *E. coli* and *K. pneumoniae* uropathogenic isolates were seeded in a well plate for colorimetric growth detection by means of a 10-plex test strip that was dipped into the reservoirs. In particular, the possible impact of reducing the test volume (1 μL samples, *i.e.* by 100-fold from microplates) was investigated to understand if miniaturisation affects AST performance.[296] Hsu *et al.* used a pneumatically-driven microfluidic chip, comprising micromixers, micropumps and 24 reaction chambers, for automated colorimetric AST. Four UTI pathogens were tested (*E. coli*, *K. pneumoniae*, *P. aeruginosa*, and *E. faecalis*) and AST was completed in 4.5–9 h (depending on the initial bacteria concentration, spiked urine).[297] Gao *et al.* developed assays for multiplex pathogen identification and AST based on carbon nanotube enhanced microwave electroporation of viable bacteria. Off-chip electroporation was used for intracellular delivery of molecular probes and fluorescence detection after hybridization to species-specific regions of bacterial 16S rRNA. The assays allowed identification of clinical isolates at single cell level from urine (*E. coli*, *P. aeruginosa*, and *K. pneumoniae*) and blood (*E. coli*). Rapid phenotypic AST by monitoring the bacterial growth at the single-cell level was achieved by physical trapping of identified bacteria on a microfluidic channel array. Comprehensive microbiological analysis could be performed in 3 h.[298]

# 5 Gastrointestinal tract infections

## 5.1 Scope and common pathogens

In most cases, gastrointestinal tract infection (GTI), in particular of the small intestine (enteritis), is acquired through fecal-contaminated food or drinking-water, by transmission from person-to-person or by contact with contaminated surfaces. Foodborne diseases represent a significant burden to public health.[299] Ingested pathogens that escape the host defence in the upper gastrointestinal tract potentially may invade and multiply in the intestine, thus generating infection and disease, possibly progressing to infection of other body systems *via* the lymphatic system or the bloodstream (septic infection). Diarrhoeal disease is the most common outcome of GTI, with nearly 1.7 billion cases of childhood diarrhoeal disease every year. In the developing world diarrhoeal disease represents a major health problem, causing high morbidity and mortality rate, in particular through dehydration (WHO 2017).[300] Many cases could be prevented by safe drinking-water and adequate sanitation. GTI may be caused by a host of bacteria, viruses or parasites. Pathogenic *E. coli* strains, such as *Enterohemorrhagic E. coli* (EHEC, O157:H7),[301] *Salmonella*,[302] *Campylobacter*,[303] *Listeria monocytogenes*,[304] *Clostridium perfringens*,[305] or *S. aureus*[306] are examples for important food- or waterborne bacterial pathogens.[307] Ingestion of water or fish contaminated by pathogenic strains of *Vibrio cholerae* causes the potentially deadly acute diarrhoeal disease cholera. Cholera pandemic or endemic outbreaks regularly occur.[308,309] Other examples for diseases caused by pathogenic enteric bacteria are shigellosis, a predominantly paediatric diarrhoeal disease with an exclusively human reservoir,[310] or typhoid fever which is a life-threatening systemic infection caused by *Salmonella Typhimurium*.[311] Viral gastroenteritis is also extremely widespread, with rotaviruses (children),[312] noroviruses (adults)[313] and hepatitis A virus[314] being most prevalent pathogens transmitted by the fecal-oral route.[315] *Helicobacter pylori*, another common pathogen, causes infections of the stomach, which are often without symptoms but may generate gastritis or ulcers.[316]

### 5.2 Diagnostic methods and relevant reviews

Conventional diagnosis protocols for viral or bacterial GTI infections include pathogen isolation from feces and culture, antigen or toxin detection (*e.g.* with rapid antigen immunochromatographic assays), MALDI-TOF and nucleic-acid tests.[307,313] Emerging diagnostic tools and microfluidic assays that have been developed for other infectious pathogens and clinical samples may possibly also be adapted for GTI diagnosis.[96,120] Xpert® Norovirus assay (Cepheid, USA) is an example for a commercial RT-PCR assays targeting an important GTI pathogen. The Bosch Vivalytic HSP test differs between the pathogens *C. difficile*, norovirus and rotavirus and delivers fast and precise results.[115] Microfluidic and biosensor approaches dealing with GTI causative pathogens have been extensively reviewed in literature, in great majority with focus on pathogen detection from contaminated food- or waterborne samples. Very recently, Yin *et al.* discussed the current state-of-art and future perspectives of detection methods for foodborne viruses.[317] Other recent review articles that include microfluidic devices have been worked out, for instance by Gao *et al.*, who discussed advances in microfluidic devices for foodborne pathogen detection,[318] by Shang *et al.* with focus on advances in nanomaterial-based microfluidic platforms,[319] by Ranjbaran *et al.* on microfluidics at the interface of bacteria and fresh produce,[320] or by Quintela *et al.* on advances and limitations of portable and rapid detection technologies for foodborne pathogens.[321] Mi *et al.* summarized microfluidic biosensor tools for foodborne pathogenic bacteria and Su *et al.* investigated microfluidic nucleic acid tests of foodborne viruses.[322,323] Other reviews focused on specific pathogens, such as POC methods for detection of norovirus by Zaczek-Moczydlowska *et al.* or POC diagnosis for *E. coli* O157:H7 in food and water by Rani *et al.*[324,325] Shen *et al.* explored biosensor technologies for rapid detection of *Salmonella* in food.[326] Wang *et al.* discussed microfluidic sampling and biosensing systems for foodborne *E. coli* and *Salmonella*.[327] In the context of GTI diagnosis, only a few microfluidic devices have been designed for or tested directly with human samples, in particular fecal samples. Possible GTI diagnostic tools could also be derived from other applications, such as evolving technologies in clinical research in the gut microbiome era.[328] On the other hand,

Table 4 Selection of microfluidic devices for GTI-related pathogen detection

| Pathogen | Device and assay principle | Performance indications | Ref. |
|---|---|---|---|
| ***Systems for bacterial enteric pathogens*** | | | |
| Gut microbiome, *B. vulgatus* | Droplet microfluidics applied to complex microbiome samples | Cultivation-free single-cell genetic assays and enrichment by sorting of positive droplets | 334 |
| *Campylobacter* spp. | On-chip chambers with chromogenic medium for identification and AST | *Campylobacter spp*. detected in milk and poultry meat. AST within 24 h | 335 |
| Enterohemorrhagic *E. coli* | Cartridges for PCR amplification and microarray hybridization | Fluidic operations with combined centrifugal/pneumatic actuation. Workflow of 2 h | 336 |
| Enterotoxins and enteric bacteria | Integrated LAMP and immunoassays on a LoaD platform | Different disc designs for single or dual assays. LOD 1.35–5.50 ng $mL^{-1}$ (toxins), 1–30 cells (LAMP) | 337 |
| Foodborne pathogens | Microchip with paper pads for LAMP in multiple reaction chambers | LOD 0.013 ng $\mu L^{-1}$ for purified *E. coli* DNA, LOD 12 CFU $mL^{-1}$ for *Salmonella* spp. in milk | 338 |
| *S. typhimurium* | Colorimetric biosensor using bacteria-immune Au@Pt NP conjugates | Finger-driven mixing, LOD 168 CFU $mL^{-1}$, within 25 min | 339 |
| *E. coli* O157:H7 | Integrated biosensor chip based on the RPA-CRISPR/Cas12a reaction | Finger-pressure actuation, LOD 10 CFU $mL^{-1}$, within 2.5 h | 340 |
| Foodborne pathogens | Portable system and microfluidic cartridge with LAMP reaction wells | LOD $8 \times 10^3$ CFU mL (*Shigella*). Validated with artificially contaminated food samples | 341 |
| ***Systems for viral and parasitic enteric pathogens*** | | | |
| Human norovirus | On-chip chamber digital RT-RAA for quantitative virus detection | Sample partition (10 min), amplification (20 min). LOD 1 cRNA copy per μL | 342 |
| Norovirus (capsids and intact viruses) | LFAs immunoassay based on dispersed particle aggregates | Virus detection at single copy level from water samples | 344 |
| Rotavirus A | Paper disc for nucleic acid extraction, LAMP and readout with the naked eye | LOD $1 \times 10^3$ virus copies per mL, within 30 min. Tested with clinical stool samples | 346 |
| Porcine enteric viruses | Multiplex colorimetric LAMP for visual detection of diarrhea-related viruses | Handheld operation of a fan-shaped chip. Testing <60 min, LOD of 100 DNA copies per μL | 347 |
| Porcine enteric viruses | RT-LAMP 3D-printed microfluidic device | LOD $10^1$–$10^2$ RNA copies per reaction, appropriate for early-stage infection detection | 348 |
| Porcine enteric viruses | Multiplex RT-LAMP on LoaD | Detection of 3 viruses, LOD $10^1$–$10^2$ RNA copies per μL, 1.5 h. Clinical fecal samples tested | 349 |
| Murine norovirus | Modular nucleic acid-based detection platform with colorimetric detection | LOD 10 PFU $mg^{-1}$ within 30 min in fecal sample | 350 |
| *Giardia* | Giardia cysts purification using spiral inertial microfluidics | Recovery rates up to 75% from mouse feces with 0.75 mL $min^{-1}$ throughput | 351 |

enteric diseases are also a common problem in modern swine farming and POC devices developed for veterinary use could be suitable for adaptation to human samples and diagnostic approaches.[329] In the following, considering the lack of literature on microfluidic devices specifically applied to POC clinical diagnosis of human GTI, we will extend our discussion to a selection of recent approaches covering pathogen detection from foodborne or non-human samples. Table 4 provides an overview of recent approaches for GTI pathogen detection.

### 5.3 Microfluidic sample processing techniques

In the context of GTI diagnosis and gut microbiome studies, fecal sample processing and extraction of commensal or pathogenic bacteria colonizing the gastrointestinal tract is an important issue.[330] Sample processing steps are critical aspects in the design of realistic diagnostic POC strategies. A challenge of GTI diagnostic workflows are specific problems related to the complex matrix of stool samples involving high variability of consistency, the presence of PCR inhibitors, and possibly low target of analyte concentrations. Three examples of microfluidic approaches emphasizing fecal samples processing are cited here. One on-chip method for liquefaction and homogenization of human stool samples was based on piezoelectric actuation for generating strong acoustic microvortex streaming and sample mixing in a PDMS microchannel. Sharp structures in the main channel enhanced the microstreaming effect, whereas an array of narrow parallel microchannels filtered large debris. The device could be operated in continuous manner with a throughput of 30 μL $min^{-1}$.[331] Kang *et al.* proposed a microfluidic cartridge for automated nucleic acids purification from fecal samples for POC diagnosis of gastroenteritis or gut microbiome analysis. The cartridge included a pre-treatment chamber for stool sample homogenization by electromagnetic actuation and subsequent filtering. An air pressure system controlled microvalve operation. The performance of the system was evaluated using fecal samples spiked with *C. difficile* or *Enterovirus*, as well as through metagenomics analysis of clinical fecal samples of diseased patients.[332] Mosely *et al.* designed a sample introduction interface for on-chip nucleic acid analysis and applied the method to the detection of *Helicobacter pylori* from liquified stool samples. The multi-chamber DNA purification chip comprised a large chamber receiving liquid stool samples and a final small elution chamber. Extracted DNA was magnetically transported through interconnecting trapezoidal microfluidic conduits filled with an immiscible phase for filtration. DNA purification and 40-fold pre-concentration was achieved within 7 min from crude clinical stool samples.[333]

### 5.4 Microfluidic devices for gastroenteric pathogen detection

**Systems for bacterial enteric pathogens.** Pryszlak *et al.* presented a high-throughput microfluidic droplet assay for single-cell genetic assays of gut microbiome stool samples (Fig. 5a). The microfluidic workflow, based on off-chip PCR and subsequent droplet sorting, enabled culture-free microbial enrichment and high-quality genomic analysis from rare target cells (<1%) in complex microbiome samples. The method was applied to the endogenous gut species *Bacteroides vulgatus* spiked into human stool samples, demonstrating recovery of bacteria at a ratio as low as 1 : 250.[334] Ma *et al.* designed a microfluidic device for the identification of *Campylobacter* spp. and assessment of antimicrobial susceptibility profiles. The bacterial sample was distributed into 8 separated PDMS incubation chambers containing chromogenic agar for colorimetric growth detection. *Campylobacter* isolates from various agri-food food models were used in this study. *C. jejuni* was detected in raw milk (LOD $1 \times 10^2$ CFU $mL^{-1}$, within 48 h), and *Campylobacter* spp. in chicken meat (LOD $1 \times 10^4$ CFU, after 60 h). For on-chip multiplexed AST and multidrug resistance testing, antibiotics were preloaded onto paper disks placed in each incubation chamber, followed by adding chromogenic agar and inoculation of bacterial suspension. *C. jejuni* susceptibility profiles were accurately determined for three types of antibiotics within 24 h.[335]

Geissler *et al.* designed a microfluidic cartridge installed in a centrifugal device, enabling thermal activation, internal pneumatic liquid pumping and valve control during rotation. Thanks to this dual actuation protocol, all fluidic operations for thermal lysis, PCR amplification and DNA microarray hybridization were performed in a fully-automated fashion. The system was validated for multiplexed detection of several enterohemorrhagic *E. coli* serotypes. The workflow took less than 2 h.[336] Phaneuf *et al.* combined ultrasensitive immunoassays and isothermal amplification-based POC detection for both protein and nucleic acid targets on a portable centrifugal microfluidic platform. The panel of toxins and bacteria included three enterotoxins (cholera toxin, *Staphylococcal* enterotoxin B, and Shiga-like toxin 1) and three enteric bacteria (*C. jejuni*, *E. coli*, and *S. typhimurium*). All were detected with high sensitivity (LOD 1.35–5.50 ng $mL^{-1}$ for immunoassays and 1–30 cells for isothermal amplification, <one hour). The system was capable of handling a complex sample matrix like stool.[337] Zhang *et al.* performed LAMP of four foodborne pathogens (*E. coli* O157:H7, *Salmonella* spp., *S. aureus*, and *V. parahaemolyticus*) on a paper-embedded microchip. The device used centrifugal force for distributing the sample in radially arranged reaction chambers. Paper pads soaked by LAMP reagents were inserted in each chamber. The device was tested with milk samples spiked with *Salmonella* ssp. and on-chip DNA extraction on polydopamine-coated paper (LOD ~12 CFU $mL^{-1}$).[338]

Jin *et al.* developed a microfluidic biosensor for on-site detection of *S. typhimurium* from real pork samples (Fig. 5b).

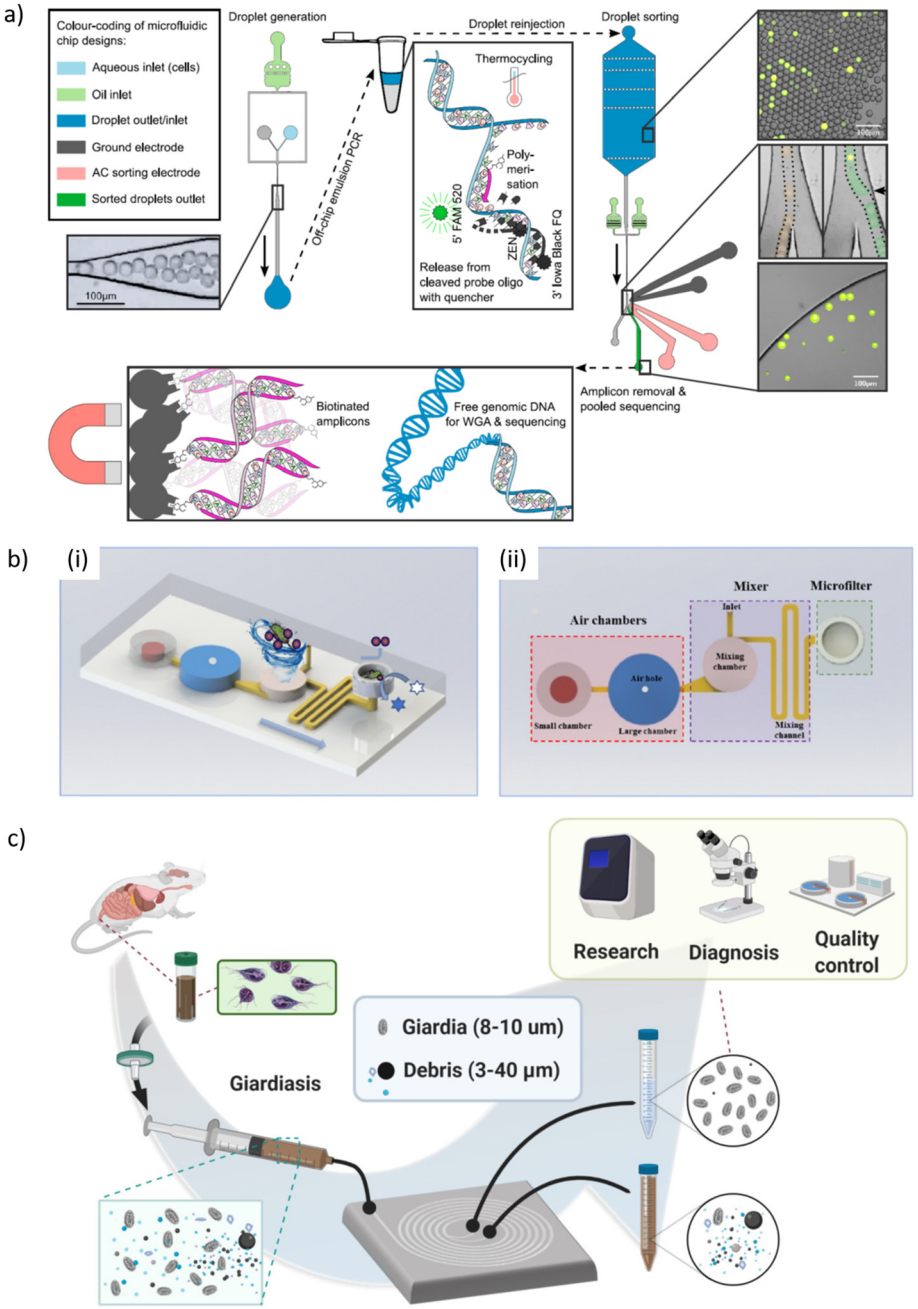


**Fig. 5** a) Microfluidic workflow, microfluidic chip designs, microscope images of their use, and schematics of molecular mechanisms of a droplet microfluidic platform for targeting individual cells from complex microbiome samples. (Top left) Droplet generation chip and photo of 39 µm-droplet generation with cells and reagents in oil. The arrow indicates the flow direction. Top center: Illustration of emulsion PCR in a thermocycler. If the target DNA sequence is present, it allows the binding of biotinylated primers and probes, thus the synthesis of corresponding amplicons. During strand extension, the TaqMan probes are cleaved, releasing fluorescent molecules. (Top right) Droplet sorting chip design and microscopy images. The microscopy pictures on the right show an emulsion before sorting and during sorting and the positive droplet enrichment post sorting. Here, fluorescent droplets indicate the presence of the gut bacterium *B. vulgatus* inside the droplet. Multiple microscopy images of the droplet sorting junction at different time points were overlaid and colored to demonstrate droplet flow-traces. In the right image, a small black arrow indicates the location of the nearby sorting electrode, and a bright green spot indicates the upstream location of fluorescence detection. The scale bars are 100 µm. (Bottom) Illustration of the removal of abundant amplicons with biotin-binding streptavidin beads (after pooling the sorted positive droplets) to purify genomic DNA for sequencing library preparation. Library preparation further involves whole-genome amplification (WGA) after binding adapter primers to the randomly broken genomic DNA fragments, followed by DNA fragment size selection. b) Schematic of the operation of a microfluidic biosensor chip for *Salmonella* detection. (i) The principle of this biosensor is based on the use of gold@platinum nanoparticles for specific bacterial labeling, a finger-driven mixer with two serial air chambers for efficient immunoreaction and a nuclear track membrane to be used as microfilter for bacterial isolation from the complex sample. (ii) Layout of the microfluidic chip. c) Schematic workflow, setup, and application of using an inertial microfluidic device to separate *Giardia* from a turbid fecal sample containing various sizes of contaminants [a) reprinted with permission from ref. 334, ©2021 Elsevier; b) reprinted with permission from ref. 339, ©2022 Elsevier; c) reprinted with permission from ref. 351, ©2022 AIP Publishing].

 

The device used finger-pressure air chambers for fluidic handing and a chamber for active on-chip mixing for forming *Salmonella*-immune Au@Pt nanoparticle conjugates. Sample concentration and colorimetric smartphone detection in $H_2O_2$-TMB substrate was carried out in a dedicated chamber. The device enabled *Salmonella* detection down to 168 CFU $mL^{-1}$ in 25 min.[339] Also Shang *et al.* developed a microfluidic cartridge with finger-pressure pneumatic actuation for fluidic manipulation. This device detected *E. coli* O157:H7 from $10^2$ to $10^8$ CFU $mL^{-1}$ in 2.5 h with a LOD of 10 CFU $mL^{-1}$. The workflow on the fully integrated device included immunomagnetic microbial separation, nucleic acid extraction and signal detection based on the RPA-CRISPR/Cas12a reaction. Spiked and real food samples were tested for system validation.[340] A 10-well microfluidic chip was used by Cao *et al.* for the detection of multiple foodborne pathogens (*Salmonella*, *S. aureus*, *E. coli* O157:H7, and *Shigell*). Each reaction well was pre-loaded with lyophilized LAMP primers prior to multiplex on-chip LAMP with a LOD reaching reached $8 \times 10^3$ CFU $mL^{-1}$ and an assay time of 45 min.[341]

**Systems for viral and parasitic enteric pathogens.** Qin *et al.* implemented a digital nucleic acid amplification assay for norovirus detection in microfluidic chip format. The chip consisted of an array of 5120 nL-volume chambers that hold the partitioned samples and reaction components. Amplification occurred only in microchambers containing intact RNA templates thus detection was possible by simple end-point counting. On-chip recombinase-aided amplification (RT-RAA) was carried out at 39 °C for 20 min with a LOD of 1.02 copies per μL for coding RNA (cRNA) templates in buffer. The clinical performance was tested with stool samples after off-chip nucleic acid extraction.[342] In another approach for norovirus detection an electrochemical aptasensor was integrated in microfluidic chip comprising microfilters and a sensing zone with screen-printed carbon electrodes functionalized with ferrocene tagged aptamers. A LOD of 100 pM with a detection range from 100 pM to 3.5 nM for recombinant norovirus-like particles in buffer was achieved.[343]

Chung *et al.* proposed a paper-based norovirus POC assay combined with a smartphone fluorescence microscope. Norovirus solution and anti-norovirus fluorescent polystyrene particle suspension were successively added directly to the mainchannel of the μPAD from where they spread by capillary action and aggregated. The extent of particle immune-aggregation correlated to the norovirus concentration, enabling sensitive detection down to the single virus copy level, thus omitting the need of sample concentration or nucleic acid amplification steps. This protocol was also evaluated with field water samples. The LODs were 1 genome copy per μL in DI water and 10 copies per μL in reclaimed wastewater, respectively (assays time <20 min).[344,345] Ye *et al.* used simple equipment-free glass fiber paper discs for rotavirus A DNA extraction, LAMP amplification and visual readout for POC diagnosis with the naked eye. The circular sample area of the paper disc was cut out and placed in a micro-well chip for the LAMP reaction and colorimetric detection. The time from sample to answer was <30 min with a LOD of $1 \times 10^3$ viral copies per mL. The device performance was evaluated with stool samples from pediatric diarrhea patients.[346]

A handheld PMMA microfluidic chip was designed for simultaneous colorimetric detection of four swine enteric viruses. DNA was extracted from the blood of the virus-infected swine and pipetted into the on-chip LAMP reaction chambers. To perform the LAMP reaction, the microfluidic chip was sealed and heated to 65 °C in a water bath for 60 min. The LOD of this simple POC device was 100 genomic viral DNA copies. The performance of the chip assay was comparable to commercial real-time PCR test kits.[347] Another portable, 3D printed microfluidic device enabled multiplexed detection of porcine enteric viruses by real time RT-LAMP within 30 min and an analytical sensitivity of 10–100 genomic copies per reaction.[348] Likewise, a microfluidic LAMP lab-on-a-disc enabled multiplex detection of a panel of viral porcine enteric pathogens from clinical fecal swine samples with analytical sensitivities in the range of $1 \times 10^1$ copies per μL to $1 \times 10^2$ RNA copies per μL within a total processing time of 1.5 h.[349] Murine norovirus from fecal samples was detected using a foldable POC microfluidic chip module. Process steps included virus concentration by means of graphene oxide coated glass microbeads, lysis and RNA hybridization with colorimetric detection after an additional on-chip signal separation step. The detection sensitivity was 10 PFU $mg^{-1}$ feces with an assay time of 30 min.[350]

*Giardia* is a small about 10 μm long parasite that causes diarrheal disease. Ding *et al.* designed a spiral microfluidic device to separate *Giardia* or other gastrointestinal pathogens from turbid samples, such as mouse fecal samples, by means of inertial microfluidics (Fig. 5c). The device provided a simple sample preparation method for bright-field microscopy diagnosis, achieving 75% *Giardia* recovery rate and 95% debris removal rate at a flow rate of 0.75 mL $min^{-1}$.[351] Another lab-on-a-disk device for parasite detection in stool sample was used for concentrating parasite eggs and removal of sample debris.[352]

# 6 Bloodstream infection and sepsis

## 6.1 Scope and common pathogens

Microbemia, or more specifically bacteremia, occurs when bacteria enter the bloodstream *via* the lymphatic system from sites of local infection in the body or *via* disrupted skin and mucous membrane. Bacteremia may be asymptomatic if viable bacteria can be rapidly removed by activation of immune response. However, if bacterial invasion persists and proliferates, *e.g.* due to high pathogenicity of the microbes or a weakened immune system, the bloodstream infection (BSI) leads to bacteria accumulation in other locations of the body, including artificial devices (such as implants or catheters), causing remote infections and possibly a serious systemic

inflammatory response called sepsis. Sepsis is a major global health threat with a high incidence and mortality.[353] A WHO report (released in 2020) indicates an estimated 49 million cases and 11 million sepsis-related deaths in 2017, accounting for approximately 20% of all-cause deaths globally.[354] Sepsis can be defined as life-threatening organ dysfunction caused by a dysregulated host response to infection. Septic shock, triggered by dangerously low blood pressure, results in organ failure with a higher risk of mortality. Sepsis is characterized by significant alterations of clinical, laboratory and hemodynamic parameters due to circulatory and cellular/metabolic dysfunction.[355–357] Sepsis can be considered as a biphasic syndrome, with the initial phase being characterized by overactivation of the inflammatory response (cytokine storm) followed by a second phase of persistent immuno-suppression where patients are strongly exposed to reoccurring primary or secondary infection with high risk of fatal outcome.[357–359]

Pneumonia is the most common primary site of infection associated with sepsis, followed by bacteraemia without specific primary infection site location, UTIs and intraabdominal infection.[355,356] Quantitative blood cultures indicate extremely low numbers of circulating bacteria in septic adults (typically a few tenths of bacteria per mL of blood), whereas bacterial counts may be significantly higher in neonates and children (up to 100–1000 CFU $mL^{-1}$).[360] Predominant bacterial species are staphylococci (*S. aureus*, *S. epidermidis*, *S. pneumonia*), *Pseudomonas* (*P. aeruginosa*), *Enterobacter* (*E. coli*), *Klebsiella* and *Acinetobacter*.[355,356,361] Methicillin-resistant *S. aureus* (MRSA) was identified in about 10% of culture-positive patients in intensive care units.[361] In the particular context of sepsis/sepsis shock fast antimicrobial treatment can be life-saving. For this reason, administration of broad-spectrum antibiotic as soon as possible, ideally within 1 h after the outbreak of symptoms, remains a strong recommendation in sepsis management.[362]

### 6.2 Methods and technologies for sepsis diagnosis and related reviews

G. Lippi introduced current strategies and their limitations for early sepsis diagnosis.[363] The conventional culture-based workflow from incubation to pathogen identification is very time-consuming (typically in the range of 2 to 7 days) and additional subculture steps are needed for phenotypic AST.[364] MALDI-TOF applied after positive BCs has significantly accelerated the pathogen identification process.[365] Culture-independent molecular techniques using blood samples directly have been developed with an estimated reduction of the time to result to 6 from 48 h. Furthermore, array approaches enable multiplexing and identification of panels of relevant pathogen targets.[364,366] Examples for commercial microfluidic systems include the Xpert® MRSA/SA Blood Culture assay (Cepheid, USA) that was designed for identification of methicillin-resistant *S. aureus* (MRSA) on a benchtop PCR system (GeneXpert®, Cepheid, USA). Time-to-result is 1 h after positive blood culture.[367] The BioFire® FilmArray® Blood Culture Identification panels (BCID2) (BioFire® Diagnostics, USA) tests for 43 BSI targets (bacteria and antimicrobial resistance genes). Results are also available in 1 h from positive BC.[365] The ePlex® system (GenMark Diagnostics, USA) takes advantage of an integrated assay based on droplet microfluidics, multiplex PCR amplification and electrochemical detection. The Sepsis Flow Chip® (Vitro/Master Diagnostica, Spain) detects a large panel of bacteria, fungus and antibiotic resistance genes. The multiplex PCR microarray is implemented in the 3D environment of a porous membrane enabling improved flow-through interaction of the DNA samples with immobilized probes.[368] The abioSCOPE® POC platform detects an early protein biomarker of sepsis (pancreatic stone protein). The immunoassay-based system takes advantage of nanofluidic technology to accelerate molecular interactions, with test results obtained in a few minutes (Abionic SA, Epalinges, Switzerland).[369]

A host of review articles covers the field of BSI diagnostics. Peker *et al.* provided an exhaustive overview of commercially available methods for the identification of microorganisms and detection of antimicrobial-resistant genes from positive blood cultures or directly from whole blood, respectively.[364] Peri *et al.* reviewed culture-independent BSI detection systems.[366] Sinha *et al.* also outlines the limitations of routine blood culture testing and discusses emerging molecular technologies.[370] Jyoti *et al.* emphasized POC sensor-based methods for diagnosis of neonatal sepsis (including microfluidics).[371] Zhang *et al.* more specifically focused on microfluidics for sepsis diagnosis.[372] POC technologies were discussed by Oeschger *et al.*, including pathogen removal devices and commercial systems for BSI detection.[373] Other reviews on biosensors for BSI diagnostics have been elaborated by Kumar *et al.* or Tsounidi *et al.*, respectively, including microfluidic approaches.[374,375] Liu *et al.* reviewed detection of bacteria and sepsis-related biomarkers with aptamer-based biosensors.[376] Pilecky *et al.* investigated pathogen enrichment from human whole blood,[377] and also Burklund *et al.* looked into microfluidics tools for organism isolation from whole blood.[378] In an earlier review, Li *et al.* discussed paper microfluidics for blood analysis from a more general perspective.[379] In the following, we will explore different microfluidic approaches related to BSI and sepsis diagnosis. Table 5 provides an overview of selected recent systems.

### 6.3 Microfluidic devices for isolation and detection of sepsis-causing pathogens in whole blood

Blood is a complex matrix that often compromises direct application of molecular methods for pathogen detection, for instance due to the presence of PCR inhibitors or abundant interfering human DNA.[400] Moreover, detection of extremely low pathogen concentrations encountered in clinical BSI/sepsis (as low as 1–10 bacteria per mL) in a background of

Table 5 Selection of microfluidic or biosensor devices for BSI diagnostics

| Analyte | Device and assay principle | Performance indications | Ref. |
|---|---|---|---|
| ***Detection and AST of sepsis-causing pathogens in whole blood*** | | | |
| Sepsis-inducing bacteria | Micro-PCR chip with membrane-based filtration module | Rapid isolation of bacteria from blood by stirring-enhanced filtration and PCR within 4 h | 380 |
| Engineered *E. coli* strains, clinical isolates | Droplet digital PCR for rapid bacterial detection and AST in 10% whole blood | 3D droplet counter enabled high throughput (assay time 1 h, LOD 10 CFU $mL^{-1}$). Applicable for a wide range of antibiotic resistance genes | 381 |
| *E. coli*, *K. pneumoniae*, *E. faecalis*, *S. aureus* | Culture-free detection and phenotypic AST by single-cell trapping | RBC depletion *via* dextran sedimentation. AST in <2 h. LOD 1–10 CFU $mL^{-1}$ | 382 |
| ***Biomarker detection related to sepsis diagnosis*** | | | |
| PCT, CRP, cytokines | Multiplexed electrochemical biosensor for rapid sepsis endotyping | ZnO/Au electrodes enhanced sensitivity. LOD of 1 pg $mL^{-1}$, <5 min. Validation with clinical samples | 383–386 |
| PCT, CRP | Sensor microarray for nanoparticle-enhanced plasmonic detection | LOD 21 pg $mL^{-1}$ for PCT and 36 pg $mL^{-1}$ for CRP. Clinically relevant PCT levels in <15 min | 387 |
| CRP, NP | Immunoassays in microchannels with integrated optical detection | LOD 10 ng $mL^{-1}$ for CRP and 2.1 ng $mL^{-1}$ for spiked serum. Assay time 20 min | 388 |
| PCT | On-chip electrokinetically driven electrochemical immunoassay | LOD 0.04 ng $mL^{-1}$ for PCT, time <20 min | 389 |
| CRP | ELISA on a sliding-strip 3D μPAD | Detection range 1–100 μg $mL^{-1}$ in undiluted blood | 390 |
| IL-6 | Plasmonic immunosensor on paper | Portable device with smartphone detection. LOD 0.1 pg $mL^{-1}$, within 17 min | 391 |
| IL-6 | Differential electrical counting of modified beads | LOD 127 pg $mL^{-1}$, within 5 min | 392 |
| Cell-free DNA | Simple thread-based silicone tube device | cfDNA quantification (1–3 μg $mL^{-1}$) spiked in plasma within 20 min | 393 |
| ***Sepsis diagnosis based on alterations of leucocyte properties*** | | | |
| Neutrophils | Measurement of spontaneous motility in a channel array/maze chip | Machine-learning-based sepsis scoring validated with clinical samples | 394 |
| Leukocytes | Inertial cell sorting and isodielectric cell profiling | Continuous sepsis monitoring based on detecting activated/inactivated leukocytes | 395 |
| Leukocytes | Hydrodynamic interactions of immune cells with an on-chip pillar-array | Label-free immune profiling assay from unprocessed blood using shaped pillars, 15 min | 396 |
| Leukocytes | Microfluidic assay for combined CD64 and CD69 cell capture | Total analysis time 2 h. Assay validation with clinical samples | 397, 398 |
| Neutrophils | Quantification of CD64 expression by cell capture and differential counting | Multivariate regression using artificial neural networks. Validation with clinical samples | 399 |

blood cell concentrations that are orders of magnitude higher (RBCs $\sim 10^9$ per mL; platelets $\sim 10^8$ per mL; leukocytes $\sim 10^7$ per mL) is extremely challenging.[378] Sample preparation and pathogen enrichment therefore remains an important issue for implementing sepsis diagnosis strategies with high sensitivity.[377,378] Kalyan *et al.* recently addressed inertial microfluidics enabling clinical research and blood cell/pathogen separation.[401] In an earlier review, Pitt *et al.* considered various methods, including microfluidic approaches, for rapid separation of bacteria from blood, with emphasis on devices that are designed for processing mL-quantities enabling detection of extremely low pathogen concentrations.[402] In the following, we present a selection of devices using different methods for bacteria isolation from blood cells for on-chip or off-chip detection.

Fang *et al.* developed a PDMS microfluidic device for isolation and early detection of sepsis-causing bacteria directly from whole blood (Fig. 6a). The microfluidic chip assembly comprises different modules, namely (i) a pneumatically-actuated stirring-enhanced blood filtration module for extraction of bacteria-laden plasma, (ii) an adjacent chamber for bacteria capture on magnetic beads, and (iii) a micro-PCR module with four on-chip PCR chambers. Active on-chip micromixing prevented clogging of the filter membrane by the blood matrix and efficient bacteria isolation. Multiplex detection of relevant pathogens (*E. coli*, *K. pneumoniae*, *P. aeruginosa*, *S. epidermidis* and *S. saprophyticus*) was achieved within 4 h (LOD of 10 CFU $mL^{-1}$ for the on-chip PCR reaction).[380] Ohlsson *et al.* proposed a semi-integrated microfluidic method for bacteria detection from blood by preforming successive assay steps in connected devices. The process started with differential separation of bacteria from blood cells by on-chip acoustophoresis in a straight microchannel. The channel acted as ultrasonic resonant cavity in which blood cells migrate laterally and focus into a central stream, whereas live bacteria in plasma could be recovered from the off-center fluid fractions. The bacteria-containing plasma was then further processed in a glass capillary by acoustic-assisted bacteria trapping/enrichment on polystyrene particle clusters.

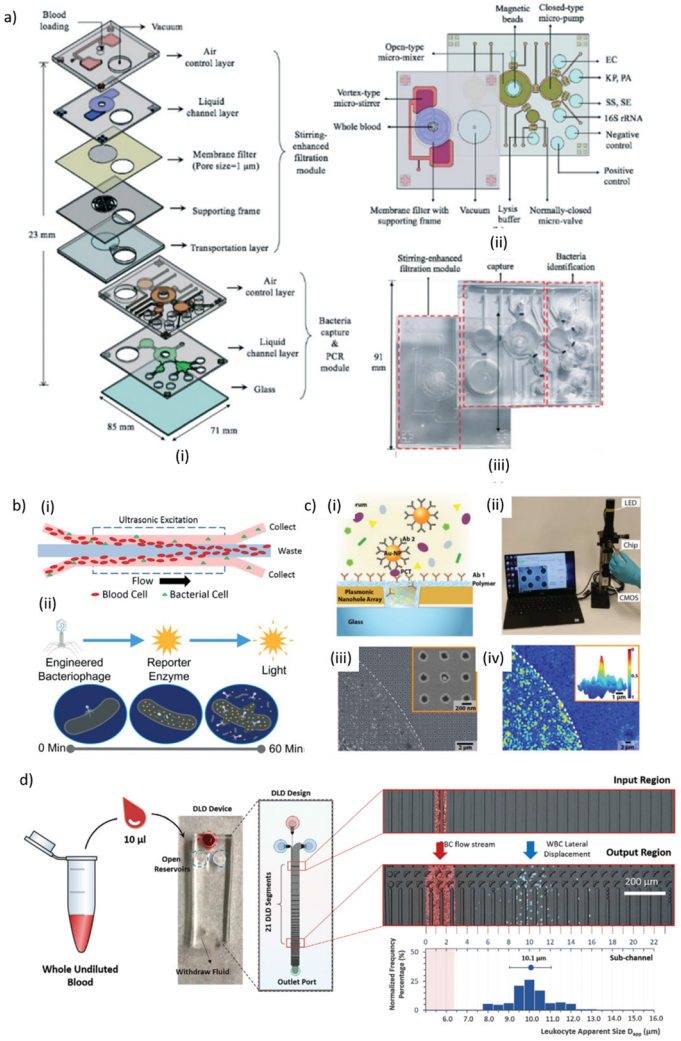


**Fig. 6** a) (i) Exploded view of an integrated microfluidic chip for early detection of sepsis-inducing bacteria, featuring a stirring-enhanced filtration module, a bacteria-capturing module, and a micro-PCR module. (ii) The chip was equipped with microfluidic components (*e.g.* micro-stirrers, micro-pumps, micro-mixers, micro-valves, & microchambers). A magnet was placed underneath the micro-mixer for bead collection (not shown), and a thermo-electric cooler was placed under the four microchambers for PCR thermocycling (not shown). Microchambers for positive and negative PCR controls were also incorporated. EC, KP, PA, SS and SE stand for *E. coli*, *K. pneumoniae*, *P. aeruginosa*, *S. saprophyticus*, and *S. epidermidis*, respectively. (iii) Photograph of the integrated microfluidic chip. b) (i) Illustration of acoustic separation of bacteria from blood. A sample of bacteria and blood flows in the side inlets in laminar flow while a density-matched buffer flows in the center inlet. Acoustophoresis causes the blood cells (red and white blood cells) to migrate laterally toward the center of the channel and out the center outlet, while bacteria respond weakly to the acoustic field. This differential is the basis of isolation from blood cells. (ii) Illustration of the luminescent bacteriophage assay. Bacteriophage modified to incorporate a reporter luminescent protein are added to the blood sample and infect the target bacteria, using the host bacteria's machinery to amplify the reporter. Within one hour of incubation, a complementary substrate is added to induce the luminescent signal generation, which is recorded with a luminometer. c) Portable digital nanoparticle-enhanced plasmonic imager for biomarkers detection. (i) PCT and CRP, which are blood-circulating protein biomarkers secreted by the host body in response to systemic inflammation, are detected. A single-step bioassay directly in human serum enables rapid molecular results, critical for the early diagnosis of sepsis, by detecting individual Au nanoparticles (NPs) binding to the Au nanohole array (NHA). (ii) Prototype reader developed for highly sensitive and multiplexed detection of biomarkers. The device uses a CMOS camera and a narrow-band LED source to record the transmitted images from a nanoplasmonic chip. (iii) SEM image of an Au-NHA area after a bioassay showing the bound NPs. Inset shows a single nanoparticle bound inside a nanohole. (iv) Plasmonic image of the Au-NHA area with bound nanoparticles. The binding of Au-NPs on Au-NHAs causes local transmission suppression through distortion of plasmonic excitations in the Au-NHA and can be digitally detected using far-field imaging. The inset shows a normalized intensity contrast induced by a single nanoparticle trapped in a nanohole. d) Schematics of experiment and immune profiling workflow using deterministic lateral displacement (DLD) assays using L and $L^{-1}$ pillar shapes for sorting. The whole blood DLD assay proceeds by loading the blood into the sample reservoirs of the PDMS DLD device which is used to simultaneously sort and measure the distribution of cells across the output region allowing size frequency distribution analysis. The device consists of two additional buffer reservoirs that sandwich the sample stream resulting in a precise injection of sample into the DLD region. The DLD region is composed of 21 DLD segments corresponding to 21 step measurement resolution ranging from size 6.0 to 16.0 μm in steps of 0.5 μm. The streams in input and output regions are in pseudo-color to show the differences between input and output. Scale bar is 200 μm [a) reproduced from ref. 380 with permission from the Royal Society of Chemistry; b) reproduced from ref. 404 with permission from the Royal Society of Chemistry; c) reprinted with permission from ref. 387, ©2020 John Wiley and Sons; d) reprinted with permission from ref. 396, ©2021 John Wiley and Sons].

Finally, bacteria were detected on a disposable PCR chip. A LOD of 1000 bacteria per mL was achieved within <2 h (*P. putida* spiked into whole blood).[403] Dow *et al.* used microfluidic acoustophoretic separation and off-chip detection based on bacteriophage luminescence as optical reporter of the bacteria concentration (Fig. 6b). The system achieved a 40–60% recovery yield for concentrations from $10^2$ to $10^6$ CFU $mL^{-1}$ (*P. aeruginosa*, *E. coli*, or *S. aureus* spiked in diluted whole blood). Acoustic purification resulted in a 33-fold LOD improvement of the bioluminescence assay.[404] Microfluidic dielectrophoresis or elasto-inertial microfluidics are other techniques that have been explored earlier for label-free isolation of bacteria.

### 6.4 Systems based on single-cell detection enabling fast AST in whole blood sample

Abram *et al.* implemented a digital one-step blood droplet PCR assay on a rapid diagnostic platform. Unprocessed whole blood samples spiked with target pathogens were mixed with reagents enabling inhibitor-resistant PCR and then compartmentalized on-chip. High-throughput droplet generation was achieved with four flow-focusing units in parallel. Subsequently, the blood droplets were collected for off-chip PCR and 3D volumetric fluorescence detection for digital target quantification. The assay achieved an analytical sensitivity of 10 CFU $mL^{-1}$ within <1 h (10% blood spiked with an antibiotic resistant *E. coli* model strain containing the synthetic $bla_{CTX\text{-}M\text{-}9}$ target gene). The applicability of the technology for rapid diagnosis of BSI was demonstrated with clinical isolates that have been interrogated for different molecular targets, including antibiotic resistance molecular markers.[381] Forsyth reported a culture-free sample preparation and bacteria enrichment workflow for microbiological analysis of BSI and phenotypic AST by single-cell observation. Dextran sedimentation was used for efficient depletion of erythrocytes in whole blood spiked with clinically relevant bacteria (*E. coli*, *K. pneumoniae*, *E. faecalis*, and *S. aureus*). A centrifugation step was incorporated to enrich the sample. Subsequently, dextran-isolated bacteria were trapped in narrow microfluidic channels for single-cell detection and phenotypic AST based on bacteria growth dynamics upon exposure to different antibiotic concentrations. The workflow took less than 2 h and was performed with a clinically relevant pathogen concentration (10 CFU $mL^{-1}$).[382]

### 6.5 Biomarker detection for diagnosis of sepsis

A major challenge is to identify reliable biomarkers or combinations enabling rapid sepsis diagnosis and prognosis of outcome. As sepsis is an inflammatory syndrome involving numerous cellular processes most of the currently used biomarkers are not specific but may be indicative for other infectious conditions. The panel of relevant sepsis biomarkers has been reviewed by Pierrakos *et al.* and Biron *et al.*, for instance.[405,406] Reviews on biosensors also include discussions of biomarkers in sepsis diagnostics.[371,375]

Two important sepsis-related biomarkers are C-reactive protein (CRP), a non-specific marker for acute immune response, and procalcitonin (PCT), a clinically relevant biomarker of sepsis diagnosis at early stages. Tanak *et al.* developed a dual-marker non-faradaic electrochemical impedimetric biosensor for the detection of sepsis. Zinc oxide coating of the interdigitated Au electrodes provided enhanced sensitivity. The choice of biomarkers, *i.e.* the early sepsis marker PCT and the late onset marker CRP, was expected to be useful for evaluating the severity of infection. Detection in whole blood with LODs of 0.10 ng $mL^{-1}$ for PCT and 0.10 mg $mL^{-1}$ for CRP, respectively, was reported.[383] Further sensor array integration for monitoring five cytokines by means of a handheld electrochemical reader enhanced the capability of rapid POC sepsis endotyping (LOD 1 pg $mL^{-1}$, results available in <5 min from a single drop of undiluted plasma).[384] Subsequently, the system was validated by cohort studies with clinical samples.[385,386] Belushkin *et al.* developed a digital nanoparticle-enhanced plasmonic imager for rapid and sensitive detection of CRP and PCT (Fig. 6c). A plasmonic gold nanohole array (Ti/Au film with 200 nm holes on a silica substrate) enabled detection of single Au nanoparticle (NP)-labeled molecules by means of a portable optical reader. The functionalized AuNP suspension mixed with blood serum was directly injected in the detection chamber of the microfluidic cartridge. Multiplexing was achieved by bioprinting different capture antibodies on the sensor array. The system showed very high sensitivity with LODs of 21 pg $mL^{-1}$ for PCT and 36 pg $mL^{-1}$ for CRP, respectively. Clinical validation with patient blood serum demonstrated that PCT levels typical for sepsis can be monitored in <15 min.[387]

Giannetti *et al.* implemented immunoassays for multiplex optical detection of CRP and neopterin (NP) on a multi-channel microfluidic flow cell in a sepsis diagnostic device. Combined measurement of both non-specific markers is expected to improve early diagnosis of systemic infection. A LOD of 10 ng $mL^{-1}$ for CRP and 2.1 ng $mL^{-1}$ for NP (spiked in human serum) was achieved, respectively, with a total assay time of 20 min.[388] Molinero-Fernández *et al.* combined a PCT magneto-immunoassay format with flow-based electrochemical on-chip detection. The immunocomplex was injected in a cross-channel microfluidic chip and retained in the main channel while an enzymatic substrate was electrokinetically driven over the magnetic bead plug for downstream in-channel amperometric detection (LOD of 0.04 ng $mL^{-1}$ for PCT standard solutions, analysis time <20 min).[389] Verma *et al.* implemented a CRP ELISA assay in a microfluidic sliding-strip paper device. The paper strip, which contains the sensing area, was inserted in a functional dock, built up from multiple wax-patterned paper layers, defining the fluidic operations and for storage of dry reagents/detection antibody. The strip receives the blood sample at the initial position and is then moved further step-

wise under successive reaction areas to perform the colorimetric ELISA assay. This simple device could be suitable for diagnosis of suspected neonatal sepsis, in particular in resource-limited setting.[390] Kim *et al.* designed a microfluidic cartridge that incorporates an immuno-flow strip with colorimetric read-out for on-site sepsis diagnosis. The hybrid biosensor was designed for conducting a biochemical analysis (lactate assay) and immunoassays (PCT and CRT) simultaneously on the same membrane strip. In contrast to conventional LFAs, a 2D crossing flow protocol was implemented to perform the immunoassays.[407]

A plasmonic immunosensor for rapid detection of sepsis biomarkers in unprocessed blood, in this case the interleukin proinflammatory marker (IL-6), was proposed by Alba-Patino. Quantification of the colorimetric nanoprobe signal on a simple filter paper substrate was done in real time by means of a smartphone (LOD 0.1 pg $mL^{-1}$, recombinant human IL-6 in buffer, within 17 min).[391] Valera *et al.* used latex beads carrying the IL-6 biomarker that selectively binding to functionalized pillars in a capture chamber. On-chip coulter counting provided a measure for the IL-6 concentration (LOD 127 pg $mL^{-1}$, within 5 min).[392] A POC integrated magneto-electrochemical biosensor platform for sepsis diagnosis produced test results within 1 h from blood samples and detected IL-3 at a sensitivity of $<10$ pg $mL^{-1}$.[408]

The content of circulating cell-free DNA (cfDNA) in plasma has been considered as an indicator for possibly sepsis fatality. Damodara *et al.* proposed a very simple microfluidic approach for low-cost POC detection of cfDNA. Sample and DNA-binding fluorescent dye were loaded into a silicone tube (length 1 cm) with twisted polyester threads and mixed by squeezing, prior to incubation and imaging. Quantification of cfDNA spiked in plasma in the range of 1–3 μg $mL^{-1}$ was demonstrated, possible suitable to identify sepsis patients at high fatality risk.[393]

### 6.6 Sepsis diagnosis based on alterations of leucocyte properties

Microfluidic assays that analyse biochemical or biophysical properties of white blood cells have been developed as a tool for sepsis diagnosis. Neutrophils play an essential role in the response of the innate immune system.[409] Babatunde *et al.* reviewed microfluidic devices that have been designed to investigate complex neutrophil migration behaviors.[410]

Ellett *et al.* developed a microfluidic device for investigating sepsis-specific spontaneous migration signatures. The chip comprises RBC filters, an array of narrow neutrophil migration channels for measuring motility parameters and mazes allowing spontaneous binary changes of direction. Neutrophil track analysis and a machine-learning leveraged sepsis scoring system enabled accurate diagnosis of sepsis with clinical blood samples.[394] Jeon *et al.* designed an integrated platform comprising two subsystems, namely (i) a multidimensional double-spiral microfluidic device for inertial isolation of leukocytes from peripheral blood, and (ii) an isodielectric separation chip for subsequent discrimination of activated/inactivated leukocytes based on dielectric cell properties. The authors demonstrated that leukocytes from septic and healthy human subjects could be discriminated.[395] Zeming *et al.* proposed a microfluidic approach for monitoring rapidly changing host inflammatory response and severe immune response signatures, as occurs in acute septic conditions (Fig. 6d). For this purpose, an unprocessed blood sample was flushed through arrays of specifically designed pillars, enabling very rapid (15 min) profiling of immune response based on hydrodynamic interactions and sensing of biophysical signatures of white blood cells (size and deformability).[396]

A microfluidic chip developed by Zhou *et al.* took advantage of multiple affinity capture regions. Leukocytes with upregulated CD64 or CD69 expression levels due to inflammation or sepsis were retained in the flow channels by immunoaffinity on the functionalized sections. The interaction between cells and the substrate was increased *via* secondary flow patterns induced by herringbone structures in the channel.[397,398] This assay builds on an earlier approach for capture of CD64+ cells only.[411] Hassan *et al.* also proposed a microfluidic device for quantification of CD64 expression on neutrophils. The chip comprises two inlets for whole blood and RBC lysing buffer, respectively. Leukocytes were transported downstream through an anti-CD64 functionalized chamber enabling differential immunoaffinity counting of CD64+ cells.[399,412]

## 7 Sexually transmitted infections

### 7.1 Sexually transmitted pathogens and diseases

Sexually transmitted infections (STIs) are generally spread through unprotected sexual activity, whereas other transmission modes, for instance during pregnancy, child birth or through contact with infected body fluids, in particular blood, are possible. STIs have a profound impact on health and represent a major global burden for the public health system.[413] More than 30 different pathogens can cause sexually transmitted diseases and over 1 million STIs are acquired every day worldwide (WHO STIs factsheet 2023).[414] The four most common STIs are: chlamydia, a bacterial infection mainly caused by the species *Chlamydia trachomatis* (CT),[415] gonorrhea with *Neisseria gonorrhoeae* (NG) as bacterial causative organism,[416] trichomoniasis provoked by the protozoan parasite *Trichomonas vaginalis* (TV),[417] and syphilis, which is due to infection with the bacterium *Treponema pallidum* (TP).[418] These STIs are often asymptomatic or show non-specific symptoms, as a consequence most infected patients do not seek medical treatment. These diseases are actually curable with antimicrobial treatments, however, if untreated, serious impact on health may occur, including neurological and cardiovascular disease, infertility, stillbirths, and an increased risk of human immunodeficiency virus (HIV)

 

infection.[419] Rapidly increasing antimicrobial resistance is a growing threat for untreatable gonorrhea.[420]

Most important currently incurable viral STIs or related causative pathogens are:[414] hepatitis B virus (HBV),[421] genital herpes simplex virus (HSV),[422] HIV/AIDS[423] and human papillomavirus (HPV).[424] Hepatitis, in particular types B and C, leads to chronic disease such as liver cirrhosis and liver cancer. WHO estimates that 296 million people were living with chronic HBV infection in 2019, resulting in an estimated 820 000 deaths, even though vaccines are available to prevent fatal outcome.[425,426] Diagnostic devices focusing specifically on hepatitis C viruses (HCV) will be included in this section, even if transmission generally occurs by infected blood samples (*e.g.* by sharing syringes for drug injection) and not by sexual intercourse. Acquired immunodeficiency syndrome (AIDS) is a potentially life-threatening condition caused by HIV that continues to be a major global public health issue with an estimated 39.0 million people living with HIV infection at the end of 2022.[414] HIV attacks the body's immune system, specifically white blood cells (CD4 cells), thus increasing the risk of morbidity through co-infections.[419] HIV, as well as HSV, generate lifelong infections, but efficient antiviral therapies may suppress the viral load sufficiently to maintain manageable chronic conditions.[427,428] Vaccines against HPV have been developed to prevent HPV-associated cancers, in particular cervical cancer.[429]

### 7.2 Current STI diagnostics landscape and recent reviews

Diagnostic procedures to detect STIs include both direct and indirect methods based on various samples, including blood, urine, and vaginal or endocervical swabs. Direct pathogen detection, like pathogen culture, antigen tests or nucleic acid tests can be used to examine localized and acute infections. On the other hand, antibody response to infection may become detectable only after weeks to months, thus are more suitable for diagnostic evaluation of chronic infection or the patient's actual immune status.[430] Rapid LFA STI diagnostic tests for antibody/antigen detection are available, such as syphilis treponemal antibody tests (for instance Syphilis Health Check™, Diagnostics Direct, USA).[431] These tests have limited sensitivity but deliver qualitative results in less than 30 min at the POC. NAAT-based commercial systems have been developed or adapted for POC STI diagnostics. As an example, Xpert® microfluidic PCR assays running on the GeneXpert® system have been designed for sexual health testing, including CT/NG and TV assays, as well as tests for viral STIs (including HIV, HBV/HCV and HPV). The Bosch Vivalytic STI PCR test can reliably analyse a patient sample for ten different pathogens at once. A urine sample or a urogenital swab is used as the sample type, results are available in 30–90 min.[115] Another promising approach is the Visby Medical Sexual Health Test (Visby Medical, USA), which is a rapid (results within 30 min), handheld and easy-to-use PCR device with excellent sensitivity and specificity for CT, NG and TV detection.[432]

Cristillo *et al.* reviewed the frame of POC STI diagnostics from a larger perspective, including current and emerging technologies, clinical and public health benefits and other aspects,[433] whereas Wi *et al.* discussed challenges of STI diagnosis in resource-constrained settings.[434] Caruso *et al.* compared current STI laboratory diagnostic tools with respect to performance, applicability, and adaptability to POC format.[435] Toskin *et al.* looked at the state of STI POC testing technologies and the implications for health system integration.[436] Discussions including commercial POC systems for STI testing, in particular for the four major curable STIs and HIV, have been provided by Adamson *et al.*, Gaydos *et al.* or Hsieh *et al.*, for instance.[437–439] Hsieh *et al.* also investigated the gap of near-POC NAAT devices and the requirement to move to real POC applications. Thakur *et al.* recently reviewed high-performance biosensing systems for STI diagnostics,[440] and Farokhzad *et al.* analyzed progress towards POC platforms from a materials chemistry-enabling perspective.[441] Other reviews by Tharakan *et al.*, Pai *et al.* or Eid *et al.* focused on novel technologies for HIV diagnostics, including nanotechnology and microfluidics.[442–444] Xiao *et al.* provided an overview of POC tests for hepatitis B,[445] other reviews addressed more specifically HCV diagnosis *via* microfluidics or biosensors for hepatitis diagnostics (HBV and others).[446,447] Nath *et al.* discussed laboratory and POC techniques for diagnosis of HSV infections.[448]

Even if a wide range of STI diagnostic tools is currently available, high actual incidence rates of STI, emergence of antimicrobial drug resistance and the requirement of extended screening campaigns in low and middle-income countries motivate the development of new truly POC diagnostic devices with high sensitivity and short time-to-result. In the following we will discuss a selection of recent microfluidic and biosensor developments for STI diagnosis. Table 6 provides an outline.

### 7.3 Microfluidic systems and assays for HIV/AIDS diagnostics

In clinical settings, HIV/AIDS disease progression is monitored by CD4 counts,[465] whereas p24 viral capsid protein antigen immunoassays or antigen/antibody combination assays are used for detecting acute HIV infection.[466] NAAT-based RNA detection allows quantification of the viral load and early detection of infection. Trick *et al.* proposed a filtration-assisted magnetofluidic blood-to-PCR workflow for HIV RNA detection from blood (Fig. 7a).[449] As described below, a similar approach was also used for other pathogens.[462,467] In the present case, viral HIV particles were extracted from a droplet of whole blood by means of a filtration module and collected in a vial for lysis and RNA capture on magnetic beads. Subsequently, the filtered plasma mixture was loaded into the assay cartridge and inserted in the magnetofluidic qPCR platform. The system achieved a LOD of down to 1000 copies of HIV RNA per blood sample

Table 6 Selection of recent microfluidic devices for STI-related pathogen detection

| Analyte | Device and assay principle | Performance indications | Ref. |
|---|---|---|---|
| ***Microfluidic systems and assays for HIV/AIDS diagnostics*** | | | |
| HIV viral particles | Filtration-assisted magnetofluidic cartridge qPCR platform | Uses a separate 3D-printed filter module, LOD $10^5$ mL$^{-1}$ HIV RNA (whole blood), 30 min | 449 |
| HIV-1 RNA | Fingerpick blood RT-LAMP test cartridge using magnetic transport | Viral load tests performed within 60 min in whole blood (threshold at 1000 copies per mL) | 450 |
| HIV-1 p24 antigen | Colorimetric ELISA assay on a 3D origami paper-based device | Semi-quantified results, LOD 0.03 ng mL$^{-1}$ (spiked plasma), 10 min | 451 |
| HIV-1 RNA, HIV-1 virus | Cartridge for autonomous RT-LAMP with integrated LFA detection | LOD $3 \times 10^5$ HIV-1 viral particles per mL of whole blood, within 90 min | 452 |
| HIV-1 p24 antigen | HRP-linked immunoassay and Au nanorod based multicolor assay | Semi-quantitative analysis by naked eye in 1 h, LOD 0.5 ng mL$^{-1}$ (buffer) | 453 |
| HIV-1 synthetic target | RCA combined with microfluidic affinity chromatography | Padlock probe-mediated detection, LOD <30 fM | 454 |
| HIV-1 plasmids | Wearable device for HIV-1 DNA RPA using human body heat | LOD 100 copies per mL (buffer), within 24 min | 455 |
| ***Microfluidic systems for HBV/HCV and HPV detection*** | | | |
| HCV and HIV cDNA | Multiplexed digital droplet LAMP with scorpion-shaped probes | Quantification with LOD of 4 copies per reaction. Clinical plasma samples tested. | 456 |
| HCV RNA | LAMP assay cartridge with lateral flow detection | Result in <40 min. Tested with clinical samples | 457 |
| HBV, HCV, HIV nucleic acid targets | Self-driven microfluidic multiplex LAMP chip | Sample loading *via* on-chip vacuum. LOD 2 copies of target nucleic acid per μL | 458 |
| HPV | LAMP on LoaD with Chelex-100 based nucleic acid isolation | Multiplex detection of 5 high-risk HPV virus types, within 40 min | 459 |
| Up to 24 HPV genotypes | Reverse dot hybridization for HPV genotyping on a palm-sized cartridge | Automated operation with LOD of $10^3$ copies per mL. Tested with clinical samples | 460 |
| HPV-16 and HPV-18 | SlipChip approach for viral load quantification with digital LAMP | On-chip self-partitioning of reaction droplets. Tested with clinical samples | 461 |
| ***Microfluidic systems for non-viral STIs*** | | | |
| *N. gonorrhoeae* | Cartridge-based automated magneto-fluidic PCR platform | Detection in clinical samples with simultaneous antimicrobial resistance genotyping, <15 min | 462 |
| STI pathogens | Isothermal nucleic acid amplification on LoaD | Multiplex pathogen detection directly from genitourinary secretions, within 50 min | 463 |
| *N. gonorrhoeae* | Foldable paper platform based on thermophilic HDA and LFA detection | Clinically relevant LOD of 500 NG cells per device, run time 80 min | 464 |

with a typical fingerprick volume of 10 μL (*i.e.* a LOD of $10^5$ per mL) within in <30 min.[449] The platform also enabled HCV RNA viral load quantitation from blood serum in approximately 1 h. The assay had a sensitivity of 45 IU per sample (corresponding to 4.500 IU mL$^{-1}$) and may be suitable for screening patients with chronic HCV infections.[468] Liu *et al.* developed a compact automated USB-interfaced analyzer aiming HIV self-testing. 100 μL of finger-prick blood would be collected and mixed in a tube containing lysis buffer and magnetic beads. In the present case, the device was tested with purified HIV RNA spiked into whole blood. The mixture is then manually transferred into a microfluidic cartridge and magnetically transported through a RNA binding chamber, a washing chamber and a RT-LAMP reaction chamber. Oil valve sections separate successive assay steps. Differentiating clinically relevant viral loads (threshold at 1000 copies per mL) was demonstrated with a turnaround time of 60 min. The RT-LAMP assay (validation in reaction tubes) had a LOD of 214 viral HIV RNA copies per mL for spiked whole blood.[450] An immunoassay for HIV p24 antigen quantification was implemented by Li *et al.* in a centrifugal microchannel array chip format with a smartphone detection unit. Horseradish peroxidase (HRP)-catalyzed oxidation of tetramethylbenzidine (TMB) induced a color intensity change in the presence of the p24 antigen. LODs obtained were 0.17 ng mL$^{-1}$ and 0.11 ng mL$^{-1}$ for p24 antigen spiked in buffer or human serum, respectively.[469]

Paper-based devices open the way to real POC applications, based on electricity- and instrument-free infectious disease diagnosis. Chen *et al.* performed a colorimetric ELISA assay on a 3D origami μPAD sensor for HIV-1 p24 antigen detection. The μPAD contained wells with pre-dried detection antibodies and capture antibodies. Assay steps were sequentially performed by sliding a paper strip over the 3D stack inserted in a 3D-printed holder. Appropriate self-timing of the multistep assay was achieved by adjusting the buffer viscosity and the volume of the fluid path. Semi-quantitative evaluation of the signal visible to the naked eye on the μPAD was possible by comparison with a color chart diagram. The linear detection range for HIV-1 p24 antigen was 0.03 ng to 3 ng mL$^{-1}$ with human plasma samples.[451] Phillips *et al.* reported a fully-integrated autonomous POC analysis platform comprising a microfluidic μPAD installed in a small plastic housing with

 

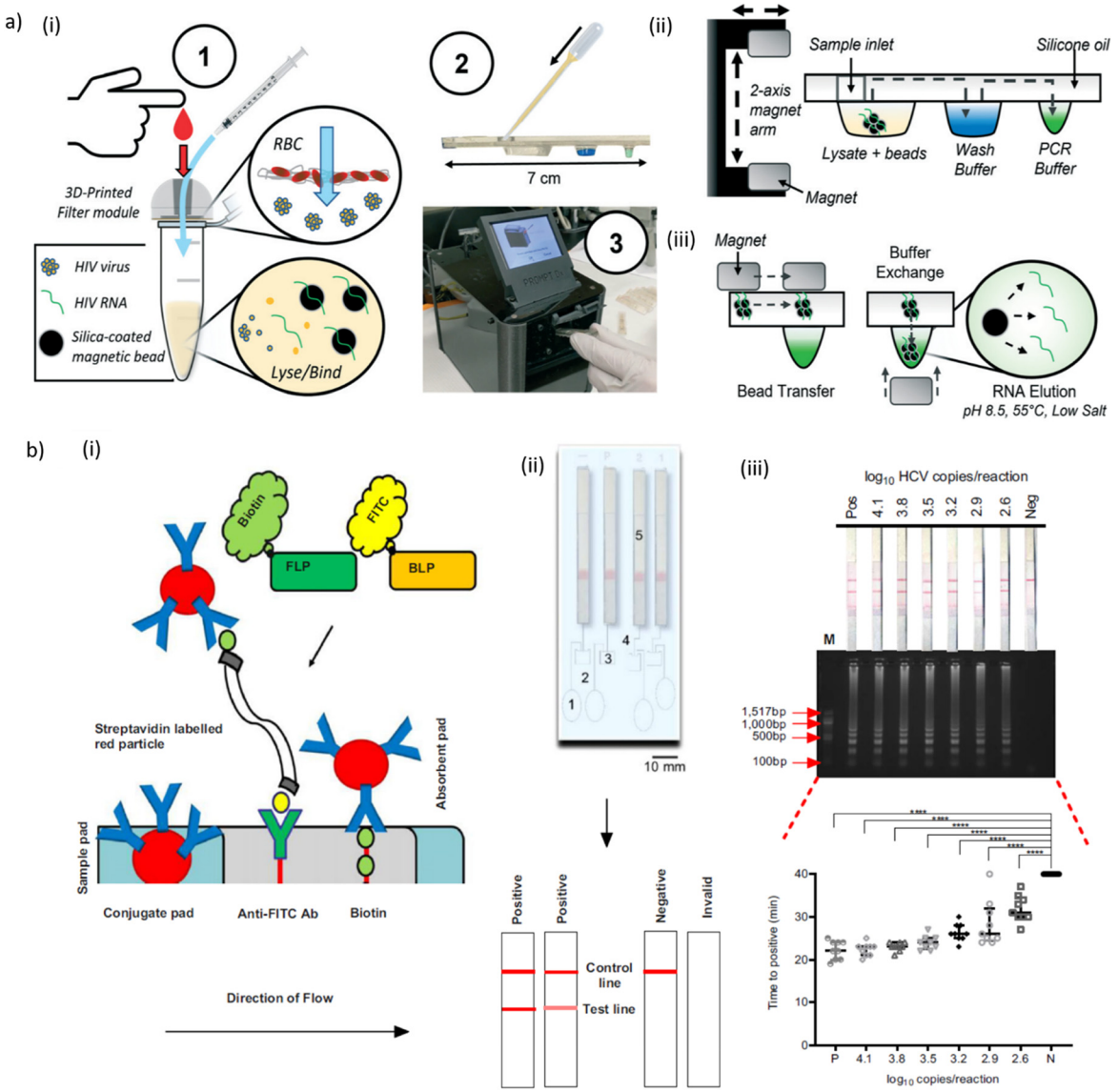


**Fig. 7** a) Filtration-assisted magnetofluidic blood-to-PCR workflow. (i) To begin the test, (1) a droplet of blood is first deposited into the filter module and viral particles are rinsed through the filter membrane with phosphate buffered saline (PBS) using a syringe. The filter traps red blood cells (RBCs) while viral particles are small enough to pass through into a lysis and binding solution containing magnetic beads for capture of viral RNA. This entire filtered plasma mixture is (2) loaded into the assay cartridge, which is then (3) inserted into the instrument. (ii) The magnetic beads are transferred through an immiscible silicone oil layer into the cartridge's extruded wells containing preloaded reagent buffers using a 2-axis motorized magnet arm. (iii) Bead transfer between wells is conducted by lateral movement of the top permanent magnet with bead exchange into buffers using vertical translation of the magnet arm to attract beads into the well with the bottom magnet. The final transfer of beads into the PCR buffer allows direct elution of RNA due to the relatively alkaline pH, elevated temperature, and low salt conditions. b) Lateral flow detection of HCV LAMP assay. (i) The mechanism of the lateral flow strip. Two primers, FLP and BLP, are pre-labelled with biotin and FITC, respectively. The amplicon resulting from the LAMP reaction, contains both labelled primers as double-stranded DNA represented schematically by two gray lines. It is added onto the sample pad and moves towards the conjugate *via* capillary action. The streptavidin-labelled red particles bind with the biotin (from the FLP primer) on the amplicon and together move towards the test line. The anti-FITC antibody (Ab) on the strip captures the amplicon *via* its FITC label (from the BLP primer) at the test line forming a band. Any unbound red particles move towards the control line where they are captured *via* the biotin forming a second band. (ii) The assembly and interpretation of the lateral flow devices. The device consists of the water chamber (1), connecting channels (2), four LAMP reaction chambers (3), channels (4) and lateral flow strips (5). Following the incubation period, two bands indicate a positive reaction, one band indicates a negative and no bands indicate invalid results. P – positive, N – negative, 1 and 2 – sample in duplicate. (iii) Analytical sensitivity of the lateral flow method (top panel) compared to gel electrophoresis (middle panel) and fluorescence over time (bottom panel). Serial dilutions of plasmid JFH1 replicon were made based on copy number per reaction ($\log_{10}$). Black lines indicate median with interquartile range ($n$ = 3 biologically independent experiments, each with three technical replicates). The different symbols are for each dilution, to ease visualisation (grey and white disc – 4.1, white lozenges – 3.8, inverse triangles – 3.5, black diamond – 3.2, grey circles – 2.9 and white squares – 2.6 $\log_{10}$ copies per reaction, black disc is negative control – DI water). Statistical analysis for the fluorescence over time was performed using a parametric, one-way ANOVA. The F ratio = 55.56 and the degrees of freedom = 65. ****$p \leq 0.0001$, Pos – positive HCV control, Neg – no template control, M – 100 bp NEB DNA ladder, C – control line, T – test line [a) reproduced from ref. 449 with permission from the Royal Society of Chemistry; b) reproduced from ref. 457, ©2021, Creative Commons license, CC BY 4.0 (**http://creativecommons.org/licenses/by/4.0/**)].

resistive heating elements, powered *via* a smartphone. The system was designed for automatically isolating HIV-1 RNA from whole blood, *in situ* RT-LAMP amplification, valve-controlled fluid transfer and detection on an internal LFA. The time-to-result was 90 min with a LOD of $3 \times 10^5$ HIV-1 viral particles (corresponding to $2.3 \times 10^7$ virus copies per mL of whole blood).[452]

A microfluidic immunosensor device for visual detection of HIV-1 p24 antigen with the naked eye was developed by Liu *et al.* The polymer cartridge for the multicolor immunosensor comprised an alternating alignment of circular reservoirs for assay reagents and elliptical reservoirs filled with mineral oil barriers. A HRP-linked magnetic bead-based immunoassay was implemented for detecting HIV-1 p24 antigens. Gold nanorods (AuNR) were used as chromogenic substrates. HRP-catalyzed TMB oxidation quantitatively mediated AuNR etching to produce a color change, which was visible within a HIV-1 p24 concentration range of 0–7 ng $mL^{-1}$ (spiked serum samples). The assay enabled semiquantitative detection of HIV-1 p24 with a LOD of 0.5 ng $mL^{-1}$ in buffer within 1 h. A significant color signal was displayed with 2 ng $mL^{-1}$ HIV-1 p24 spiked in serum.[453] Soares *et al.* used an agarose bead-based microfluidic device for affinity chromatographic capture and detection of padlock probe-mediated RCA products with a LOD below 30 fM for HIV-1 synthetic targets.[454] Song *et al.* designed a microfluidic chip reactor for RT LAMP-based detection of HIV or HPV. Paraffin-encapsulated reagents were prestored in the reactor and a nucleic acid binding membrane decoupled the sample from the reaction volume. The device was tested with HPV-16 DNA spiked in saliva and human plasma laden with HIV (subtype C) virions.[470] Kong *et al.* developed a wearable microfluidic device for rapid detection of HIV-1 DNA. The flexible chip, featuring a single fluidic 50 μL chamber containing RPA reagents and HIV-1 DNA, was immobilized by a wristband. The compatible temperature range for performing the RPA-based assay was simply provided by heat transfer from the human body. After incubation the chip was removed for fluorescence detection with a cellphone. HIV-1 DNA detection was achieved at 100 copies per mL in buffer within 24 min.[455]

A nanofluidic concentration device enabled highly efficient enrichment of nucleic acids and proteins directly from clinical samples. The approach, developed by Ouyang *et al.*, took advantage of a hierarchical architecture with vertically stacked massively parallel microchannels in a first stage and downscaling to a single microchannel in the final stage of the device. The analytes were electrokinetically transported and concentrated through the nanochannel network construct comprising a cation-selective Nafion membrane held by plasma-bonded PDMS layers. The performance of the device was demonstrated by detecting the HIV p24 protein in a 3200-plex concentration device (0.6 mL sample volume). Fluorescence signals could be detected within 60 min for an initial target concentration of 10 to 100 aM (in diluted serum), representing a nearly 6 order-of-magnitude enhancement compared to the same assay without pre-concentration.[471] Kadimisetty *et al.* discussed a self-powered flow-through membrane-based 3D-printed sample concentrator for highly sensitive molecular detection of HIV in whole blood at the POC.[472]

### 7.4 Microfluidic systems for HBV/HCV detection and other viral pathogens

Tan *et al.* adapted a droplet microfluidic technology for multiplexed LAMP and fluorescence detection of viral RNA. Multiplex detection in droplets was enabled by scorpion-shaped probes which, after activation by the LAMP reaction, generate a target specific color. Digital quantification of HCV and HIV cDNA with LOD as low as 4 copies was reported.[456] Witkowska McConnell *et al.* proposed a low-cost pan-genotypic RT-LAMP assay for HCV detection (Fig. 7b). The cartridge-like assembly comprises four RT-LAMP reaction chambers, transfer channels and lateral flow strips for visual detection of amplification products in less than 40 min. Fluidic manipulation was done *via* finger pumps. Using optimized primers, the method was validated as part of a clinical study with samples from patients with a range of viral loads and genotypes.[457] Li *et al.* designed a lab-on-a-disc for real-time PCR HBV DNA detection from whole blood. Versatility of the automated fluidic manipulation was enhanced by using a centrifugal device with two rotating shafts. On-chip wax valves were actuated by means of a laser diode. Detection of HBV in whole blood samples was feasible down to $10^2$ copies per mL with a total assay time of about 48 min.[469] LAMP-based multiplex detection of HBV, HCV and HIV was performed on a microfluidic chip designed by Xie *et al.* The PDMS chip comprises an array of 60 reaction chambers with target-specific primer solutions, fluidic channels and a vacuum chamber generating a negative pressure gradient for self-driven sample loading. An analytical sensitivity of 2 copies per μL of target viral nucleic acid after 50 min of isothermal amplification was reported.[458]

A LAMP-based microfluidic lab-on-a-disc system designed by Zhao *et al.* provided automated diagnosis of five high-risk HPV types with high specificity within 40 min. The system integrated Chelex-100 based nucleic acid isolation and is capable of performing 40 detections simultaneously.[459] A palm-sized PCR microfluidic cartridge, installed in a custom-made operating platform, enabled testing of 24 HPV genotypes. The whole cartridge comprised 3 functional areas for DNA extraction, for amplification in attached PCR tubes and a DNA microarray for reverse dot hybridization assay to identify multiple HPV genotypes, respectively. The LOD of the system for the detection of 24 HPV genotypes was $10^3$ copies per mL.[460] SlipChip technology for slip-induced self-partitioning and on-chip stationary droplet formation was applied to the quantification of HPV viral load by means of digital LAMP. The assay correctly identified clinical HPV-16 and HPV-18

 

positive samples with viral loads ranging from $7.0 \times 10^2$ copies per mL to $1.4 \times 10^7$ copies per mL.[470] Goux *et al.* discussed the performance of nanophosphor lateral-flow assay for self-testing for HSV-2 seropositivity.[473]

### 7.5 Microfluidic systems for non-viral STIs

Shin *et al.* designed a stationary droplet NAAT magnetofluidic platform for CT screening. The core of the device is a thermoformed polymer cartridge with distinct fluidic compartments separated by a fluorinated oil layer. In the present case, the clinical sample matrix presented in the form of a vaginal swab was first expressed in a tube for cell lysis before being transferred into the cartridge. Pathogen DNA was captured on magnetic particles and magnetically transported through the cartridge for performing the assay protocol, *i.e.* successive rinsing steps, subsequent elution and LAMP amplification. The cartridge was installed in a compact processing unit for mechanical and thermal control, as well as for fluorescence signal acquisition. The duration of the automated workflow was 65 min with an assay sensitivity in the range of $10^2$–$10^3$ target copies per sample. The performance of the platform was successfully tested in a clinical setting.[467] More recently the platform has been used for detecting NG with simultaneous genotyping for resistance to ciprofloxacin. A clinical study was carried out with penile swab samples from sexual health clinics. In this case, rapid on-chip PCR (40 cycles were completed within 12 min) was implemented resulting in sample-to-answer diagnosis in less than 15 min. Initial manual operations were limited to swab elution and mixing with magnetic bead suspension. Depending on the amplified gene sequence an assay sensitivity in the range of 10 to 100 CFU was determined.[462] The technology and assay principle were also adapted for HIV and HCV detection (see above).[449,468]

Magnetic actuation was also implemented in another automated droplet-array platform with a 3D printed fluidic cartridge. The system was tested by microfluidic screening of STI pathogens directly from clinical urine samples.[474] A microfluidic lab disc assay based on isothermal amplification was designed for processing eight clinical samples simultaneously targeting CT, NG, *Mycoplasma hominis*, and *Ureaplasma urealyticum* from genitourinary swabs. The turnaround time was 50 min with good detection limits and specificity.[463] Horst *et al.* presented a POC paper-fluidic device for POC diagnosis of NG that is expected to bridge the gap between RDTs and laboratory NAATs. Patient samples derived from clinical urethral and vaginal swabs were mixed with lysis/DNA precipitation buffer and pipetted into the reaction chamber of the device for nucleic acid extraction and multiplexed thermophilic HDA, followed by visual lateral flow assay detection. The assay run time was 80 min from sample-to-result with a LOD of 500 genomic NG copies per reaction.[464]

## 8 Vector-borne infections

### 8.1 Scope of vector-borne infections

Vector-borne diseases are caused by parasites, bacteria or arboviruses that are transmitted mainly by bloodsucking infected arthropod insects, such as mosquitoes or ticks. The ingested disease-producing microorganisms reproduce in the animal (vector) and are (re-)transmitted to humans by insect bites. Vector-borne diseases account for more than 17% of all infectious diseases, causing more than 700 000 deaths annually.[475] The burden is highest in tropical and subtropical areas, but vector-borne diseases are also widespread in Europe. The prevalence strongly depends on environmental conditions, such as climate factors, habit destruction or pesticide application, that impact the vector distribution. Vector control is a fundamental approach in WHO response to preventing disease.[476,477] Global patterns are evolving with climate change.[18,478,479] For instance, climate change enables the expansion of Lyme borreliosis, the most common bacterial (*Borrelia burgdorferi*) tick-borne disease in Europe.[480,481] Invasive mosquito species, such as the Asian tiger mosquito (*Aedes albopictus*) are causing increasing concern in public health due to the possible transmission of tropical pathogens.[482]

Dengue is the most prevalent arthropod-borne viral disease.[483,484] The dengue virus (DENV) is transmitted by *Aedes* mosquitoes. About half of the world's population is at risk of dengue with an estimated 100–400 million infections occurring each year.[485] Dengue currently is endemic in more than 100 countries with strongly growing incidence.[486] Traditional methods for dengue virus detection are based on virus isolation in cell culture, serological assays, and molecular techniques.[487] Emerging diagnostic biosensor technologies, including POC approaches, specifically focusing on dengue virus infection have been reviewed previously by Eivazzadeh-Keihan *et al.* or Darwish *et al.*[488,489] Other viral mosquito-borne pathogens and diseases, mainly found in tropical and subtropical areas, include Lymphatic filariasis, Chikungunya virus (CHIKV), Zika virus (ZIKV), Yellow fever, Japanese encephalitis and West Nile viruses (listed according to global health significance).[478] Review articles discussing microfluidic and biosensor devices for virus detection from a more general perspective generally also include tropical viruses such as DENV, ZIKV or CHIKV.[96,120]

Malaria, caused by the parasite *Plasmodium*, remains one of the most important vector-borne infectious diseases worldwide. This disease will therefore be discussed more extensively in a separate section. In the following, we first introduce systems for the detection of panels of fever-causing tropical pathogens and then discuss a selection of recent microfluidic or chip-based diagnostic systems for viral and bacterial vector-borne diagnostics. Table 7 provides an overview.

Table 7 Selection of recent microfluidic devices for VBI-related pathogen detection

| Analyte | Device and assay principle | Performance indications | Ref. |
|---|---|---|---|
| ***Microfluidic platforms and devices for viral vector-borne diseases*** | | | |
| 12-plex panel of fever-causing pathogens | LoaD platform for diagnosis of febrile illnesses | Tested with biobanked clinical samples. POC detection of coinfection within 2 h | 76 |
| 8 vector-borne viruses | Real-time or colorimetric LAMP assays on a self-powered microfluidic chip | LOD 50–500 plasmid copies per μL, 50 min | 490 |
| DENV, ZIKV, CHIKV and SARS-CoV-2 antibodies | Multiplex immunoassay platform incorporating a functionalized bead line array | Vacuum-driven fluid transfer. Chip with staggered herringbone micromixer. Test within 30 min | 491 |
| ZIKV RNA or virus | Modular design for sample pre-processing and LAMP. Spatial signal distribution readout | <32 min to distinguish pos/neg samples. LOD 2.7 × $10^2$ RNA copies per μl (buffer) | 492 |
| ZIKV | LAMP assay chip with successive chambers and oil-filled valving sections | LOD $10^2$ copies per mL (ZIKV spiked plasma), within 40 min | 493 |
| DENV | Paper origami/polymer device for a multiplex LAMP-based assay | Detection of 4 DENV serotypes, within 30 min (serum) | 494 |
| DENV, ZIKV, CHIKV | Lab-on-paper in LFA format for all-in-one molecular diagnostics | Multiplex detection of 3 viruses, within 60 min (serum) | 495 |
| CHIKV IgM | Paper-based device with CHIKV pseudo-particles for antibody capture | CHIKV IgM detected within <10 min (serum) | 496 |
| ***Microfluidic methods for Lyme disease diagnosis*** | | | |
| Lyme-specific antibodies | Plasmonic biochip with antigen spot array for multiplex target screening | LOD in the fM range (clinical serum) | 497 |
| Lyme-specific antibodies | Paper-based multiplexed serodiagnostic test for early-stage Lyme disease | Sensing array with 7 *Borrelia* antigens. Machine learning based colorimetric detection | 498, 499 |
| Lyme-specific antibodies and biomarkers | Multiplexed serologic tests in microfluidic cassette functionalized with *Borrelia* proteins | Diagnosis of early and late Lyme disease using panels of clinical serum samples | 500 |

### 8.2 Microfluidic platforms enabling the detection of panels of fever-causing pathogens

Efficient management of febrile tropical illnesses, including patients presenting non-specific fever or fever with unknown origin, is a significant health care challenge.[501,502] The availability of fast infection-specific true POC diagnostic tests, in particular for malaria and dengue, is indispensable to avoid presumptive therapy. Diagnostics of vector-borne infections and febrile illnesses in general, would greatly benefit from POC devices enabling the detection of wide panels of relevant pathogen simultaneously, by this reducing the important risk of misdiagnosis. Nonvector-borne emerging or reemerging tropical viruses, for instance the Ebola virus, could be included in the panel of fever-causing pathogens. Mitsakakis *et al.* elaborated a comprehensive review covering (commercial) diagnostic technologies and platforms for tackling febrile illness, including vector-borne diseases.[108] The chip-based NAAT assay VereFever™ (VerePLEX™ Biosystem Veredus Laboratories, Singapore) is an example for a commercial approach that was designed for multiplex detection of a panel of viral pathogens (including DENV serotypes, ZIKV, CHIKV and others), as well as *Plasmodium* spp for malaria detection. Tan *et al.* evaluated the system performance and found a detection range from 250 to 4 × $10^7$ PFU for CHIKV.[503]

Hin *et al.* presented the FeverDisk platform, a LabDisk-format centrifugal device designed for differential diagnosis of tropical febrile illness with unknown origin.[76] The platform enables simultaneous detection of a 12-plex panel of different infectious fever-causing pathogens, including several arboviruses collected during epidemics outbreaks (dengue, chikungunya), bacteria (*e.g. Salmonella*), and malaria parasite species. FeverDisk assays feature fully-automated integrated magnetic bead-based DNA purification and LAMP with fluorescence detection. Thanks to pre-stored reagents on the disc, only a single manual pipetting step for sample addition was required, providing fully integrated sample-to-answer operation. To validate POC capabilities of the device, two test series in African reference laboratories have been conducted with different types of biobanked or bacterial culture samples. Assays were performed in a total run time of less than two hours and in good agreement with reference method results. Malaria infections could be successfully confirmed in malaria-positive whole blood samples on a very short time scale. Likewise, the system confirmed different viral infections and co-infections. The analytical sensitivity of salmonella species was determined in a separate test series using cultured samples.[76] The same authors also adapted this technology for vector monitoring (VectorDisk), *i.e.* for identifying mosquito and malaria parasite species, as well as insecticide resistance mechanisms.[504]

Yao *et al.* proposed a microfluidic RT-LAMP chip for multiplex detection of eight vector-borne viruses (DENV serotypes, CHIKV, yellow fever virus, Rift Valley fever, Japanese encephalitis virus). Rapid self-powered sample loading was achieved by PDMS-film vacuum pumping. Detection was either based on real-time LAMP or colorimetric read-out. The whole analysis could be completed in 50 min. The system was tested with human blood serum samples and infected mosquito samples.[490] Moutallier *et al.* used a

 

commercial microfluidic digital PCR system (Biomark™ HD, Standard BioTools, USA) for high-throughput detection of 64 mosquito-borne viruses in pools of mosquitoes from ZIKV endemic/epidemic areas.[505]

### 8.3 Microfluidic approaches for viral vector-borne human diseases

**Lab-on-a-chip systems for detection of arboviruses.** Commercial benchtop microfluidic systems for arbovirus detection are under development or available on the market. As an example, the ViroTrack™ (Blusense Diagnostics, Demark) is a system that has been designed for dengue or Zika biomarker detection with sample-to-answer in 15 min, possibly with multiplex operation. The microfluidic cartridge separates plasma from whole blood by centrifugation. The opto-magnetic readout technique of the on-chip immuno-magnetic assays that takes advantage of light scattering by rotating nanoparticle chains. The system has been evaluated by recently in several clinical studies.[506,507]

Ganguli *et al.* used a microfluidic diagnostics card with multiplex capability (ZIKV, DENV, CHIV) for detection of ZIKV in spiked whole human blood. The device comprises a sample PDMS preparation module and a second silicon chip module for the RT-LAMP assay. The integrated system allowed for hands-free sample processing and smartphone detection with a LOD corresponding to $1.56 \times 10^5$ PFU $mL^{-1}$ for ZIKV within 35 min.[508] Lee *et al.* designed a PDMS microfluidic chip inspired by conventional LFAs for multiplex one-step immunoassay detection (including DENV, ZIKV, CHIKV and SARS-CoV-2 biomarkers). Microfluidic on-chip components comprise a dried reagent storage chamber, a passive micromixer, and a vacuum-driven fluid transfer void. Self-assembled lines of functionalized polystyrene microbeads served as antigen or antibody capture/detection zones. Various biomarker combinations have been tested to demonstrate the versatility of the approach.[491]

An interesting assay for arbovirus detection was based isothermal amplification of ZIKV cDNA using padlock probes and RCA, combined with a bead-based microfluidic affinity chromatography enrichment platform.[509] Jankelow *et al.* implemented LAMP assays for ZIKV detection from whole blood samples in a 3D printed microfluidic cartridge. The cartridge consists of two separate modules, involving several manual operations for mixing and other fluidic handling steps. A drop of unprocessed whole blood was introduced in the first module where viral RNA was released by chemical lysis and mixed with RT-LAMP reagents. The preprocessed sample solutions were then pipetted into the RT-LAMP reaction module, comprising parallel microfluidic compartments for spatial analysis of early fluorescent events of positive samples *via* smartphone real-time readout. A LOD of $2.7 \times 10^2$ viral RNA copies per μL (buffer) and $10^3$ virus particles (in a 12.5 μl blood droplet) was determined. Discrimination of positive/negative samples was possible in less than 32 min.[492] A LOC platform detected ZIKV within 40 min in spiked human plasma samples and a LOD of $10^2$ copies per mL (spiked ZIKV nucleic acid plasma samples). The chip design featured successive reaction/washing and oil-filled valving chambers for automated sample transport by magnetic actuation, sequential on-chip assay steps, LAMP and colorimetric detection.[493] In another approach, chitosan-modified $SiO_2$ capillaries were embedded in a PDMS chip for on-chip sample lysis, ZIKV RNA enrichment and *in situ* RT-PCR amplification. A LOD of 50 TU (transduction units) per mL was reported with virus-like particles containing the ZIKV RNA sequences spiked in human raw saliva samples.[510]

**Paper-based devices for arbovirus detection.** Several immunochromatographic LFAs for rapid DENV diagnosis are available on the market, mainly based on the NS1 (nonstructural protein 1) antigen, which is detectable during the acute phase of DENV infections, or on IgG/IgM antibody detection.[511–513] Over the last years, a host of microfluidic paper devices and biosensors has been developed for improved detection of DENV, ZIKV or other flaviviruses. Only a few examples will be discussed here. For instance, Biswas *et al.* implemented an integrated paper-mediated sample processing workflow for multiplex detection of four DENV serotypes on a multilayered paper-origami/polymer device (Fig. 8a). The protocol took 30 min, comprising nucleic acid isolation, isothermal amplification and colorimetric detection. The approach was validated with clinical human blood serum.[494] Seok *et al.* demonstrated a lateral flow type device for RT-LAMP molecular diagnostics of multiple viral RNAs from human serum (DENV, ZIKV, CHIKV). The whole process of nucleic acid testing was integrated on the lab-on-paper strip with an assay time of 60 min.[495] Another paper microfluidic ZIKV RT-LAMP assay was carried out on a simple capillary flow channel that filters contaminants in the ZIKV RNA-spiked sample matrices (human urine or human blood plasma). RT-LAMP and colorimetric smartphone detection was selectively performed on the circular end of the strip. Detection time was a fast as 15 min with a LOD of 1 ZIKV RNA copy per μL.[514] Shehata Draz *et al.* implemented a nanoparticle signal amplification technology on a paper microchip with a screen-printed graphene-silver electrode for electrical sensing. A change in conductivity of the sample solution is observed upon the release of charged molecules by the ZIKV-nanoparticle complex.[515] Theillet *et al.* designed a laser-cut glass-fiber chip using chikungunya pseudo-particles and virus-like particles as alternative antigens to the viral lysates as proof-of-concept for CHIKV IgM serology. Colorimetric detection of CHIKV IgM in human sera was possible in less than 10 min.[496]

### 8.4 Microfluidic methods for Lyme disease diagnosis

The Sofia 2 Lyme FIA (QuidelOrtho, USA) is a commercially available immunofluorescence LFA for rapid detection of human IgM and IgG antibodies to *B. burgdorferi*. Flynn *et al.*

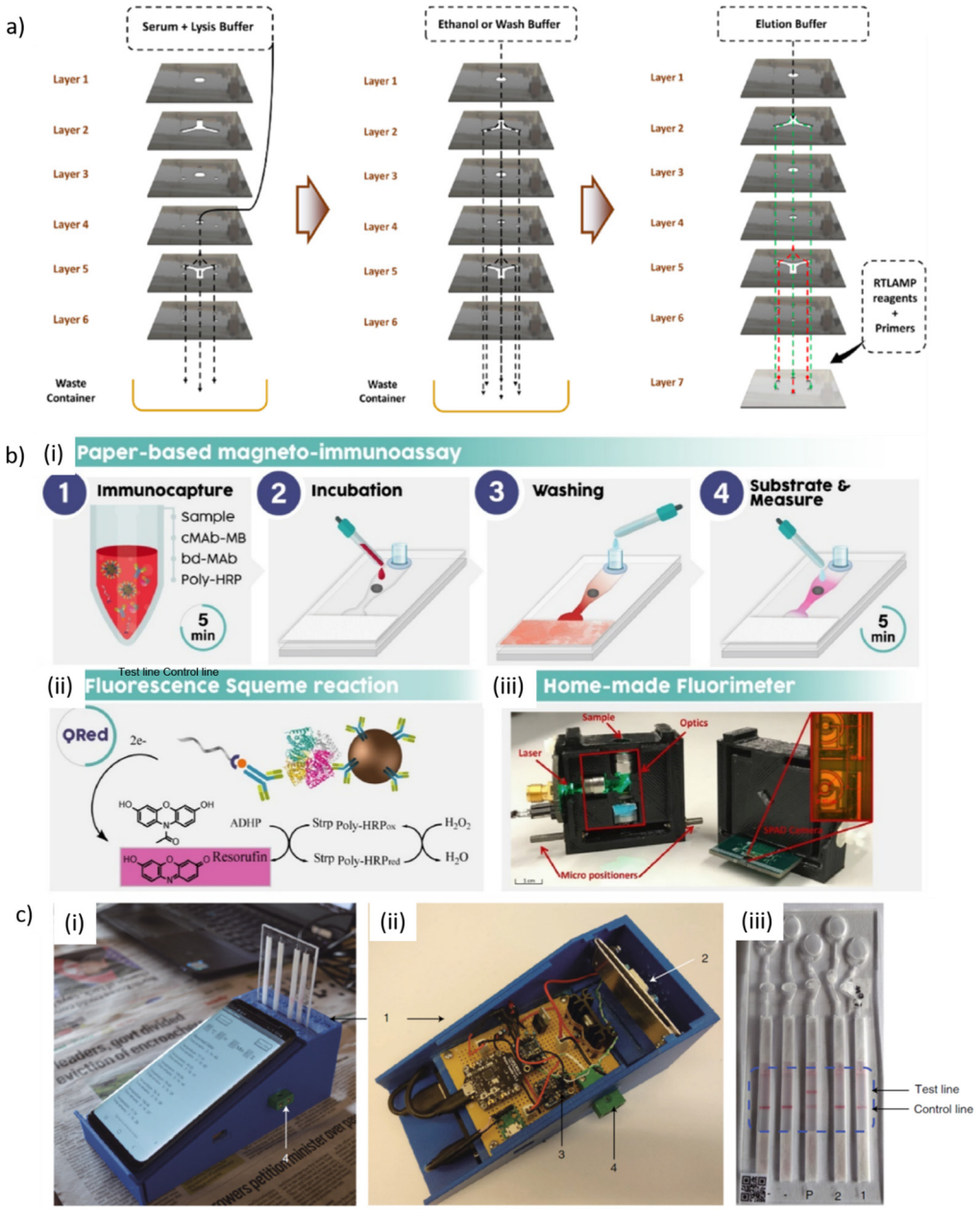


**Fig. 8** a) Schematic of the working principle of an origami-based paper device. The flow of the buffers is described with arrows. Layers 1–3 were made of Whatman 1 filter paper, except for the fact that the central region on layer 4 was constituted of a piece of a glass fiber filter membrane with a diameter of 5 mm for RNA extraction. Layer 5 consisted of a Y-shaped paper disc at the center and three pieces of 3 mm Whatman 1 filter paper circles in the periphery. These paper materials were sandwiched by a laminating film. Layer 6 was made of a double-sided adhesive tape, and six pieces of 3 mm Whatman 1 filter paper discs were sandwiched between the two layers of the adhesive film. Holes were created on two sides of the laminating film, and the upper layer of the adhesive film allowed the liquid to flow from layers 4 to 6. Layer 7 was made of PDMS to execute the LAMP reaction. Once the filter paper discs in layer 6 got wetted by the solution flowing from the above layers, the adhesive film got peeled off and pasted onto layer 7. An RT-LAMP reagent was added directly onto layer 7 for amplification and visualization of the result on top of the portable isothermal heating device. b) (i) Schematic representation of a single-step magneto-immunoassay operated using partial automation and based on a paper strip, in which magnetic particles washing, concentration and fluorescent detection are performed directly on-chip. (ii) Fluorescent reaction product catalyzed by the poly-HRP enzyme using a substrate (QuantaRed). (iii) Portable fluorimeter used for detection. c) Design of smartphone-based malaria detection. (i) The assembled device, showing the phone used to supply power, control the assay conditions (on/off, start/stop and temperature), collect results, communicate with the cloud, analyse data and provide geotagging. The diagnostic chip is shown, inserted into the heating element. The whole device, including the mobile phone, is lightweight (<500 g) and can be held in one hand, with the potential to enable diagnostics to be delivered anywhere. (ii) Open section view of the device and associated circuit. The numbered parts, respectively, are (1) the casing and main body of the device, (2) the aluminium band for receiving the diagnostic device and conducting heat for the nucleic acid amplification assay, (3) circuit components including a microcontroller, heater controller and power supply unit, and (4) the external port for thermal calibration. (iii) The plastic cartridge including a microfluidic circuit with chambers for the LAMP reaction and lateral flow strips for readout, as well as the QR code for traceability [a) reprinted with permission from ref. 494, ©2022 American Chemical Society; b) reprinted with permission from ref. 516, ©2022 Elsevier; c) reprinted with permission from ref. 517, ©2021 Springer Nature].

 

recently discussed biosensors with focus on Lyme disease.[518] Chou *et al.* presented a *B. burgdorferi* antigen microarray designed for the detection of serum antibodies in patients with active and convalescent Lyme disease. High sensitivity was achieved by plasmon-enhanced fluorescence signal detection. The approach has potential for screening of antibody targets predictive for disease status using microliter samples.[497] Joung *et al.* developed a paper-based vertical flow immunodiagnostic assay comprising a spatially-multiplexed sensing membrane containing antigens against Lyme-specific antibodies in human sera. The assay was performed in 20 min with smartphone colorimetric readout and optimized by a deep-learning diagnostic algorithm.[498,499] Arumugam *et al.* used a microfluidic platform for multiplexed serologic diagnosis of Lyme disease and screening of diagnostic biomarkers from clinical serum samples.[500] The assay was improved by selecting a panel of 12 best-performing *B. burgdorferi* proteins. Diagnosis could differentiate different stages of the disease. The protocol uses microfluidic plastic cartridges featuring distinct channels with adsorbed Lyme antigens, enabling optical detection *via* gold-labeled detection antibodies and silver amplification reagents. Diagnostic tests can be performed in 15 min thus have potential for rapid POC diagnosis.[519] Banović *et al.* took advantage of the fact that tick-borne pathogens may concentrated in the platelet fraction of blood.[520] Differential detection of tick-borne pathogens was performed in human platelets, whole blood and ticks using a commercial digital PCR system. The assay allows detecting a large panel of relevant pathogens, including 27 bacterial species.

### 8.5 Malaria

**Scope of the malaria diagnostics and reviews.** Malaria is caused by the protozoan parasite *Plasmodium* that spreads to humans through the bites of infected *Anopheles* mosquitoes.[521] The mosquitoes inoculate *Plasmodium* spp. sporozoites into the bloodstream of the mammalian host where they migrate to the liver and develop into merozoites in infected hepatocytes, initiating replication cycles with increasing parasite load.[522,523] Among *Plasmodium* species, *P. falciparum* and *P. vivax* represent the greatest risk, being the most life-threatening and the most geographically widespread, respectively.[523,524] Access to diagnosis and treatment of all suspected malaria cases is still core of the WHO's global strategy for malaria.[525] A significant concern arises from performance limitations of actual malaria POC diagnostic tests, in particular for diagnosis in young children and for the detectability of asymptomatic malaria in patients with low parasitaemia.[526] Another mayor challenge in informed patient management is to differentiate between malaria and other febrile tropical illnesses, requiring multiplex detection of co-infections by other pathogens that circulate in malaria-endemic regions.[108,527]

Three methods are commonly used for malaria diagnosis,[528,529] *i.e.* microscopy slide examination, NAATs, and immunochromatographic LFAs. Optical microscopic examination of patient blood smears remains the golden standard, allowing quantification of parasitaemia and identification of parasite species. However, these tests are often performed with suboptimal sensitivity, typically in the range a few 50–200 parasites per μL of blood.[530] NAATs owing high sensitivity and specificity are suitable for detecting very low parasitaemia.[531,532] The LOD for PCR diagnosis is in the range of 0.5–5 parasites per μL of blood. More recently, the potential of multiplex LAMP for POC malaria diagnosis has been assessed.[533] Some NAAT-based LOC systems for malaria POC diagnostics are commercially available. The VereFever™ (VerePLEX™ Biosystem, Veredus Laboratories, Singapore) designed for multiplex detection of tropical viruses, also enables differentiation of *Plasmodium* species (200 to $4 \times 10^5$ for *P. falciparum* with spiked human blood).[503] Truenat® Malaria Pv/Pf (Molbio Diagnostics, India), an on-chip real-time duplex microPCR test for *P. vivax* and *P. falciparum*, achieves a LOD comparable with PCR (<5 parasites per microlitre).[534] Malaria rapid diagnostic tests are designed for detection of *P. falciparum* histidine-rich protein 2 (*Pf*HRP2), *P. falciparum* lactase dehydrogenase (*Pf*LDH), *P. vivax* lactate dehydrogenase (*Pv*LDH), as well as for pan-pLDH and pan-aldolase antigen detection that are common to all human-infecting *Plasmodium* spp.[535,536] Jimenez *et al.* evaluated the best performance of RTDs and determined a LOD of 0.4 to 1.6 ng $mL^{-1}$ for *Pf*HRP2 of 12.5 to 50 ng $mL^{-1}$ for *Pv*LDH ng $mL^{-1}$ for samples derived from parasite culture or isolates.[537] As an indication, Marquart *et al.* estimated an amount of $1.4 \times 10^{-13}$ g of *Pf*HRP2 produced per parasite per replication cycle.[538]

Current and emerging malaria diagnostics methods have been reviewed for instance by Mbanefo *et al.*[529] Pham *et al.* also included LOC devices and specifications of market technologies.[530] Thorne *et al.* more specifically focused on microfluidic devices for blood sample pre-concentration to facilitate malaria diagnosis.[539] Kolluri *et al.* compared three different categories of LOC approaches, *i.e.* protein tests, nucleic acid tests and cell-based malaria assays.[540] Ragavan *et al.* analysed biosensor technologies for malaria diagnosis.[541] Mitsakakis *et al.* discussed the vision of a holistic approach in malaria management, comprising differential fever diagnosis and mosquito vector monitoring.[542] Malaria diagnostics, in particular microfluidic approaches, may also probe biophysical properties for differentiating infected and non-infected red blood cells.[540,543] in the following, we discuss different categories of microfluidic devices for malaria diagnosis. Table 8 provides an overview of selected recent approaches.

**Paper-based devices for malaria antigen detection.** Arias-Alpízar *et al.* proposed a single-step *Pf*LDH magneto-immunoassay with enhanced sensitivity (Fig. 8b). The assay was partly carried out on a disposable device, featuring a simple paper sensor pad with a small magnet for concentrating the magneto-immunocomplex and fluorescence readout. The sensor provided *Pf*LDH quantification within 20 min and a LOD of 0.9 ng $mL^{-1}$

Table 8 Selection of recent microfluidic devices for malaria diagnostics

| Analyte | Device and assay principle | Performance indications | Ref. |
|---|---|---|---|
| ***Malaria antigen detection*** | | | |
| *Pf*LDH | Paper-based magneto-immunoassay with fluorescence detection | LOD 0.92 ng $mL^{-1}$, <20 min | 516 |
| *Pf*HRP2 | 3D paper immunoassay with on-chip mass spectrometry detection | Proof-of-concept, 4 test zones, LOD ≤5 nM, <10 min | 544 |
| *Pf*LDH | Aptamer-based paper-based LFA with colorimetric enzymatic detection | Proof-of-concept, LOD in nM region | 545 |
| *Pf*HRP2 | Microchannel capillary flow platform for chemiluminescence based ELISA | Autonomous sequential flow protocol LOD 8 ng $mL^{-1}$, within 20 min | 546 |
| *Pf*HRP2 | Immunoassay on capillary-driven chip with electroless Ag staining. | Ag film masks the fluorescent core of the Au labels. LOD <6 ng $mL^{-1}$, within 20 min | 547 |
| *Pf*LDH and *Pv*LDH | Polymer film-based immuno-chromatographic device | LOD 50 ng $mL^{-1}$ (*Pf*LDH) and 100 ng $mL^{-1}$ (*Pv*LDH) | 548 |
| ***LAMP-based devices with different microfluidic formats*** | | | |
| *P. falciparum*, pan-*Plasmodium* | Foldable multiplex LAMP paper device with lateral flow DNA detection | POC field-based diagnosis in <50 min, combined with deep learning for decision support | 549, 517 |
| *Plasmodium* spp., other pathogens | LoaD platform for diagnosis of febrile illnesses, including malaria | Tested with biobanked clinical samples. POC detection of coinfection within 2 h | 76 |
| *P. falciparum*, *P. vivax* | LoaD with quadruplex test capability | LOD ~0.5 parasites per μl (blood), 50 min | 550 |
| *P. falciparum* (DNA amplicons) | Diffusion-based sensing of target amplicon/bead conjugates | 3 parasites per μL (blood) detectable within 45 min without DNA extraction | 551 |

(spiked in lysed whole blood).[516] A mass-based detection strategy was implemented on a 3D μPAD, using a *Pf*HRP2 immunocomplex comprising a cleavable ionic label for paper spray mass spectrometry analysis.[544] Also, the enzymatic activity of *Pf*LDH captured on a lateral flow μPAD aptasensors was explored as means to detect this biomarker.[545] Ruiz-Vega *et al.* reported a electrochemical POC paper device for quantitative detection of *Pf*LDH. The device featured a double-sided, screen-printed carbon electrode for detection of poly-HRP amplified magneto-immunoassays. The system detected *Pf*LDH in lysed whole blood in less than 20 min with a LOD of 200 ng $mL^{-1}$.[552] Singh *et al.* functionalized magnetic beads with two aptamers to capture simultaneously pLDH and *P. falciparum* glutamate dehydrogenase (*Pf*GDH) in serum samples. The biomarker enzymes were then detected colorimetrically on an absorbent paper wick through substrate-dependent dye-coupled reactions.[553]

**Devices with autonomous on-chip fluidic control for malaria biomarker detection.** Several LOC malaria devices mimic the flow actuation in cellulose test strips by custom-designed on-chip capillary pumps. Ghosh *et al.* reported the development of a microchannel capillary flow assay platform that performs chemiluminescence-based ELISA for the *Pf*HRP2 biomarker.[546,554] The microfluidic design of the polymer chip cartridge comprises two separate fluidic paths where enzyme-labelled detection antibodies and the chemiluminescent substrate were lyophilized, respectively. The serial arrangement of test and control spiral chambers was connected to the on-chip capillary pump for autonomous fluidic control. The test cartridge was implementing in a custom-designed smartphone analyzer together with optical detectors for assay ready out. A LOD of 8 ng $mL^{-1}$ was achieved within an assay time of 20 min. Antigen-spiked artificial serum was used as reconstituting reagent.[554] Pham *et al.* developed an immunoassay strategy based on Ag staining of Au nanoparticle conjugated detection antibodies to improve the sensitivity of malaria RDTs. Electroless Ag deposition on functionalized fluorescent beads in the presence of *Pf*HRP2 antigens resulted in an attenuation of the signal. The assay was carried out on a Si-SU8 capillary-driven microfluidic chip, comprising a sample flow channel and a perpendicular lane for bead immobilization.[547] As a cheaper alternative to conventional nitrocellulose membrane LFAs, Choi *et al.* proposed an immunochromatographic microfluidic polycarbonate film device with integrated capillary pump. This simple device used spiked blood samples for simultaneous fluorescent detection of two malaria biomarkers. The LOD was in the range of 50 to 100 ng $mL^{-1}$.[548]

**Paper microfluidics for DNA-based malaria diagnostics.** A LAMP diagnostic device for multiplex of *P. falciparum* and pan-*Plasmodium* detection assays has been developed by Reboud *et al.*[549] The microfluidic chip comprised a foldable paper origami flow unit for DNA extraction from pre-treated human blood samples and flow distribution for multiplexing. After several folding steps the paper stack sits on top of the three independent LAMP chambers to which the DNA samples were delivered and amplified. DNA amplicons were then transferred to adjacent lateral flow strips for visual colorimetric readout. An analytical sensitivity of down to 5 parasites per mL was reported (cultured samples in whole blood). The performance of the system was assessed in a field study demonstrating malaria diagnosis with a high sensitivity and an assay time of 45 min.[549] The same group implemented a similar cartridge in an autonomous smartphone DNA diagnostic platform combined with deep learning algorithms for local decision support and

 

blockchain technology for secure data management (Fig. 8c).[517] In another approach, Clément *et al.* proposed an efficient paper pad functionalization method for *P. falciparum* DNA LAMP amplification and detection by square wave voltammetry. A LOD of 0.1 parasites per μL in diluted whole blood was reported.[555]

**Lab-on-a-disc devices and other on-chip formats.** A LAMP lab-on-a-disc platform (FeverDisk) designed by Hin *et al.* for differential diagnosis of tropical febrile illness was already discussed in a previous section. Among the panel of fever-causing pathogens also *Plasmodium* spp. were detected. In the frame of test series in African reference laboratories malaria infections could be confirmed in malaria-positive whole blood samples on a very short time scale.[76] Choi *et al.* presented another small benchtop lab-on-a-disc LAMP analyzer for automated quantitative molecular diagnostics. The disc was designed for processing four samples simultaneously with 50 min turnaround time, requiring only a single pipetting step for sample input is needed. The analytical sensitivity for *P. falciparum* infected whole blood was 0.5 parasites per μl, which is low enough to identify asymptomatic patients.[550]

Polymer-based diagnostic devices for malaria have been designed for a wide range assay formats and detection methods. Colbert *et al.* used a shallow sample well in a plastic chip for smartphone-enabled particle diffusometry. In this assay, LAMP amplicons of *Plasmodium* target genes bind on 400 nm polystyrene beads. Analysing the particle diffusivity allowed for detection of low concentrations of malaria DNA from unprocessed blood samples (3 parasites per μL were detectable within 45 min).[551] Real-time fully-electronic DNA sensing of *P. falciparum* was achieved by electrochemically detecting pH changes during LAMP amplification on an ion-sensitive field-effect transistor (ISFET) sensor array incorporated in a LOC platform. Identification of drug-resistant mutations was.[556]

## Conclusion

Infectious diseases represent a serious burden on global healthcare. This situation is particularly difficult in low-resource environments where infections are highly prevalent, with a broad spectrum of different pathogens, large variations in virulence and local distribution, as well as uncontrolled transmission routes. Nevertheless, the recent COVID-19 pandemic has underscored the fact that from the perspective of an infectious agent there is only one world without traceable boundaries. In developed countries, high-resolution diagnostics are available in centralized laboratories, albeit at a high cost due to specialized settings, instrumentation, and trained personnel. Unfortunately, these barriers limit the application of such solutions in the developing world. According to WHO recommendations, the ideal diagnostic test should satisfy the ASSURED criteria, *i.e.* being affordable, sensitive, specific, user-friendly, rapid and robust, equipment-free, and deliverable. Microfluidics-based technology has the potential to meet these criteria, thereby significantly reducing healthcare diagnosis costs and opening up new diagnostic markets.

Microfluidic point-of-care (POC) diagnostics has become increasingly valuable with respect to the management of infectious diseases. Typically, this routine involves conducting diagnostic tests outside of a centralized laboratory and in close proximity to the patient. Microfluidics technology serves as an integrating force by enabling the seamless conjunction of multiple assay steps on a single disposable device. These steps include sample pre-processing and purification, signal amplification, and detection, ensuring rapid and reliable test results. Integration also facilitates the development of portable, automated, and autonomous diagnostic systems. Accurate POC diagnostic testing already supports infection control and prevention strategies, primarily through the use of rapid lateral flow immunoassays. In a broader perspective, more advanced cheap and disposable paper-based microfluidic analytical devices are of particular interest for POC detection of infectious pathogens in real-world low-resource settings.

Meeting all ASSURED characteristics within a single device without compromises remains a challenging task. Currently existing immune-reaction-based and molecular assays integrated into microfluidic systems offer relatively sensitive pathogen detection but they often require prior knowledge of the infectious strains and specific assay designs. Furthermore, critical protocol steps such as patient sample pre-processing or pathogen culture and enrichment involve laboratory-based procedures, resulting in prolonged turnaround times. In fact, many of present-day microfluidic diagnostic tools may remain at a demonstrator stage, mainly due to the challenges of skilled operation, but also because of the absence of standardized microfluidic operations. Nevertheless, the number of microfluidic cartridge-based systems on the market is increasing. As an example, the GeneXpert® systems (Cepheid, USA), designed for PCR-based POC testing of a large panel of pathologies, are widely regarded as a valuable choice on the current market. However, the platform still incurs relatively high instrumentation and assay costs, and a trained technician is needed for sample pre-processing. An emerging alternative to PCR, which has gained increasing attention over the past years, is the isothermal LAMP technology for nucleic acid amplification. LAMP protocols allow for simpler instrumentation compared to thermal cycling for PCR amplification while retaining the essential features of gold standard nucleic acid-based testing. LAMP-based assays have been successfully performed on microfluidic devices but still need further development for effective implementation in clinical settings and POC testing.

Microfluidic approaches also offer promising capabilities and perspectives in phenotypic antibiotic susceptibility testing (AST). This is of particular importance with regard to the emerging major global health threat related to fast-spreading antibiotic resistance. Informed treatment,

associated with the administration of the appropriate type and quantity of antibiotics, are crucial factors in this battle. AST protocols, which are based on differential bacterial growth in different antibiotic concentrations, reliably detect antibiotic resistance and allow for the determination of the minimum inhibitory concentration. Traditional AST methods involve time-consuming bacteria culturing with a time-to-result of up to several days, depending on the specific condition. This presents a serious bottleneck for timely diagnosis. Consequently, these methods often fail to guide medical treatment in the early stages of infection. While fast genotypic AST is possible, a detailed knowledge of the specific genetic antibiotic resistance marker to be tested is required. Shifting from conventional bacterial cultures to monitoring the growth of individual cells paves the way for rapid phenotypic AST. Microfluidic devices play a prominent role in this context by offering the possibility of confining single bacteria within microchannels or nanoliter droplets. Such devices enable the detection of changes in bacterial metabolism, morphology, or replication cycles in response to antibiotic stress with single-bacteria resolution. Single-cell technologies facilitate rapid AST protocols, with results obtained in less than 30 min. For the time being, there is a need to implement the capability to generate antibiograms within single-cell AST approaches. This can be achieved on-chip thanks to the possibility of precise fluidic control and the implementation of complex fluidic protocols. Scaling up this principle for fast multiplex phenotypic AST is an important area of current research. In general, diagnostic systems on the market provide varying levels of multiplexing capability, enabling the detection and differentiation of various infectious agents, as well as the quantification of their abundance in the mix. Additionally, the ability to process multiple patient samples simultaneously is an important feature. Unfortunately, there is usually a trade-off between high-throughput diagnostics and the extent of multiplexing, limiting the number of patient samples and/or pathogens that can be tested simultaneously. Highly integrated microfluidic systems can overcome these limitations by implementing parallel assay protocols strategies on a single chip or cartridge.

Next-generation diagnostic platforms will take advantage of optimized microfluidic designs, innovative detection schemes such as isothermal amplification or CRISPR-based assays, and potentially new functionalized nanomaterials. Screening campaigns are greatly facilitated by the use of inexpensive disposable test cartridges on portable devices, as well as large-scale POC monitoring of environmental samples for surveillance against potential health threats and infectious disease outbreaks. The convergence of wireless communication technologies with microfluidic sensors already enables instantaneous on-site monitoring, enhancing the real-time accessibility of diagnostic information. Smartphones may be used for optical detection of assay results at a remote location and seamless data transmission to centralized facilities. This integration of microfluidic and information technologies holds promise for enhancing the versatility, reliability, and widespread adoption of POC testing across diverse geographic regions. Recent advancements in medical informatics and data processing are expected to further support the efficiency and effectiveness of novel microfluidic diagnostic tools. Artificial intelligence algorithms will enable advanced analysis of large datasets, leading to diagnostics with improved prediction capabilities. Upcoming trends certainly also focus on personalized medicine initiatives, tailoring microfluidic systems to individual patient needs and contributing to precision medicine approaches. Additionally, the establishment of standardized protocols and quality control is necessary to facilitate regulatory approval and promote the implementation of microfluidic-based diagnostics in clinical settings. These steps are crucial for guiding the future development of microfluidics-based infectious disease diagnostics and harnessing the vast potential of microfluidics to address emerging healthcare challenges.

## Conflicts of interest

There are no conflicts of interest to declare.

## Acknowledgements

Support to this work was provided by the École Polytechnique Fédérale de Lausanne.

## References

1 R. E. Baker, A. S. Mahmud, I. F. Miller, M. Rajeev, F. Rasambainarivo, B. L. Rice, S. Takahashi, A. J. Tatem, C. E. Wagner, L.-F. Wang, A. Wesolowski and C. J. E. Metcalf, *Nat. Rev. Microbiol.*, 2022, **20**, 193–205.
2 K. B. Patterson and T. Runge, *Am. J. Med. Sci.*, 2002, **323**, 216–222.
3 J. K. Taubenberger and D. M. Morens, *Emerging Infect. Dis.*, 2006, **12**, 15–22.
4 D. Flecknoe, B. Charles Wakefield and A. Simmons, *Med. Confl. Surviv.*, 2018, **34**, 61–68.
5 K. F. Smith, M. Goldberg, S. Rosenthal, L. Carlson, J. Chen, C. Chen and S. Ramachandran, *J. R. Soc., Interface*, 2014, **11**, 20140950.
6 A. Cassini, E. Colzani, A. Pini, M.-J. J. Mangen, D. Plass, S. A. McDonald, G. Maringhini, A. van Lier, J. A. Haagsma, A. H. Havelaar, P. Kramarz, M. E. Kretzschmar and on behalf of the Bc. Consortium, *Eurosurveillance*, 2018, **23**, 17.
7 GBD 2019 Diseases and Injuries Collaborators, *Lancet*, 2020, **396**, 1204–1222.
8 WHO Coronavirus (COVID-19) Dashboard, **https://covid19.who.int**, (accessed 5 January 2024).
9 I. Bates, C. Fenton, J. Gruber, D. Lalloo, A. M. Lara, S. B. Squire, S. Theobald, R. Thomson and R. Tolhurst, *Lancet Infect. Dis.*, 2004, **4**, 267–277.

 

10 I. Bates, C. Fenton, J. Gruber, D. Lalloo, A. M. Lara, S. B. Squire, S. Theobald, R. Thomson and R. Tolhurst, *Lancet Infect. Dis.*, 2004, **4**, 368–375.
11 Z. A. Bhutta, J. Sommerfeld, Z. S. Lassi, R. A. Salam and J. K. Das, *Infect. Dis. Poverty*, 2014, **3**, 21.
12 H.-B. Weng, H.-X. Chen and M.-W. Wang, *Infect. Dis. Poverty*, 2018, **7**, 67.
13 C. Guo, Z. Zhou, Z. Wen, Y. Liu, C. Zeng, D. Xiao, M. Ou, Y. Han, S. Huang, D. Liu, X. Ye, X. Zou, J. Wu, H. Wang, E. Y. Zeng, C. Jing and G. Yang, *Front. Cell. Infect. Microbiol.*, 2017, **7**, 317.
14 C. E. M. Coltart, B. Lindsey, I. Ghinai, A. M. Johnson and D. L. Heymann, *Philos. Trans. R. Soc., B*, 2017, **372**, 20160297.
15 R. Balasubramanian, J. Im, J.-S. Lee, H. J. Jeon, O. D. Mogeni, J. H. Kim, R. Rakotozandrindrainy, S. Baker and F. Marks, *Hum. Vaccines Immunother.*, 2019, **15**, 1421–1426.
16 D. E. Bloom and D. Cadarette, *Front. Immunol.*, 2019, **10**, 549.
17 WHO (ID 2023) Disease Outbreak News, **https://www.who.int/emergencies/disease-outbreak-news**, (accessed 5 January 2024).
18 C. Caminade, K. M. McIntyre and A. E. Jones, *Ann. N. Y. Acad. Sci.*, 2019, **1436**, 157–173.
19 N. E. Nnadi and D. A. Carter, *PLoS Pathog.*, 2021, **17**, e1009503.
20 J. T. Ladner, N. D. Grubaugh, O. G. Pybus and K. G. Andersen, *Nat. Med.*, 2019, **25**, 206–211.
21 S. Plotkin, *Proc. Natl. Acad. Sci. U. S. A.*, 2014, **111**, 12283–12287.
22 WHO Vaccines, **https://www.who.int/teams/immunization-vaccines-and-biologicals/diseases**, (accessed 3 February 2024).
23 M. B. Laurens, *Hum. Vaccines Immunother.*, 2020, **16**, 480–489.
24 N. Aderinto, G. Olatunji, E. Kokori, S. Sikirullahi, J. E. Aboje and R. E. Ojabo, *Malar. J.*, 2024, **23**, 16.
25 M. Brisse, S. M. Vrba, N. Kirk, Y. Liang and H. Ly, *Front. Immunol.*, 2020, **11**, 583077.
26 J.-L. Excler, M. Saville, S. Berkley and J. H. Kim, *Nat. Med.*, 2021, **27**, 591–600.
27 F. Wong, C. De La Fuente-Nunez and J. J. Collins, *Science*, 2023, **381**, 164–170.
28 D. M. P. De Oliveira, B. M. Forde, T. J. Kidd, P. N. A. Harris, M. A. Schembri, S. A. Beatson, D. L. Paterson and M. J. Walker, *Clin. Microbiol. Rev.*, 2020, **33**, e00181-19.
29 A. S. Lee, H. de Lencastre, J. Garau, J. Kluytmans, S. Malhotra-Kumar, A. Peschel and S. Harbarth, *Nat. Rev. Dis. Primers*, 2018, **4**, 18033.
30 Antimicrobial Resistance Collaborators, *Lancet*, 2022, **399**, 629–655.
31 C. Lange, R. E. Aarnoutse, J. W. C. Alffenaar, G. Bothamley, F. Brinkmann, J. Costa, D. Chesov, R. van Crevel, M. Dedicoat, J. Dominguez, R. Duarte, H. P. Grobbel, G. Günther, L. Guglielmetti, J. Heyckendorf, A. W. Kay, O. Kirakosyan, O. Kirk, R. A. Koczulla, G. G. Kudriashov, L. Kuksa, F. van Leth, C. Magis-Escurra, A. M. Mandalakas, B. Molina-Moya, C. A. Peloquin, M. Reimann, R. Rumetshofer, H. S. Schaaf, T. Schön, S. Tiberi, J. Valda, P. K. Yablonskii and K. Dheda, *Int. J. Tuberc Lung Dis.*, 2019, **23**, 645–662.
32 C. Llor, A. Moragas, C. Bayona, J. M. Cots, J. M. Molero, J. Ribas, J. F. Fóthy, I. Gutiérrez, C. Sánchez, J. Ortega, J. Arranz, J. Botanes and P. Robles, *BMJ Open*, 2017, **7**, e015814.
33 S. G. Llanos-Soto, N. Vezeau, M. Wemette, E. Bulut, A. Greiner Safi, P. Moroni, M. A. Shapiro and R. Ivanek, *Prev. Vet. Med.*, 2021, **188**, 105253.
34 E. Tacconelli, F. Sifakis, S. Harbarth, R. Schrijver, M. van Mourik, A. Voss, M. Sharland, N. B. Rajendran, J. Rodríguez-Baño, J. Bielicki, M. de Kraker, S. Gandra, P. Gastmeier, K. Gilchrist, A. Gikas, B. P. Gladstone, H. Goossens, H. Jafri, G. Kahlmeter, F. Leus, C. Luxemburger, S. Malhotra-Kumar, G. Marasca, M. McCarthy, M. D. Navarro, M. Nuñez-Nuñez, A. Oualim, J. Price, J. Robert, H. Sommer, M. von Cube, C. Vuong, I. Wiegand, A. T. Witschi and M. Wolkewitz, *Lancet Infect. Dis.*, 2018, **18**, e99–e106.
35 R. Laxminarayan, A. Duse, C. Wattal, A. K. M. Zaidi, H. F. L. Wertheim, N. Sumpradit, E. Vlieghe, G. L. Hara, I. M. Gould, H. Goossens, C. Greko, A. D. So, M. Bigdeli, G. Tomson, W. Woodhouse, E. Ombaka, A. Q. Peralta, F. N. Qamar, F. Mir, S. Kariuki, Z. A. Bhutta, A. Coates, R. Bergstrom, G. D. Wright, E. D. Brown and O. Cars, *Lancet Infect. Dis.*, 2013, **13**, 1057–1098.
36 A. van Belkum and W. M. Dunne, *J. Clin. Microbiol.*, 2013, **51**, 2018–2024.
37 A. van Belkum, T. T. Bachmann, G. Lüdke, J. G. Lisby, G. Kahlmeter, A. Mohess, K. Becker, J. P. Hays, N. Woodford, K. Mitsakakis, J. Moran-Gilad, J. Vila, H. Peter, J. H. Rex and W. M. Dunne, *Nat. Rev. Microbiol.*, 2019, **17**, 51–62.
38 S. Puttaswamy, S. K. Gupta, H. Regunath, L. P. Smith and S. Sengupta, *Arch. Clin. Microbiol.*, 2018, **09**(3), 83.
39 S. H. Needs, S. I. Donmez, S. P. Bull, C. McQuaid, H. M. I. Osborn and A. D. Edwards, *Front. Mech. Eng.*, 2020, **6**, 73.
40 N. Qin, P. Zhao, E. A. Ho, G. Xin and C. L. Ren, *ACS Sens.*, 2021, **6**, 3–21.
41 B. Behera, G. K. Anil Vishnu, S. Chatterjee, V. S. N. Sitaramgupta V, N. Sreekumar, A. Nagabhushan, N. Rajendran, B. H. Prathik and H. J. Pandya, *Biosens. Bioelectron.*, 2019, **142**, 111552.
42 G. Maugeri, I. Lychko, R. Sobral and A. C. A. Roque, *Biotechnol. J.*, 2019, **14**, 1700750.
43 A. J. Trotter, A. Aydin, M. J. Strinden and J. O'Grady, *Curr. Opin. Microbiol.*, 2019, **51**, 39–45.
44 P. Yager, T. Edwards, E. Fu, K. Helton, K. Nelson, M. R. Tam and B. H. Weigl, *Nature*, 2006, **442**, 412–418.
45 N. P. Pai, C. Vadnais, C. Denkinger, N. Engel and M. Pai, *PLoS Med.*, 2012, **9**, e1001306.
46 S. Ombelet, J.-B. Ronat, T. Walsh, C. P. Yansouni, J. Cox, E. Vlieghe, D. Martiny, M. Semret, O. Vandenberg, J. Jacobs, O. Lunguya, M.-F. Phoba, P. Lompo, T. Phe, S. Kariuki, P. N. Newton, D. A. B. Dance, C. Muvunyi, S. El Safi, B. Barbe, D. Falay, D. Affolabi, M. Page, C. Langendorf, Y. Gille, T.

Leenstra, J. Stelling, T. Naas, T. Kesteman, D. Seifu, E. Delarocque-Astagneau, C. Schultsz, H. Schutt-Gerowitt, J. Letchford, H. Wertheim, G. Kahlmeter and A. Aidara Kane, *Lancet Infect. Dis.*, 2018, **18**, e248–e258.
47 S. Bistafa, *Rev. Bras. Ensino Fis.*, 2017, **40**, e2603.
48 J. P. Brody, P. Yager, R. E. Goldstein and R. H. Austin, *Biophys. J.*, 1996, **71**, 3430–3441.
49 E. M. Purcell, *Am. J. Phys.*, 1977, **45**, 3–11.
50 C.-Y. Lee and L.-M. Fu, *Sens. Actuators, B*, 2018, **259**, 677–702.
51 A. Olanrewaju, M. Beaugrand, M. Yafia and D. Juncker, *Lab Chip*, 2018, **18**, 2323–2347.
52 T. Thorsen, R. W. Roberts, F. H. Arnold and S. R. Quake, *Phys. Rev. Lett.*, 2001, **86**, 4163–4166.
53 J. Zhang, S. Yan, D. Yuan, G. Alici, N.-T. Nguyen, M. Ebrahimi Warkiani and W. Li, *Lab Chip*, 2016, **16**, 10–34.
54 T. M. Squires and S. R. Quake, *Rev. Mod. Phys.*, 2005, **77**, 977–1026.
55 G. M. Whitesides, *Nature*, 2006, **442**, 368–373.
56 M. A. Unger, H.-P. Chou, T. Thorsen, A. Scherer and S. R. Quake, *Science*, 2000, **288**, 113–116.
57 T. Thorsen, S. J. Maerkl and S. R. Quake, *Science*, 2002, **298**, 580–584.
58 J. Melin and S. R. Quake, *Annu. Rev. Biophys. Biomol. Struct.*, 2007, **36**, 213–231.
59 K. Zhang, S. Qin, S. Wu, Y. Liang and J. Li, *Chem. Sci.*, 2020, **11**, 6352–6361.
60 A. Burmeister and A. Grünberger, *Curr. Opin. Biotechnol.*, 2020, **62**, 106–115.
61 F. J. H. Hol and C. Dekker, *Science*, 2014, **346**, 1251821.
62 M. Cornaglia, T. Lehnert and M. A. M. Gijs, *Lab Chip*, 2017, **17**, 3736–3759.
63 M. A. M. Gijs, F. Lacharme and U. Lehmann, *Chem. Rev.*, 2010, **110**, 1518–1563.
64 M. T. Guo, A. Rotem, J. A. Heyman and D. A. Weitz, *Lab Chip*, 2012, **12**, 2146.
65 L. Shang, Y. Cheng and Y. Zhao, *Chem. Rev.*, 2017, **117**, 7964–8040.
66 T. S. Kaminski and P. Garstecki, *Chem. Soc. Rev.*, 2017, **46**, 6210–6226.
67 Y. Ding, P. D. Howes and A. J. deMello, *Anal. Chem.*, 2020, **92**, 132–149.
68 K. Matuła, F. Rivello and W. T. S. Huck, *Adv. Biosyst.*, 2020, **4**, 1900188.
69 H. Song, M. R. Bringer, J. D. Tice, C. J. Gerdts and R. F. Ismagilov, *Appl. Phys. Lett.*, 2003, **83**, 4664–4666.
70 P. C. Gach, K. Iwai, P. W. Kim, N. J. Hillson and A. K. Singh, *Lab Chip*, 2017, **17**, 3388–3400.
71 J. Sánchez Barea, J. Lee and D.-K. Kang, *Micromachines*, 2019, **10**, 412.
72 O. Strohmeier, M. Keller, F. Schwemmer, S. Zehnle, D. Mark, F. von Stetten, R. Zengerle and N. Paust, *Chem. Soc. Rev.*, 2015, **44**, 6187–6229.
73 J. Ducrée, *Microsyst. Nanoeng.*, 2021, **7**, 104.
74 C. M. Miyazaki, E. Carthy and D. J. Kinahan, *Processes*, 2020, **8**, 1360.
75 V. Sunkara, S. Kumar, J. Sabaté Del Río, I. Kim and Y.-K. Cho, *Acc. Chem. Res.*, 2021, **54**, 3643–3655.
76 S. Hin, B. Lopez-Jimena, M. Bakheit, V. Klein, S. Stack, C. Fall, A. Sall, K. Enan, M. Mustafa, L. Gillies, V. Rusu, S. Goethel, N. Paust, R. Zengerle, S. Frischmann, M. Weidmann and K. Mitsakakis, *PLoS Neglected Trop. Dis.*, 2021, **15**, e0009177.
77 E. B. Bahadır and M. K. Sezgintürk, *TrAC, Trends Anal. Chem.*, 2016, **82**, 286–306.
78 V.-T. Nguyen, S. Song, S. Park and C. Joo, *Biosens. Bioelectron.*, 2020, **152**, 112015.
79 Y. Liu, L. Zhan, Z. Qin, J. Sackrison and J. C. Bischof, *ACS Nano*, 2021, **15**, 3593–3611.
80 H. Sohrabi, M. R. Majidi, M. Fakhraei, A. Jahanban-Esfahlan, M. Hejazi, F. Oroojalian, B. Baradaran, M. Tohidast, M. D. L. Guardia and A. Mokhtarzadeh, *Talanta*, 2022, **243**, 123330.
81 E. Fu and C. Downs, *Lab Chip*, 2017, **17**, 614–628.
82 A. W. Martinez, S. T. Phillips, G. M. Whitesides and E. Carrilho, *Anal. Chem.*, 2010, **82**, 3–10.
83 L. Magro, C. Escadafal, P. Garneret, B. Jacquelin, A. Kwasiborski, J.-C. Manuguerra, F. Monti, A. Sakuntabhai, J. Vanhomwegen, P. Lafaye and P. Tabeling, *Lab Chip*, 2017, **17**, 2347–2371.
84 J. Ma, S. Yan, C. Miao, L. Li, W. Shi, X. Liu, Y. Luo, T. Liu, B. Lin, W. Wu and Y. Lu, *Adv. Healthcare Mater.*, 2019, **8**, 1801084.
85 E. Noviana, T. Ozer, C. S. Carrell, J. S. Link, C. McMahon, I. Jang and C. S. Henry, *Chem. Rev.*, 2021, **121**, 11835–11885.
86 X. Qin, J. Liu, Z. Zhang, J. Li, L. Yuan, Z. Zhang and L. Chen, *TrAC, Trends Anal. Chem.*, 2021, **143**, 116371.
87 A. M. Caliendo, D. N. Gilbert, C. C. Ginocchio, K. E. Hanson, L. May, T. C. Quinn, F. C. Tenover, D. Alland, A. J. Blaschke, R. A. Bonomo, K. C. Carroll, M. J. Ferraro, L. R. Hirschhorn, W. P. Joseph, T. Karchmer, A. T. MacIntyre, L. B. Reller, A. F. Jackson and for the Infectious Diseases Society of America (IDSA), *Clin. Infect. Dis.*, 2013, **57**, S139–S170.
88 S. Sachdeva, R. W. Davis and A. K. Saha, *Front. Bioeng. Biotechnol.*, 2021, **8**, 602659.
89 A. Cassedy, A. Parle-McDermott and R. O'Kennedy, *Front. Mol. Biosci.*, 2021, **8**, 637559.
90 C. Deusenbery, Y. Wang and A. Shukla, *ACS Infect. Dis.*, 2021, **7**, 695–720.
91 B. Purohit, P. R. Vernekar, N. P. Shetti and P. Chandra, *Sens. Int.*, 2020, **1**, 100040.
92 F. Huang, Y. Zhang, J. Lin and Y. Liu, *Biosensors*, 2021, **11**, 190.
93 S. M. Yoo and S. Y. Lee, *Trends Biotechnol.*, 2016, **34**, 7–25.
94 O. Simoska and K. J. Stevenson, *Analyst*, 2019, **144**, 6461–6478.
95 E. Cesewski and B. N. Johnson, *Biosens. Bioelectron.*, 2020, **159**, 112214.
96 K. Y. Goud, K. K. Reddy, A. Khorshed, V. S. Kumar, R. K. Mishra, M. Oraby, A. H. Ibrahim, H. Kim and K. V. Gobi, *Biosens. Bioelectron.*, 2021, **180**, 113112.

 

97 D. Gao, X. Guo, Y. Yang, H. Shi, R. Hao, S. Wang, Z. J. Li, R. Zhao and H. Song, *J. Biol. Eng.*, 2022, **16**, 33.
98 M. De Falco, M. De Felice, F. Rota, D. Zappi, A. Antonacci and V. Scognamiglio, *TrAC, Trends Anal. Chem.*, 2022, **148**, 116538.
99 I. M. Artika, Y. P. Dewi, I. M. Nainggolan, J. E. Siregar and U. Antonjaya, *Genes*, 2022, **13**, 2387.
100 L. Becherer, N. Borst, M. Bakheit, S. Frischmann, R. Zengerle and F. von Stetten, *Anal. Methods*, 2020, **12**, 717–746.
101 Y. Shang, J. Sun, Y. Ye, J. Zhang, Y. Zhang and X. Sun, *Crit. Rev. Food Sci. Nutr.*, 2020, **60**, 201–224.
102 Y. Bai, J. Ji, F. Ji, S. Wu, Y. Tian, B. Jin and Z. Li, *Talanta*, 2022, **240**, 123209.
103 S. Barreda-García, R. Miranda-Castro, N. de-los-Santos-Álvarez, A. J. Miranda-Ordieres and M. J. Lobo-Castañón, *Anal. Bioanal. Chem.*, 2018, **410**, 679–693.
104 L. Xu, J. Duan, J. Chen, S. Ding and W. Cheng, *Anal. Chim. Acta*, 2021, **1148**, 238187.
105 M. M. Kaminski, O. O. Abudayyeh, J. S. Gootenberg, F. Zhang and J. J. Collins, *Nat. Biomed. Eng.*, 2021, **5**, 643–656.
106 J. de D. Habimana, R. Huang, B. Muhoza, Y. N. Kalisa, X. Han, W. Deng and Z. Li, *Biosens. Bioelectron.*, 2022, **203**, 114033.
107 X. Wang, X.-Z. Hong, Y.-W. Li, Y. Li, J. Wang, P. Chen and B.-F. Liu, *Mil. Med. Res.*, 2022, **9**, 11.
108 K. Mitsakakis, V. D'Acremont, S. Hin, F. von Stetten and R. Zengerle, *Microelectron. Eng.*, 2018, **201**, 26–59.
109 P. P. Nelson, B. A. Rath, P. C. Fragkou, E. Antalis, S. Tsiodras and C. Skevaki, *Front. Cell. Infect. Microbiol.*, 2020, **10**, 181.
110 Cepheid|GeneXpert System, **www.cepheid.com**, (accessed 8 January 2024).
111 BioFire Diagnostics, **https://www.biofiredx.com/**, (accessed 8 January 2024).
112 VerePLEXTM Biosystem, **vereduslabs.com**, (accessed 8 January 2024).
113 Bosch Vivalytic Analyser, **https://www.bosch-vivalytic.com/en/**, (accessed 1 February 2024).
114 D. Podbiel, L. Boecking, H. Bott, J. Kassel, D. Czurratis, F. Laermer, R. Zengerle and J. Hoffmann, *J. Micromech. Microeng.*, 2020, **30**, 115012.
115 Bosch Vivalytic tests, **https://www.bosch-vivalytic.com/en/tests/**, (accessed 1 February 2024).
116 Hahn-Schickard, **https://www.hahn-schickard.de/forschung-entwicklung/laborautomatisierung/labdisk-plattform**, (accessed 8 January 2024).
117 Dialunox, **https://labdiskplayer.com/**, (accessed 1 February 2024).
118 E. A. Flores-Contreras, R. B. González-González, I. P. Rodríguez-Sánchez, J. F. Yee-De León, H. M. N. Iqbal and E. González-González, *Biosensors*, 2022, **12**, 179.
119 C. Wang, M. Liu, Z. Wang, S. Li, Y. Deng and N. He, *Nano Today*, 2021, **37**, 101092.
120 A. Basiri, A. Heidari, M. F. Nadi, M. T. P. Fallahy, S. S. Nezamabadi, M. Sedighi, A. Saghazadeh and N. Rezaei, *Rev. Med. Virol.*, 2021, **31**, e2154.
121 N. Rezvani Jalal, P. Mehrbod, S. Shojaei, H. I. Labouta, P. Mokarram, A. Afkhami, T. Madrakian, M. J. Los, D. Schaafsma, M. Giersig, M. Ahmadi and S. Ghavami, *ACS Appl. Nano Mater.*, 2021, **4**, 4307–4328.
122 A. Tay, A. Pavesi, S. R. Yazdi, C. T. Lim and M. E. Warkiani, *Biotechnol. Adv.*, 2016, **34**, 404–421.
123 G. L. Damhorst, M. Murtagh, W. R. Rodriguez and R. Bashir, *Proc. IEEE*, 2015, **103**, 150–160.
124 X. Fu, J. Sun, R. Liang, H. Guo, L. Wang and X. Sun, *Trends Food Sci. Technol.*, 2021, **116**, 115–129.
125 X. Weng, C. Zhang and H. Jiang, *LWT*, 2021, **151**, 112172.
126 K. Subbarao and S. Mahanty, *Immunity*, 2020, **52**, 905–909.
127 J. P. Mizgerd, *N. Engl. J. Med.*, 2008, **358**, 716–727.
128 N. Jain, R. Lodha and S. K. Kabra, *Indian J. Pediatr.*, 2001, **68**, 1135–1138.
129 The top 10 causes of death, **https://www.who.int/news-room/fact-sheets/detail/the-top-10-causes-of-death**, (accessed 5 January 2024).
130 K. M. Robinson, J. K. Kolls and J. F. Alcorn, *Curr. Opin. Immunol.*, 2015, **34**, 59–67.
131 Influenza (Seasonal), **https://www.who.int/news-room/fact-sheets/detail/influenza-(seasonal)**, (accessed 5 January 2024).
132 G. R. S. Budinger, A. V. Misharin, K. M. Ridge, B. D. Singer and R. G. Wunderink, *J. Clin. Invest.*, 2021, **131**, e149412.
133 D. Dandachi and M. C. Rodriguez-Barradas, *J. Invest. Med.*, 2018, **66**, 957–965.
134 T. M. File, *The American Journal of Medicine Supplements*, 2004, **117**, 39–50.
135 S. Aliberti, G. S. Cook, B. L. Babu, L. F. Reyes, A. H. Rodriguez, F. Sanz, N. J. Soni, A. Anzueto, P. Faverio, R. F. Sadud, I. Muhammad, C. Prat, E. Vendrell, J. Neves, E. Kaimakamis, A. Feneley, R. Swarnakar, F. Franzetti, M. Carugati, M. Morosi, E. Monge and M. I. Restrepo, *J. Infect.*, 2019, **79**, 300–311.
136 A. de Roux, S. Ewig, E. García, M. A. Marcos, J. Mensa, H. Lode and A. Torres, *Eur. Respir. J.*, 2006, **27**, 795–800.
137 S. B. A. Sattar and S. Sharma, *Bacterial Pneumonia*, 2022, **https://www.ncbi.nlm.nih.gov/books/NBK513321**.
138 K. B. Waites, L. Xiao, Y. Liu, M. F. Balish and T. P. Atkinson, *Clin. Microbiol. Rev.*, 2017, **30**, 747–809.
139 R. N. Jones, *Clin. Infect. Dis.*, 2010, **51**, S81–S87.
140 WHO (2023) Tuberculosis (TB), **https://www.who.int/news-room/fact-sheets/detail/tuberculosis**, (accessed 5 January 2024).
141 H.-S. Huang, C.-L. Tsai, J. Chang, T.-C. Hsu, S. Lin and C.-C. Lee, *Clin. Microbiol. Infect.*, 2018, **24**, 1055–1063.
142 K. Mjøsund, M. Ghaleb, L. Kolsrud, J. Carrabre, F. Kainzinger, D. Boehm, F. Bitterling and B. Wolfarth, *Front. Sports Act. Living*, 2023, **5**, 1217463.
143 L. A. Heger, N. Elsen, M. Rieder, N. Gauchel, U. Sommerwerck, C. Bode, D. Duerschmied, M. Oette and I. Ahrens, *BMC Infect. Dis.*, 2022, **22**, 486.
144 J. Zhuang, J. Yin, S. Lv, B. Wang and Y. Mu, *Biosens. Bioelectron.*, 2020, **163**, 112291.

145 L. E. Breshears, B. T. Nguyen, S. Mata Robles, L. Wu and J.-Y. Yoon, *SLAS Technol.*, 2022, **27**, 4–17.
146 Z. Zhang, P. Ma, R. Ahmed, J. Wang, D. Akin, F. Soto, B.-F. Liu, P. Li and U. Demirci, *Adv. Mater.*, 2022, **34**, 2103646.
147 E. A. Tarim, B. Karakuzu, C. Oksuz, O. Sarigil, M. Kizilkaya, M. K. A. A. Al-Ruweidi, H. C. Yalcin, E. Ozcivici and H. C. Tekin, *Emergent Mater.*, 2021, **4**, 143–168.
148 Z. Qin, R. Peng, I. K. Baravik and X. Liu, *Matter*, 2020, **3**, 628–651.
149 B. V. Ribeiro, T. A. R. Cordeiro, G. R. Oliveira e Freitas, L. F. Ferreira and D. L. Franco, *Talanta Open*, 2020, **2**, 100007.
150 R. Zenhausern, C.-H. Chen and J.-Y. Yoon, *Biomicrofluidics*, 2021, **15**, 011503.
151 S. Krokhine, H. Torabi, A. Doostmohammadi and P. Rezai, *Colloids Surf., B*, 2021, **206**, 111962.
152 I. Lee, E. Jeon and J. Lee, *TrAC, Trends Anal. Chem.*, 2023, **158**, 116880.
153 E. Shabani, S. Dowlatshahi and M. J. Abdekhodaie, *Eur. J. Clin. Microbiol. Infect. Dis.*, 2021, **40**, 225–246.
154 Y. Chen, S. Huang, L. Zhou, X. Wang, H. Yang and W. Li, *J. Clin. Lab. Anal.*, 2022, **36**, e24152.
155 N. L. Welch, M. Zhu, C. Hua, J. Weller, M. E. Mirhashemi, T. G. Nguyen, S. Mantena, M. R. Bauer, B. M. Shaw, C. M. Ackerman, S. G. Thakku, M. W. Tse, J. Kehe, M.-M. Uwera, J. S. Eversley, D. A. Bielwaski, G. McGrath, J. Braidt, J. Johnson, F. Cerrato, G. K. Moreno, L. A. Krasilnikova, B. A. Petros, G. L. Gionet, E. King, R. C. Huard, S. K. Jalbert, M. L. Cleary, N. A. Fitzgerald, S. B. Gabriel, G. R. Gallagher, S. C. Smole, L. C. Madoff, C. M. Brown, M. W. Keller, M. M. Wilson, M. K. Kirby, J. R. Barnes, D. J. Park, K. J. Siddle, C. T. Happi, D. T. Hung, M. Springer, B. L. MacInnis, J. E. Lemieux, E. Rosenberg, J. A. Branda, P. C. Blainey, P. C. Sabeti and C. Myhrvold, *Nat. Med.*, 2022, **28**, 1083–1094.
156 C. M. Ackerman, C. Myhrvold, S. G. Thakku, C. A. Freije, H. C. Metsky, D. K. Yang, S. H. Ye, C. K. Boehm, T.-S. F. Kosoko-Thoroddsen, J. Kehe, T. G. Nguyen, A. Carter, A. Kulesa, J. R. Barnes, V. G. Dugan, D. T. Hung, P. C. Blainey and P. C. Sabeti, *Nature*, 2020, **582**, 277–282.
157 I. Rutten, D. Daems, K. Leirs and J. Lammertyn, *Biosensors*, 2023, **13**, 100.
158 M. Rombach, S. Hin, M. Specht, B. Johannsen, J. Lüddecke, N. Paust, R. Zengerle, L. Roux, T. Sutcliffe, J. R. Peham, C. Herz, M. Panning, O. Donoso Mantke and K. Mitsakakis, *Analyst*, 2020, **145**, 7040–7047.
159 J. Liu, H. Wang, L. Zhang, Y. Lu, X. Wang, M. Shen, N. Li, L. Feng, J. Jing, B. Cao, X. Zou, J. Cheng and Y. Xu, *Small*, 2022, **18**, 2200854.
160 H. Wang, J. Xu, S. Li, X. Wang, G. Liu, S. Yang, F. Zhao, Q. Liu, X. Chen, C. He and M. Li, *Anal. Chim. Acta*, 2023, **1242**, 340812.
161 M. Ji, Y. Xia, F.-C. Loo, L. Li, H.-P. Ho, J. He and D. Gu, *RSC Adv.*, 2020, **10**, 34088–34098.
162 H. Xiong, X. Ye, Y. Li, L. Wang, J. Zhang, X. Fang and J. Kong, *Anal. Chem.*, 2020, **92**, 14297–14302.
163 W. Xing, Y. Liu, H. Wang, S. Li, Y. Lin, L. Chen, Y. Zhao, S. Chao, X. Huang, S. Ge, T. Deng, T. Zhao, B. Li, H. Wang, L. Wang, Y. Song, R. Jin, J. He, X. Zhao, P. Liu, W. Li and J. Cheng, *Engineering*, 2020, **6**, 1130–1140.
164 E. Huang, Y. Wang, N. Yang, B. Shu, G. Zhang and D. Liu, *Anal. Bioanal. Chem.*, 2021, **413**, 1787–1798.
165 H. Yin, Z. Tong, C. Shen, X. Xu, H. Ma, Z. Wu, Y. Qi and H. Mao, *Lab Chip*, 2022, **22**, 2671–2681.
166 H. Huang, K. Huang, Y. Sun, D. Luo, M. Wang, T. Chen, M. Li, J. Duan, L. Huang and C. Dong, *Micromachines*, 2022, **13**, 1650.
167 Y. Zai, C. Min, Z. Wang, Y. Ding, H. Zhao, E. Su and N. He, *Lab Chip*, 2022, **22**, 3436–3452.
168 R. Siavash Moakhar, C. del Real Mata, M. Jalali, H. Shafique, A. Sanati, J. de Vries, J. Strauss, T. AbdElFatah, F. Ghasemi, M. McLean, I. I. Hosseini, Y. Lu, S. G. Yedire, S. S. Mahshid, M. A. Tabatabaiefar, C. Liang and S. Mahshid, *Adv. Sci.*, 2022, **9**, 2204246.
169 D. Najjar, J. Rainbow, S. Sharma Timilsina, P. Jolly, H. de Puig, M. Yafia, N. Durr, H. Sallum, G. Alter, J. Z. Li, X. G. Yu, D. R. Walt, J. A. Paradiso, P. Estrela, J. J. Collins and D. E. Ingber, *Nat. Biomed. Eng.*, 2022, **6**, 968–978.
170 W. Teixeira, Y. Pallás-Tamarit, A. Juste-Dolz, A. Sena-Torralba, R. Gozalbo-Rovira, J. Rodríguez-Díaz, D. Navarro, J. Carrascosa, D. Gimenez-Romero, Á. Maquieira and S. Morais, *Biosens. Bioelectron.*, 2022, **213**, 114454.
171 J. Yang, V. M. Phan, C.-K. Heo, H. V. Nguyen, W.-H. Lim, E.-W. Cho, H. Poo and T. S. Seo, *Sens. Actuators, B*, 2023, **380**, 133331.
172 G. Qiu, Z. Gai, Y. Tao, J. Schmitt, G. A. Kullak-Ublick and J. Wang, *ACS Nano*, 2020, **14**, 5268–5277.
173 G. Seo, G. Lee, M. J. Kim, S.-H. Baek, M. Choi, K. B. Ku, C.-S. Lee, S. Jun, D. Park, H. G. Kim, S.-J. Kim, J.-O. Lee, B. T. Kim, E. C. Park and S. I. Kim, *ACS Nano*, 2020, **14**, 5135–5142.
174 F. Li, J. Qi, Z. Ren, X. Hu, Y. Chen, B. Li and X. Fu, *Microchem. J.*, 2023, **185**, 108304.
175 P. Robin, L. Barnabei, S. Marocco, J. Pagnoncelli, D. Nicolis, C. Tarantelli, A. C. Tavilla, R. Robortella, L. Cascione, L. Mayoraz, C. M. A. Journot, M. Mensi, F. Bertoni, I. Stefanini and S. Gerber-Lemaire, *Biosens. Bioelectron.: X*, 2023, **13**, 100302.
176 P.-H. Lu, Y.-D. Ma, C.-Y. Fu and G.-B. Lee, *Lab Chip*, 2020, **20**, 789–797.
177 Y.-T. Yeh, K. Gulino, Y. Zhang, A. Sabestien, T.-W. Chou, B. Zhou, Z. Lin, I. Albert, H. Lu, V. Swaminathan, E. Ghedin and M. Terrones, *Proc. Natl. Acad. Sci. U. S. A.*, 2020, **117**, 895–901.
178 A. Ramachandran, D. A. Huyke, E. Sharma, M. K. Sahoo, C. Huang, N. Banaei, B. A. Pinsky and J. G. Santiago, *Proc. Natl. Acad. Sci. U. S. A.*, 2020, **117**, 29518–29525.
179 Y. Yu, Z. Yu, X. Pan, L. Xu, R. Guo, X. Qian and F. Shen, *Analyst*, 2022, **147**, 625–633.
180 A. Wang, Z. Wu, Y. Huang, H. Zhou, L. Wu, C. Jia, Q. Chen and J. Zhao, *Biosensors*, 2021, **11**, 427.

181 H. Wang, Z. Ma, J. Qin, Z. Shen, Q. Liu, X. Chen, H. Wang, Z. An, W. Liu and M. Li, *Biosens. Bioelectron.*, 2019, **126**, 373–380.
182 M. Dou, J. Sanchez, H. Tavakoli, J. E. Gonzalez, J. Sun, J. Dien Bard and X. Li, *Anal. Chim. Acta*, 2019, **1065**, 71–78.
183 M. Dou, N. Macias, F. Shen, J. Dien Bard, D. C. Domínguez and X. Li, *EClinicalMedicine*, 2019, **8**, 72–77.
184 G. Huang, Q. Huang, L. Xie, G. Xiang, L. Wang, H. Xu, L. Ma, X. Luo, J. Xin, X. Zhou, X. Jin and L. Zhang, *Sci. Rep.*, 2017, **7**, 6441.
185 E. D. Carrol, J. E. Clark and A. J. Cant, *Paediatr. Respir. Rev.*, 2001, **2**, 113–119.
186 B. A. Forbes, G. S. Hall, M. B. Miller, S. M. Novak, M.-C. Rowlinson, M. Salfinger, A. Somosköví, D. M. Warshauer and M. L. Wilson, *Clin. Microbiol. Rev.*, 2018, **31**, e00038-17.
187 C. J. Cambier, S. Falkow and L. Ramakrishnan, *Cell*, 2014, **159**, 1497–1509.
188 B. B. Aldridge, M. Fernandez-Suarez, D. Heller, V. Ambravaneswaran, D. Irimia, M. Toner and S. M. Fortune, *Science*, 2012, **335**, 100–104.
189 J. Millard, C. Ugarte-Gil and D. A. J. Moore, *BMJ*, 2015, **350**, h882.
190 A. Paul, N. Dutta, D. Moschou and G. Dutta, *Sens. Int.*, 2020, **1**, 100036.
191 G. L. Hobby, A. P. Holman, M. D. Iseman and J. M. Jones, *Antimicrob. Agents Chemother.*, 1973, **4**, 94–104.
192 F. Rageade, N. Picot, A. Blanc-Michaud, S. Chatellier, C. Mirande, E. Fortin and A. van Belkum, *Eur. J. Clin. Microbiol. Infect. Dis.*, 2014, **33**, 867–870.
193 WHO consolidated guidelines on tuberculosis, **https://www.who.int/publications-detail-redirect/9789240029415**, (accessed 5 January 2024).
194 J. M. Hong, H. Lee, N. V. Menon, C. T. Lim, L. P. Lee and C. W. M. Ong, *Sci. Transl. Med.*, 2022, **14**, eabj4124.
195 L. Nandlal, R. Perumal and K. Naidoo, *Infect. Drug Resist.*, 2022, **15**, 4971–4984.
196 S. D. Lawn, P. Mwaba, M. Bates, A. Piatek, H. Alexander, B. J. Marais, L. E. Cuevas, T. D. McHugh, L. Zijenah, N. Kapata, I. Abubakar, R. McNerney, M. Hoelscher, Z. A. Memish, G. B. Migliori, P. Kim, M. Maeurer, M. Schito and A. Zumla, *Lancet Infect. Dis.*, 2013, **13**, 349–361.
197 C. Nikam, M. Kazi, C. Nair, M. Jaggannath, M. Manoj, R. Vinaya, A. Shetty and C. Rodrigues, *Int. J. Mycobact.*, 2014, **3**, 205–210.
198 J. Schlanderer, H. Hoffmann, J. Lüddecke, A. Golubov, W. Grasse, E. V. Kindler, T. A. Kohl, M. Merker, C. Metzger, V. Mohr, S. Niemann, C. Pilloni, S. Plesnik, B. Raya, B. Shresta, C. Utpatel, R. Zengerle, M. Beutler and N. Paust, *Lab Chip*, 2024, **24**, 74–84.
199 K. R. Steingart, V. Ng, M. Henry, P. C. Hopewell, A. Ramsay, J. Cunningham, R. Urbanczik, M. D. Perkins, M. A. Aziz and M. Pai, *Lancet Infect. Dis.*, 2006, **6**, 664–674.
200 J. Flores, J. C. Cancino and L. Chavez-Galan, *Front. Microbiol.*, 2021, **12**, 638047.
201 S. D. Lawn, *BMC Infect. Dis.*, 2012, **12**, 103.
202 M. A. Bulterys, B. Wagner, M. Redard-jacot, A. Suresh, N. R. Pollock, E. Moreau, C. M. Denkinger, P. K. Drain and T. Broger, *J. Clin. Med.*, 2020, **9**, 111.
203 X.-J. Cao, Y.-P. Li, J.-Y. Wang, J. Zhou and X.-G. Guo, *BMC Infect. Dis.*, 2021, **21**, 336.
204 D. Qiao, L. Li, J. Guo, S. Lao, X. Zhang, J. Zhang and C. Wu, *Infect. Immun.*, 2011, **79**, 3358–3365.
205 V. Boggaram, K. R. Gottipati, X. Wang and B. Samten, *J. Biol. Chem.*, 2013, **288**, 25500–25511.
206 S. Gupta and V. Kakkar, *Biosens. Bioelectron.*, 2018, **115**, 14–29.
207 S. K. Srivastava, C. J. M. van Rijn and M. A. Jongsma, *RSC Adv.*, 2016, **6**, 17759–17771.
208 A. Niemz and D. S. Boyle, *Expert Rev. Mol. Diagn.*, 2012, **12**, 687–701.
209 V. Mani, S. Wang, F. Inci, G. De Libero, A. Singhal and U. Demirci, *Adv. Drug Delivery Rev.*, 2014, **78**, 105–117.
210 S. Wang, F. Inci, G. De Libero, A. Singhal and U. Demirci, *Biotechnol. Adv.*, 2013, **31**, 438–449.
211 K. Dheda, M. Ruhwald, G. Theron, J. Peter and W. C. Yam, *Respirology*, 2013, **18**, 217–232.
212 G. A. S. Minero, M. Bagnasco, J. Fock, B. Tian, F. Garbarino and M. F. Hansen, *Anal. Bioanal. Chem.*, 2020, **412**, 2705–2710.
213 G. A. S. Minero, E. Tefiku, F. Garbarino and M. F. Hansen, *IEEE Magn. Lett.*, 2020, **11**, 3100105.
214 A. R. Homann, L. Niebling, S. Zehnle, M. Beutler, L. Delamotte, M.-C. Rothmund, D. Czurratis, K.-D. Beller, R. Zengerle, H. Hoffmann and N. Paust, *Lab Chip*, 2021, **21**, 1540–1548.
215 M. Beutler, A. R. Homann, M. Mihalic, S. Plesnik, L. Niebling, M. Eckart, V. Allerheiligen, D. Czurratis, B. Maharjan, B. Shrestha, N. Parpieva, L. Turaev, Z. Sayfutdinov, S. Hofmann-Thiel, W. Grasse, C. Metzger-Boddien, N. Paust and H. Hoffmann, *J. Mol. Diagn.*, 2021, **23**, 643–650.
216 N. Kaur, J. S. Michael and B. J. Toley, *Sci. Rep.*, 2019, **9**, 15367.
217 L. B. Pinheiro, V. A. Coleman, C. M. Hindson, J. Herrmann, B. J. Hindson, S. Bhat and K. R. Emslie, *Anal. Chem.*, 2012, **84**, 1003–1011.
218 H. Li, R. Bai, Z. Zhao, L. Tao, M. Ma, Z. Ji, M. Jian, Z. Ding, X. Dai, F. Bao and A. Liu, *Biosci. Rep.*, 2018, **38**, BSR20181170.
219 R. Nyaruaba, C. Mwaliko, K. K. Kering and H. Wei, *Tuberculosis*, 2019, **117**, 85–92.
220 N. Song, Y. Tan, L. Zhang, W. Luo, Q. Guan, M. Yan, R. Zuo, W. Liu, F. Luo and X.-L. Zhang, *Emerging Microbes Infect.*, 2018, **7**, 1–9.
221 M. Yamamoto, R. Ushio, H. Watanabe, T. Tachibana, M. Tanaka, T. Yokose, J. Tsukiji, H. Nakajima and T. Kaneko, *Int. J. Infect. Dis.*, 2018, **66**, 80–82.
222 J. Luo, M. Luo, J. Li, J. Yu, H. Yang, X. Yi, Y. Chen and H. Wei, *Int. J. Tuberc. Lung Dis.*, 2019, **23**, 219–225.
223 C.-H. Wang, J.-R. Chang, S.-C. Hung, H.-Y. Dou and G.-B. Lee, *Sens. Actuators, B*, 2022, **365**, 131968.

224 A. C. Kukhtin, T. Sebastian, J. Golova, A. Perov, C. Knickerbocker, Y. Linger, A. Bueno, P. Qu, M. Villanueva, R. C. Holmberg, D. P. Chandler and C. G. Cooney, *Lab Chip*, 2019, **19**, 1217–1225.
225 A. V. Kukhtin, R. Norville, A. Bueno, P. Qu, N. Parrish, M. Murray, D. P. Chandler, R. C. Holmberg and C. G. Cooney, *Anal. Chem.*, 2020, **92**, 5311–5318.
226 I. M. Mbano, T. Mandizvo, J. Rogich, T. T. R. Kunota, J. S. Mackenzie, M. Pillay and F. K. Balagaddé, *J. Appl. Lab. Med.*, 2020, **5**, 440–453.
227 D. Martens, P. Ramirez-Priego, M. S. Murib, A. A. Elamin, A. B. Gonzalez-Guerrero, M. Stehr, F. Jonas, B. Anton, N. Hlawatsch, P. Soetaert, R. Vos, A. Stassen, S. Severi, W. V. Roy, R. Bockstaele, H. Becker, M. Singh, L. M. Lechuga and P. Bienstman, *Anal. Methods*, 2018, **10**, 3066–3073.
228 P. Ramirez-Priego, D. Martens, A. A. Elamin, P. Soetaert, W. Van Roy, R. Vos, B. Anton, R. Bockstaele, H. Becker, M. Singh, P. Bienstman and L. M. Lechuga, *ACS Sens.*, 2018, **3**, 2079–2086.
229 N. Singh, B. Dahiya, V. S. Radhakrishnan, T. Prasad and P. K. Mehta, *Int. J. Nanomed.*, 2018, **13**, 8523–8535.
230 S. Gupta, P. Bhatter and V. Kakkar, *Tuberculosis*, 2021, **127**, 102055.
231 N. Ariffin, N. A. Yusof, J. Abdullah, S. F. Abd Rahman, N. H. Ahmad Raston, N. Kusnin and S. Suraiya, *J. Sens.*, 2020, **2020**, 1–10.
232 H. Ghorbanpoor, A. N. Dizaji, I. Akcakoca, E. O. Blair, Y. Ozturk, P. Hoskisson, T. Kocagoz, H. Avci, D. K. Corrigan and F. D. Guzel, *Sens. Actuators, A*, 2022, **339**, 113515.
233 H. Wang, G. M. Conover, S.-I. Han, J. C. Sacchettini and A. Han, *Microsyst. Nanoeng.*, 2021, **7**, 37.
234 M. Elitas, N. Dhar and J. D. McKinney, *Antibiotics*, 2021, **10**, 794.
235 V. O. Baron, M. Chen, B. Hammarstrom, R. J. H. Hammond, P. Glynne-Jones, S. H. Gillespie and K. Dholakia, *Commun. Biol.*, 2020, **3**, 236.
236 R. J. H. Hammond, V. O. Baron, K. Oravcova, S. Lipworth and S. H. Gillespie, *J. Antimicrob. Chemother.*, 2015, **70**, 2823–2827.
237 A. Masajtis-Zagajewska and M. Nowicki, *Clin. Chim. Acta*, 2017, **471**, 286–291.
238 S. Aitekenov, A. Gaipov and R. Bukasov, *Talanta*, 2021, **223**, 121718.
239 E. Lepowsky, F. Ghaderinezhad, S. Knowlton and S. Tasoglu, *Biomicrofluidics*, 2017, **11**, 051501.
240 E. Mahoney, J. Kun, M. Smieja and Q. Fang, *J. Electrochem. Soc.*, 2020, **167**, 037518.
241 W.-C. Tai, Y.-C. Chang, D. Chou and L.-M. Fu, *Biosensors*, 2021, **11**, 260.
242 A. L. Flores-Mireles, J. N. Walker, M. Caparon and S. J. Hultgren, *Nat. Rev. Microbiol.*, 2015, **13**, 269–284.
243 M. Medina and E. Castillo-Pino, *Ther. Adv. Urol.*, 2019, **11**, 1756287219832172.
244 R. D. Klein and S. J. Hultgren, *Nat. Rev. Microbiol.*, 2020, **18**, 211–226.
245 R. Öztürk and A. Murt, *World J. Urol.*, 2020, **38**, 2669–2679.
246 B. Foxman, *Nat. Rev. Urol.*, 2010, **7**, 653–660.
247 C. Walsh and T. Collyns, *Surgery*, 2020, **38**, 191–196.
248 T. J. Wiles, R. R. Kulesus and M. A. Mulvey, *Exp. Mol. Pathol.*, 2008, **85**, 11–19.
249 F. M. E. Wagenlehner, T. E. Bjerklund Johansen, T. Cai, B. Koves, J. Kranz, A. Pilatz and Z. Tandogdu, *Nat. Rev. Urol.*, 2020, **17**, 586–600.
250 M. Gajdács, I. Dóczi, M. Ábrók, A. Lázár and K. Burián, *Cent. Eur. J. Urol.*, 2019, **72**, 209–214.
251 E. Paydaş Hataysal, B. Saraçlıgil, H. Türk Dağı and H. Vatansev, *Eur. Respir. J.*, 2019, **5**, 613–617.
252 D. Fallon, *J. Clin. Pathol.*, 2003, **56**, 608–612.
253 M. Oyaert and J. Delanghe, *Ann. Lab. Med.*, 2018, **39**, 15–22.
254 M.-D. Phan, K. M. Peters, S. Sarkar, S. W. Lukowski, L. P. Allsopp, D. G. Moriel, M. E. S. Achard, M. Totsika, V. M. Marshall, M. Upton, S. A. Beatson and M. A. Schembri, *PLoS Genet.*, 2013, **9**, e1003834.
255 P. Bajaj, N. S. Singh and J. S. Virdi, *Front. Microbiol.*, 2016, **7**, 417.
256 M. Santos, M. Mariz, I. Tiago, J. Martins, S. Alarico and P. Ferreira, *J. Pharm. Biomed. Anal.*, 2022, **219**, 114889.
257 M. Harris and T. Fasolino, *J. Lab. Med.*, 2022, **46**, 3–15.
258 M. S. Kumar, S. Ghosh, S. Nayak and A. P. Das, *Biosens. Bioelectron.*, 2016, **80**, 497–510.
259 M. Davenport, K. E. Mach, L. M. D. Shortliffe, N. Banaei, T.-H. Wang and J. C. Liao, *Nat. Rev. Urol.*, 2017, **14**, 298–310.
260 M. S. Kumar and A. P. Das, *Adv. Colloid Interface Sci.*, 2017, **249**, 53–65.
261 R. Lei, R. Huo and C. Mohan, *Expert Rev. Mol. Diagn.*, 2020, **20**, 69–84.
262 A. Hasandka, A. R. Singh, A. Prabhu, H. R. Singhal, M. S. G. Nandagopal and N. K. Mani, *Anal. Bioanal. Chem.*, 2022, **414**, 847–865.
263 D. J. Shin, N. Andini, K. Hsieh, S. Yang and T.-H. Wang, *Annu. Rev. Anal. Chem.*, 2019, **12**, 41–67.
264 W. Kim, J. S. Park, D. Lee, J. Seo, L. P. Lee and S. J. Kim, *Biosens. Bioelectron.*, 2022, **213**, 114350.
265 Z. D. Call, I. Jang, B. J. Geiss, D. S. Dandy and C. S. Henry, *Anal. Chem.*, 2022, **94**, 7545–7550.
266 J. Noiphung and W. Laiwattanapaisal, *Sci. Rep.*, 2019, **9**, 1555.
267 Y. Shen, J. Yi, M. Song, D. Li, Y. Wu, Y.-J. Liu, M. Yang and L. Qiao, *Analyst*, 2021, **146**, 4146–4153.
268 J. Chen, Y. Xu, H. Yan, Y. Zhu, L. Wang, Y. Zhang, Y. Lu and W. Xing, *Lab Chip*, 2018, **18**, 2441–2452.
269 A. O. Olanrewaju, A. Ng, P. Decorwin-Martin, A. Robillard and D. Juncker, *Anal. Chem.*, 2017, **89**, 6846–6853.
270 I. P. Alves and N. M. Reis, *Biosens. Bioelectron.*, 2019, **145**, 111624.
271 V. B. Barbosa, C. F. Rodrigues, L. Cerqueira, J. M. Miranda and N. F. Azevedo, *Front. Bioeng. Biotechnol.*, 2022, **10**, 987669.
272 Y. Li, T. Wang and J. Wu, *Analyst*, 2021, **146**, 1151–1156.

273 R. Moakhar, T. AbdelFatah, A. Sanati, M. Jalali, S. E. Flynn, S. S. Mahshid and S. Mahshid, *ACS Appl. Mater. Interfaces*, 2020, **12**, 23298–23310.
274 M. Basak, S. Mitra, M. Gogoi, S. Sinha, H. B. Nemade and D. Bandyopadhyay, *ACS Appl. Bio Mater.*, 2022, **5**, 5321–5332.
275 R. Pandey, Y. Lu, E. Osman, S. Saxena, Z. Zhang, S. Qian, A. Pollinzi, M. Smieja, Y. Li, L. Soleymani and T. Hoare, *ACS Sens.*, 2022, **7**, 985–994.
276 D. Yang, H. Zhou, N. E. Dina and C. Haisch, *R. Soc. Open Sci.*, 2018, **5**, 180955.
277 H. Ilhan, B. Guven, U. Dogan, H. Torul, S. Evran, D. Çetin, Z. Suludere, N. Saglam, İ. H. Boyaci and U. Tamer, *Talanta*, 2019, **201**, 245–252.
278 Y. Li, G. Xie, J. Qiu, D. Zhou, D. Gou, Y. Tao, Y. Li and H. Chen, *Sens. Actuators, B*, 2018, **258**, 803–812.
279 S. Reyes, N. Le, M. D. Fuentes, J. Upegui, E. Dikici, D. Broyles, E. Quinto, S. Daunert and S. K. Deo, *Int. J. Mol. Sci.*, 2020, **21**, 5015.
280 P. Zhang, A. M. Kaushik, K. Hsieh, S. Li, S. Lewis, K. E. Mach, J. C. Liao, K. C. Carroll and T.-H. Wang, *Small Methods*, 2022, **6**, 2101254.
281 K. E. Mach, A. M. Kaushik, K. Hsieh, P. K. Wong, T.-H. Wang and J. C. Liao, *Analyst*, 2019, **144**, 1565–1574.
282 A. M. Kaushik, K. Hsieh, K. E. Mach, S. Lewis, C. M. Puleo, K. C. Carroll, J. C. Liao and T.-H. Wang, *Adv. Sci.*, 2021, **8**, 200341.
283 K. Hsieh, K. E. Mach, P. Zhang, J. C. Liao and T.-H. Wang, *Acc. Chem. Res.*, 2022, **55**, 123–133.
284 P. Athamanolap, K. Hsieh, C. M. O'Keefe, Y. Zhang, S. Yang and T.-H. Wang, *Anal. Chem.*, 2019, **91**, 12784–12792.
285 W. Kang, S. Sarkar, Z. S. Lin, S. McKenney and T. Konry, *Anal. Chem.*, 2019, **91**, 6242–6249.
286 P. Sabhachandani, S. Sarkar, P. C. Zucchi, B. A. Whitfield, J. E. Kirby, E. B. Hirsch and T. Konry, *Microchim. Acta*, 2017, **184**, 4619–4628.
287 A. A. Sklavounos, C. R. Nemr, S. O. Kelley and A. R. Wheeler, *Lab Chip*, 2021, **21**, 4208–4222.
288 X. Li, X. Liu, Z. Yu, Y. Luo, Q. Hu, Z. Xu, J. Dai, N. Wu and F. Shen, *Lab Chip*, 2022, **22**, 3952–3960.
289 M. Osaid, Y.-S. Chen, C.-H. Wang, A. Sinha, W.-B. Lee, P. Gopinathan, H.-B. Wu and G.-B. Lee, *Lab Chip*, 2021, **21**, 2223–2231.
290 J. Avesar, D. Rosenfeld, M. Truman-Rosentsvit, T. Ben-Arye, Y. Geffen, M. Bercovici and S. Levenberg, *Proc. Natl. Acad. Sci. U. S. A.*, 2017, **114**, E5787–E5795.
291 Ö. Baltekin, A. Boucharin, E. Tano, D. I. Andersson and J. Elf, *Proc. Natl. Acad. Sci. U. S. A.*, 2017, **114**, 9170–9175.
292 H. Li, P. Torab, K. E. Mach, C. Surrette, M. R. England, D. W. Craft, N. J. Thomas, J. C. Liao, C. Puleo and P. K. Wong, *Proc. Natl. Acad. Sci. U. S. A.*, 2019, **116**, 10270–10279.
293 Y. Yang, K. Gupta and K. L. Ekinci, *Proc. Natl. Acad. Sci. U. S. A.*, 2020, **117**, 10639–10644.
294 V. Kara, C. Duan, K. Gupta, S. Kurosawa, D. J. Stearns-Kurosawa and K. L. Ekinci, *Lab Chip*, 2018, **18**, 743–753.
295 V. Shumeiko, G. Hidas, C. Nowogrodski, Y. Pinto, O. Gofrit, M. Duvdevani and O. Shoseyov, *Sensors*, 2021, **21**, 5902.
296 S. H. Needs, H. M. I. Osborn and A. D. Edwards, *J. Microbiol. Methods*, 2021, **187**, 106199.
297 K.-W. Hsu, W.-B. Lee, H.-L. You, M. S. Lee and G.-B. Lee, *Lab Chip*, 2021, **21**, 755–763.
298 J. Gao, H. Li, P. Torab, K. E. Mach, D. W. Craft, N. J. Thomas, C. M. Puleo, J. C. Liao, T.-H. Wang and P. K. Wong, *Nanomedicine*, 2019, **17**, 246–253.
299 S. M. Pires, B. N. Desta, L. Mughini-Gras, B. T. Mmbaga, O. E. Fayemi, E. M. Salvador, T. Gobena, S. E. Majowicz, T. Hald, P. S. Hoejskov, Y. Minato and B. Devleesschauwer, *Curr. Opin. Food Sci.*, 2021, **39**, 152–159.
300 WHO 2017 Diarrhoeal disease, **https://www.who.int/news-room/fact-sheets/detail/diarrhoeal-disease**, (accessed 6 January 2024).
301 Y. Nguyen and V. Sperandio, *Front. Cell. Infect. Microbiol.*, 2012, **2**, 90.
302 L. A. Knodler and J. R. Elfenbein, *Trends Microbiol.*, 2019, **27**, 964–965.
303 D. Costa and G. Iraola, *Clin. Microbiol. Rev.*, 2019, **32**, e00072-18.
304 M. M. Koopmans, M. C. Brouwer, J. A. Vázquez-Boland and D. van de Beek, *Clin. Microbiol. Rev.*, 2022, e00060-19.
305 I. Mehdizadeh Gohari, M. A. Navarro, J. Li, A. Shrestha, F. Uzal and B. A. McClane, *Virulence*, 2021, **12**, 723–753.
306 S. M. E. Toubar, A. A. Elbialy, M. M. M. Zaky and A. S. El-Shafey, *AASCIT Journal of Health*, 2018, **5**, 34–38.
307 R. M. Humphries and A. J. Linscott, *Clin. Microbiol. Rev.*, 2015, **28**, 3–31.
308 WHO Cholera – Global situation, **https://www.who.int/emergencies/disease-outbreak-news/item/2022-DON426**, (accessed 6 January 2024).
309 J. Deen, M. A. Mengel and J. D. Clemens, *Vaccine*, 2020, **38**, A31–A40.
310 S. Baker and H. C. The, *Curr. Opin. Infect. Dis.*, 2018, **31**, 449–454.
311 M. M. Gibani, C. Britto and A. J. Pollard, *Curr. Opin. Infect. Dis.*, 2018, **31**, 440–448.
312 S. E. Crawford, S. Ramani, J. E. Tate, U. D. Parashar, L. Svensson, M. Hagbom, M. A. Franco, H. B. Greenberg, M. O'Ryan, G. Kang, U. Desselberger and M. K. Estes, *Nat. Rev. Dis. Primers*, 2017, **3**, 17083.
313 E. Robilotti, S. Deresinski and B. A. Pinsky, *Clin. Microbiol. Rev.*, 2015, **28**, 134–164.
314 G. Di Cola, A. C. Fantilli, M. B. Pisano and V. E. Ré, *Int. J. Food Microbiol.*, 2021, **338**, 108986.
315 K. Bányai, M. K. Estes, V. Martella and U. D. Parashar, *Lancet*, 2018, **392**, 175–186.
316 S. E. Crowe, *N. Engl. J. Med.*, 2019, **380**, 1158–1165.
317 L. Yin, Y. Li, W. Zhang, X. Han, Q. Wu, Y. Xie, J. Fan and L. Ma, *J. Agric. Food Chem.*, 2023, **71**, 3551–3563.
318 D. Gao, Z. Ma and Y. Jiang, *TrAC, Trends Anal. Chem.*, 2022, **157**, 116788.
319 Y. Shang, X. Xiang, Q. Ye, Q. Wu, J. Zhang and J.-M. Lin, *TrAC, Trends Anal. Chem.*, 2022, **147**, 116509.

320 M. Ranjbaran and M. S. Verma, *Trends Food Sci. Technol.*, 2022, **128**, 102–117.
321 I. A. Quintela, T. Vasse, C.-S. Lin and V. C. H. Wu, *Front. Microbiol.*, 2022, **13**, 1054782.
322 W. Su, D. Liang and M. Tan, *Trends Food Sci. Technol.*, 2021, **113**, 97–109.
323 F. Mi, C. Hu, Y. Wang, L. Wang, F. Peng, P. Geng and M. Guan, *Anal. Bioanal. Chem.*, 2022, **414**, 2883–2902.
324 A. Rani, V. B. Ravindran, A. Surapaneni, N. Mantri and A. S. Ball, *Int. J. Food Microbiol.*, 2021, **349**, 109233.
325 M. A. Zaczek-Moczydlowska, A. Beizaei, M. Dillon and K. Campbell, *Trends Food Sci. Technol.*, 2021, **114**, 684–695.
326 Y. Shen, L. Xu and Y. Li, *Compr. Rev. Food Sci. Food Saf.*, 2021, **20**, 149–197.
327 B. Wang and B. Park, *Foodborne Pathog. Dis.*, 2022, **19**, 359–375.
328 A. Ajayi, T. Jolaiya and S. Smith, *J. Clin. Med.*, 2020, **9**, 2565.
329 R. Li, X. Tian, J. Pang, L. Li, J. Yuan, Z. Tian and Z. Wang, *Viruses*, 2022, **14**, 1355.
330 W.-K. Wu, C.-C. Chen, S. Panyod, R.-A. Chen, M.-S. Wu, L.-Y. Sheen and S.-C. Chang, *J. Formosan Med. Assoc.*, 2019, **118**, 545–555.
331 S. Zhao, W. He, Z. Ma, P. Liu, P.-H. Huang, H. Bachman, L. Wang, S. Yang, Z. Tian, Z. Wang, Y. Gu, Z. Xie and T. Jun Huang, *Lab Chip*, 2019, **19**, 941–947.
332 J. Kang, C. Park, J. Lee, J. Namkung, S. Y. Hwang and Y. S. Kim, *BioChip J.*, 2017, **11**, 76–84.
333 O. Mosley, L. Melling, M. D. Tarn, C. Kemp, M. M. N. Esfahani, N. Pamme and K. J. Shaw, *Lab Chip*, 2016, **16**, 2108–2115.
334 A. Pryszlak, T. Wenzel, K. W. Seitz, F. Hildebrand, E. Kartal, M. R. Cosenza, V. Benes, P. Bork and C. A. Merten, *Cells Rep. Methods*, 2022, **2**, 100137.
335 L. Ma, M. Petersen and X. Lu, *Appl. Environ. Microbiol.*, 2020, **86**, e00096-20.
336 M. Geissler, D. Brassard, L. Clime, A. V. C. Pilar, L. Malic, J. Daoud, V. Barrère, C. Luebbert, B. W. Blais, N. Corneau and T. Veres, *Analyst*, 2020, **145**, 6831–6845.
337 C. R. Phaneuf, B. Mangadu, H. M. Tran, Y. K. Light, A. Sinha, F. W. Charbonier, T. P. Eckles, A. K. Singh and C.-Y. Koh, *Biosens. Bioelectron.*, 2018, **120**, 93–101.
338 M. Zhang, J. Liu, Z. Shen, Y. Liu, Y. Song, Y. Liang, Z. Li, L. Nie, Y. Fang and Y. Zhao, *BMC Microbiol.*, 2021, **21**, 197.
339 N. Jin, L. Xue, Y. Ding, Y. Liu, F. Jiang, M. Liao, Y. Li and J. Lin, *Biosens. Bioelectron.*, 2023, **220**, 114844.
340 Y. Shang, G. Xing, X. Liu, H. Lin and J.-M. Lin, *Anal. Chem.*, 2022, **94**, 16787–16795.
341 Y. Cao, C. Ye, C. Zhang, G. Zhang, H. Hu, Z. Zhang, H. Fang, J. Zheng and H. Liu, *Food Control*, 2022, **134**, 108694.
342 Z. Qin, X. Xiang, L. Xue, W. Cai, J. Gao, J. Yang, Y. Liang, L. Wang, M. Chen, R. Pang, Y. Li, J. Zhang, Y. Hu and Q. Wu, *Microchem. J.*, 2021, **164**, 106050.
343 R. Chand and S. Neethirajan, *Biosens. Bioelectron.*, 2017, **98**, 47–53.
344 S. Chung, L. E. Breshears, S. Perea, C. M. Morrison, W. Q. Betancourt, K. A. Reynolds and J.-Y. Yoon, *ACS Omega*, 2019, **4**, 11180–11188.
345 S. Chung, L. E. Breshears, A. Gonzales, C. M. Jennings, C. M. Morrison, W. Q. Betancourt, K. A. Reynolds and J.-Y. Yoon, *Nat. Protoc.*, 2021, **16**, 1452–1475.
346 X. Ye, J. Xu, L. Lu, X. Li, X. Fang and J. Kong, *Anal. Chim. Acta*, 2018, **1018**, 78–85.
347 S. Wen, J. Zhang, R. Zhao, J. Gao, N. Wang, T. Lu, R. Xie, X. Sun, B. Xiao, Z. Duan and A. Chen, *ACS Agric. Sci. Technol.*, 2022, **2**, 805–812.
348 M. El-Tholoth, H. Bai, M. G. Mauk, L. Saif and H. H. Bau, *Lab Chip*, 2021, **21**, 1118–1130.
349 L. Zhou, Y. Chen, X. Fang, Y. Liu, M. Du, X. Lu, Q. Li, Y. Sun, J. Ma and T. Lan, *Anal. Chim. Acta*, 2020, **1125**, 57–65.
350 W. Y. Cui, H. J. Yoo, Y. G. Li, C. Baek and J. Min, *Biosens. Bioelectron.*, 2022, **199**, 113878.
351 L. Ding, S. Razavi Bazaz, T. Hall, G. Vesey and M. Ebrahimi Warkiani, *Biomicrofluidics*, 2022, **16**, 014105.
352 S. Sukas, B. van Dorst, A. Kryj, O. Lagatie, W. De Malsche and L. J. Stuyver, *Micromachines*, 2019, **10**, 852.
353 K. E. Rudd, S. C. Johnson, K. M. Agesa, K. A. Shackelford, D. Tsoi, D. R. Kievlan, D. V. Colombara, K. S. Ikuta, N. Kissoon, S. Finfer, C. Fleischmann-Struzek, F. R. Machado, K. K. Reinhart, K. Rowan, C. W. Seymour, R. S. Watson, T. E. West, F. Marinho, S. I. Hay, R. Lozano, A. D. Lopez, D. C. Angus, C. J. L. Murray and M. Naghavi, *Lancet*, 2020, **395**, 200–211.
354 World Health Organization, *Global report on the epidemiology and burden of sepsis: current evidence, identifying gaps and future directions*, World Health Organization, Geneva, 2020.
355 D. C. Angus and T. van der Poll, *N. Engl. J. Med.*, 2013, **369**, 840–851.
356 F. B. Mayr, S. Yende and D. C. Angus, *Virulence*, 2014, **5**, 4–11.
357 C. Nedeva, J. Menassa and H. Puthalakath, *Front. Cell Dev. Biol.*, 2019, **7**, 108.
358 R. S. Hotchkiss, G. Monneret and D. Payen, *Nat. Rev. Immunol.*, 2013, **13**, 862–874.
359 F. Venet and G. Monneret, *Nat. Rev. Nephrol.*, 2018, **14**, 121–137.
360 P. Yagupsky and F. S. Nolte, *Clin. Microbiol. Rev.*, 1990, **3**, 11.
361 J.-L. Vincent, J. Rello, J. Marshall, E. Silva, A. Anzueto, C. D. Martin, R. Moreno, J. Lipman, C. Gomersall, Y. Sakr, K. Reinhart and for the EPIC II Group of Investigators, *JAMA, J. Am. Med. Assoc.*, 2009, **302**, 2323–2329.
362 L. Evans, A. Rhodes, W. Alhazzani, M. Antonelli, C. M. Coopersmith, C. French, F. R. Machado, L. Mcintyre, M. Ostermann, H. C. Prescott, C. Schorr, S. Simpson, W. J. Wiersinga, F. Alshamsi, D. C. Angus, Y. Arabi, L. Azevedo, R. Beale, G. Beilman, E. Belley-Cote, L. Burry, M. Cecconi, J. Centofanti, A. Coz Yataco, J. De Waele, R. P. Dellinger, K. Doi, B. Du, E. Estenssoro, R. Ferrer, C. Gomersall, C. Hodgson, M. H. Møller, T. Iwashyna, S. Jacob, R. Kleinpell,

 

M. Klompas, Y. Koh, A. Kumar, A. Kwizera, S. Lobo, H. Masur, S. McGloughlin, S. Mehta, Y. Mehta, M. Mer, M. Nunnally, S. Oczkowski, T. Osborn, E. Papathanassoglou, A. Perner, M. Puskarich, J. Roberts, W. Schweickert, M. Seckel, J. Sevransky, C. L. Sprung, T. Welte, J. Zimmerman and M. Levy, *Intensive Care Med.*, 2021, **47**, 1181–1247.

363 G. Lippi, *Clin. Chem. Lab. Med.*, 2019, **57**, 1281–1283.

364 N. Peker, N. Couto, B. Sinha and J. W. Rossen, *Clin. Microbiol. Infect.*, 2018, **24**, 944–955.

365 B. Fiori, T. D'Inzeo, A. Giaquinto, G. Menchinelli, F. M. Liotti, F. de Maio, G. De Angelis, G. Quaranta, D. Nagel, M. Tumbarello, B. Posteraro, M. Sanguinetti and T. Spanu, *J. Clin. Microbiol.*, 2016, **54**, 576–584.

366 A. M. Peri, P. N. A. Harris and D. L. Paterson, *Clin. Microbiol. Infect.*, 2022, **28**, 195–201.

367 M. P. McHugh, B. J. Parcell, F. M. MacKenzie, K. E. Templeton and Scottish Microbiology and Virology Network (SMVN) Molecular Diagnostics Evaluation Group, *J. Med. Microbiol.*, 2020, **69**, 552–557.

368 A. Galiana, J. Coy, A. Gimeno, N. M. Guzman, F. Rosales, E. Merino, G. Royo and J. C. Rodríguez, *PLoS One*, 2017, **12**, e0177627.

369 Abionic SA, **www.abionic.com**, (accessed 09 February 2024).

370 M. Sinha, J. Jupe, H. Mack, T. P. Coleman, S. M. Lawrence and S. I. Fraley, *Clin. Microbiol. Rev.*, 2018, **31**, e00089-17.

371 A. Jyoti, S. Kumar, V. Kumar Srivastava, S. Kaushik and S. Govind Singh, *Clin. Chim. Acta*, 2021, **521**, 45–58.

372 Y. Zhang, Y. Zhou, Y. Yang and D. Pappas, *Analyst*, 2021, **146**, 2110–2125.

373 T. Oeschger, D. McCloskey, V. Kopparthy, A. Singh and D. Erickson, *Lab Chip*, 2019, **19**, 728–737.

374 S. Kumar, S. Tripathy, A. Jyoti and S. G. Singh, *Biosens. Bioelectron.*, 2019, **124–125**, 205–215.

375 D. Tsounidi, P. S. Petrou and I. Raptis, *IEEE Sens. J.*, 2021, **21**, 12840–12855.

376 L. Liu, Z. Han, F. An, X. Gong, C. Zhao, W. Zheng, L. Mei and Q. Zhou, *J. Nanobiotechnol.*, 2021, **19**, 216.

377 M. Pilecky, A. Schildberger, D. Orth-Höller and V. Weber, *Diagn. Microbiol. Infect. Dis.*, 2019, **94**, 7–14.

378 A. Burklund and J. X. J. Zhang, *Ann. Biomed. Eng.*, 2019, **47**, 1657–1674.

379 H. Li and A. J. Steckl, *Anal. Chem.*, 2019, **91**, 352–371.

380 Y.-L. Fang, C.-H. Wang, Y.-S. Chen, C.-C. Chien, F.-C. Kuo, H.-L. You, M. S. Lee and G.-B. Lee, *Lab Chip*, 2021, **21**, 113–121.

381 T. J. Abram, H. Cherukury, C.-Y. Ou, T. Vu, M. Toledano, Y. Li, J. T. Grunwald, M. N. Toosky, D. F. Tifrea, A. Slepenkin, J. Chong, L. Kong, D. V. Del Pozo, K. T. La, L. Labanieh, J. Zimak, B. Shen, S. S. Huang, E. Gratton, E. M. Peterson and W. Zhao, *Lab Chip*, 2020, **20**, 477–489.

382 B. Forsyth, P. Torab, J.-H. Lee, T. Malcom, T.-H. Wang, J. C. Liao, S. Yang, E. Kvam, C. Puleo and P. K. Wong, *Biosensors*, 2021, **11**, 288.

383 A. S. Tanak, B. Jagannath, Y. Tamrakar, S. Muthukumar and S. Prasad, *Anal. Chim. Acta: X*, 2019, **3**, 100029.

384 A. S. Tanak, S. Muthukumar, S. Krishnan, K. L. Schully, D. V. Clark and S. Prasad, *Biosens. Bioelectron.*, 2021, **171**, 112726.

385 A. S. Tanak, A. Sardesai, S. Muthukumar, S. Krishnan, D. A. Striegel, K. L. Schully, D. V. Clark and S. Prasad, *Biosens. Bioelectron.: X*, 2022, **10**, 100144.

386 A. S. Tanak, A. Sardesai, S. Muthukumar and S. Prasad, *Bioeng. Transl. Med.*, 2022, **7**, e10310.

387 A. Belushkin, F. Yesilkoy, J. J. González-López, J. C. Ruiz-Rodríguez, R. Ferrer, A. Fàbrega and H. Altug, *Small*, 2020, **16**, 1906108.

388 A. Giannetti, C. Trono, G. Porro, C. Domenici, M. Puntoni and F. Baldini, *Chemosensors*, 2020, **8**, 12.

389 A. Molinero-Fernández, M. A. López and A. Escarpa, *Analyst*, 2020, **145**, 5004–5010.

390 M. S. Verma, M.-N. Tsaloglou, T. Sisley, D. Christodouleas, A. Chen, J. Milette and G. M. Whitesides, *Biosens. Bioelectron.*, 2018, **99**, 77–84.

391 A. Alba-Patiño, S. M. Russell, M. Borges, N. Pazos-Pérez, R. A. Álvarez-Puebla and R. De La Rica, *Nanoscale Adv.*, 2020, **2**, 1253–1260.

392 E. Valera, J. Berger, U. Hassan, T. Ghonge, J. Liu, M. Rappleye, J. Winter, D. Abboud, Z. Haidry, R. Healey, N.-T. Hung, N. Leung, N. Mansury, A. Hasnain, C. Lannon, Z. Price, K. White and R. Bashir, *Lab Chip*, 2018, **18**, 1461–1470.

393 S. Damodara, J. Arora, P. C. Liaw, A. E. Fox-Robichaud and P. R. Selvaganapathy, *Microchim. Acta*, 2022, **189**, 146.

394 F. Ellett, J. Jorgensen, A. L. Marand, Y. M. Liu, M. M. Martinez, V. Sein, K. L. Butler, J. Lee and D. Irimia, *Nat. Biomed. Eng.*, 2018, **2**, 207–214.

395 H. Jeon, D.-H. Lee, B. Jundi, M. Pinilla-Vera, R. M. Baron, B. D. Levy, J. Voldman and J. Han, *ACS Sens.*, 2021, **6**, 2747–2756.

396 K. K. Zeming, R. Vernekar, M. T. Chua, K. Y. Quek, G. Sutton, T. Krüger, W. S. Kuan and J. Han, *Small*, 2021, **17**, 2006123.

397 Y. Zhang, Y. Zhou, W. Li, V. Lyons, A. Johnson, A. Venable, J. Griswold and D. Pappas, *Anal. Chem.*, 2018, **90**, 7204–7211.

398 Y. Zhou, Y. Zhang, A. Johnson, A. Venable, J. Griswold and D. Pappas, *Anal. Chim. Acta*, 2019, **1062**, 110–117.

399 U. Hassan, R. Zhu and R. Bashir, *Lab Chip*, 2018, **18**, 1231–1240.

400 N. Mancini, S. Carletti, N. Ghidoli, P. Cichero, R. Burioni and M. Clementi, *Clin. Microbiol. Rev.*, 2010, **23**, 235–251.

401 S. Kalyan, C. Torabi, H. Khoo, H. W. Sung, S.-E. Choi, W. Wang, B. Treutler, D. Kim and S. C. Hur, *Micromachines*, 2021, **12**, 257.

402 W. G. Pitt, M. Alizadeh, G. A. Husseini, D. S. McClellan, C. M. Buchanan, C. G. Bledsoe, R. A. Robison, R. Blanco, B. L. Roeder, M. Melville and A. K. Hunter, *Biotechnol. Prog.*, 2016, **32**, 823–839.

403 P. Ohlsson, M. Evander, K. Petersson, L. Mellhammar, A. Lehmusvuori, U. Karhunen, M. Soikkeli, T. Seppä, E. Tuunainen, A. Spangar, P. von Lode, K. Rantakokko-Jalava, G. Otto, S. Scheding, T. Soukka, S. Wittfooth and T. Laurell, *Anal. Chem.*, 2016, **88**, 9403–9411.

404 P. Dow, K. Kotz, S. Gruszka, J. Holder and J. Fiering, *Lab Chip*, 2018, **18**, 923–932.

405 B. M. Biron, A. Ayala and J. L. Lomas-Neira, *Biomarker Insights*, 2015, **10s4**, BMI.S29519.
406 C. Pierrakos and J.-L. Vincent, *Crit. Care*, 2010, **14**, R15.
407 S.-W. Kim, I.-H. Cho, G.-S. Lim, G.-N. Park and S.-H. Paek, *Biosens. Bioelectron.*, 2017, **98**, 7–14.
408 J. Min, M. Nothing, B. Coble, H. Zheng, J. Park, H. Im, G. F. Weber, C. M. Castro, F. K. Swirski, R. Weissleder and H. Lee, *ACS Nano*, 2018, **12**, 3378–3384.
409 C. Rosales, *Front. Physiol.*, 2018, **9**, 113.
410 K. A. Babatunde, J. M. Ayuso, S. C. Kerr, A. Huttenlocher and D. J. Beebe, *Front. Immunol.*, 2021, **12**, 781535.
411 Y. Zhang, W. Li, Y. Zhou, A. Johnson, A. Venable, A. Hassan, J. Griswold and D. Pappas, *Analyst*, 2018, **143**, 241–249.
412 U. Hassan, T. Ghonge, B. Reddy, M. Patel, M. Rappleye, I. Taneja, A. Tanna, R. Healey, N. Manusry, Z. Price, T. Jensen, J. Berger, A. Hasnain, E. Flaugher, S. Liu, B. Davis, J. Kumar, K. White and R. Bashir, *Nat. Commun.*, 2017, **8**, 15949.
413 Y. Zheng, Q. Yu, Y. Lin, Y. Zhou, L. Lan, S. Yang and J. Wu, *Lancet Infect. Dis.*, 2022, **22**, 541–551.
414 WHO STI factsheet 2023, **https://www.who.int/news-room/fact-sheets/detail/sexually-transmitted-infections-(stis)**, (accessed 7 January 2024).
415 C. Elwell, K. Mirrashidi and J. Engel, *Nat. Rev. Microbiol.*, 2016, **14**, 385–400.
416 M. K. Morgan and C. F. Decker, *Disease-a-Month*, 2016, **62**, 260–268.
417 F. Mercer and P. J. Johnson, *Trends Parasitol.*, 2018, **34**, 683–693.
418 K. G. Ghanem, S. Ram and P. A. Rice, *N. Engl. J. Med.*, 2020, **382**, 845–854.
419 S. R. Galvin and M. S. Cohen, *Nat. Rev. Microbiol.*, 2004, **2**, 33–42.
420 B. Mlynarczyk-Bonikowska, C. Kowalewski, A. Krolak-Ulinska and W. Marusza, *Int. J. Mol. Sci.*, 2022, **23**, 10499.
421 M. Iannacone and L. G. Guidotti, *Nat. Rev. Immunol.*, 2022, **22**, 19–32.
422 K. Madavaraju, R. Koganti, I. Volety, T. Yadavalli and D. Shukla, *Front. Cell. Infect. Microbiol.*, 2021, **10**, 617578.
423 J. O. Kahn and B. D. Walker, *N. Engl. J. Med.*, 1998, **339**, 33–39.
424 M. E. Sabatini and S. Chiocca, *Br. J. Cancer*, 2020, **122**, 306–314.
425 WHO Hepatitis B factsheet 2023, **https://www.who.int/news-room/fact-sheets/detail/hepatitis-b**, (accessed 7 January 2024).
426 J. K.-T. Ho, B. Jeevan-Raj and H.-J. Netter, *Viruses*, 2020, **12**, 126.
427 K. Yoshimura, *J. Infect. Chemother.*, 2017, **23**, 12–16.
428 L. A. Sadowski, R. Upadhyay, Z. W. Greeley and B. J. Margulies, *Viruses*, 2021, **13**, 1228.
429 L. Cheng, Y. Wang and J. Du, *Vaccines*, 2020, **8**, 391.
430 T. Meyer, *Microorganisms*, 2016, **4**, 25.
431 C. C. Bristow, J. D. Klausner and A. Tran, *Clin. Infect. Dis.*, 2020, **71**, S52–S57.
432 S. R. Morris, C. C. Bristow, M. R. Wierzbicki, M. Sarno, L. Asbel, A. French, C. A. Gaydos, L. Hazan, L. Mena, P. Madhivanan, S. Philip, S. Schwartz, C. Brown, D. Styers, T. Waymer and J. D. Klausner, *Lancet Infect. Dis.*, 2021, **21**, 668–676.
433 A. D. Cristillo, C. C. Bristow, R. Peeling, B. Van Der Pol, S. H. de Cortina, I. K. Dimov, N. P. Pai, D. Jin Shin, R. Y. T. Chiu, C. Klapperich, P. Madhivanan, S. R. Morris and J. D. Klausner, *Sex. Transm. Dis.*, 2017, **44**, 211–218.
434 T. E. Wi, F. J. Ndowa, C. Ferreyra, C. Kelly-Cirino, M. M. Taylor, I. Toskin, J. Kiarie, N. Santesso and M. Unemo, *J. Int. AIDS Soc.*, 2019, **22**, e25343.
435 G. Caruso, A. Giammanco, R. Virruso and T. Fasciana, *Int. J. Environ. Res. Public Health*, 2021, **18**, 1038.
436 I. Toskin, V. Govender, K. Blondeel, M. Murtagh, M. Unemo, C. Zemouri, R. W. Peeling and J. Kiarie, *Sex. Transm. Infect.*, 2020, **96**, 342–347.
437 K. Hsieh, J. H. Melendez, C. A. Gaydos and T.-H. Wang, *Lab Chip*, 2022, **22**, 476–511.
438 P. C. Adamson, M. J. Loeffelholz and J. D. Klausner, *Arch. Pathol. Lab. Med.*, 2020, **144**, 1344–1351.
439 C. A. Gaydos, Y. C. Manabe and J. H. Melendez, *Sex. Transm. Dis.*, 2021, **48**, S71–S77.
440 D. Thakur, T. Fatima, P. Sharma, M. R. Hasan, N. Malhotra, M. Khanuja, S. K. Shukla and J. Narang, *Process Biochem.*, 2023, **126**, 223–237.
441 N. Farokhzad and W. Tao, *Trends Chem.*, 2021, **3**, 589–602.
442 J. Eid, M. Mougel and M. Socol, *Viruses*, 2020, **12**, 982.
443 S. Tharakan, O. Faqah, W. Asghar and A. Ilyas, *Biosensors*, 2022, **12**, 949.
444 N. P. Pai, A. Karellis, J. Kim and T. Peter, *Lancet HIV*, 2020, **7**, e574–e581.
445 Y. Xiao, A. J. Thompson and J. Howell, *Cells*, 2020, **9**, 2233.
446 V. Narayanamurthy, Z. E. Jeroish, K. S. Bhuvaneshwari and F. Samsuri, *Anal. Methods*, 2021, **13**, 740–763.
447 S. Hassanpour, B. Baradaran, M. de la Guardia, A. Baghbanzadeh, J. Mosafer, M. Hejazi, A. Mokhtarzadeh and M. Hasanzadeh, *Microchim. Acta*, 2018, **185**, 568.
448 P. Nath, M. A. Kabir, S. K. Doust and A. Ray, *Infect. Dis. Rep.*, 2021, **13**, 518–539.
449 A. Y. Trick, H. T. Ngo, A. H. Nambiar, M. M. Morakis, F.-E. Chen, L. Chen, K. Hsieh and T.-H. Wang, *Lab Chip*, 2022, **22**, 945–953.
450 T. Liu, G. Choi, Z. Tang, A. Kshirsagar, A. J. Politza and W. Guan, *Biosens. Bioelectron.*, 2022, **209**, 114255.
451 C.-A. Chen, H. Yuan, C.-W. Chen, Y.-S. Chien, W.-H. Sheng and C.-F. Chen, *Lab Chip*, 2021, **21**, 1908–1915.
452 E. A. Phillips, T. J. Moehling, K. F. K. Ejendal, O. S. Hoilett, K. M. Byers, L. A. Basing, L. A. Jankowski, J. B. Bennett, L.-K. Lin, L. A. Stanciu and J. C. Linnes, *Lab Chip*, 2019, **19**, 3375–3386.
453 D. Liu, Y. Zhang, M. Zhu, Z. Yu, X. Ma, Y. Song, S. Zhou and C. Yang, *Anal. Chem.*, 2020, **92**, 11826–11833.
454 R. R. G. Soares, J. C. Varela, U. Neogi, S. Ciftci, M. Ashokkumar, I. F. Pinto, M. Nilsson, N. Madaboosi and A. Russom, *Biosens. Bioelectron.*, 2020, **166**, 112442.

 

455 M. Kong, Z. Li, J. Wu, J. Hu, Y. Sheng, D. Wu, Y. Lin, M. Li, X. Wang and S. Wang, *Talanta*, 2019, **205**, 120155.
456 Y.-L. Tan, A.-Q. Huang, L.-J. Tang and J.-H. Jiang, *Chem. Sci.*, 2021, **12**, 8445–8451.
457 W. Witkowska McConnell, C. Davis, S. R. Sabir, A. Garrett, A. Bradley-Stewart, P. Jajesniak, J. Reboud, G. Xu, Z. Yang, R. Gunson, E. C. Thomson and J. M. Cooper, *Nat. Commun.*, 2021, **12**, 6994.
458 C. Xie, S. Chen, L. Zhang, X. He, Y. Ma, H. Wu, B. Zou and G. Zhou, *Anal. Bioanal. Chem.*, 2021, **413**, 2923–2931.
459 X. Zhao, X. Li, W. Yang, J. Peng, J. Huang and S. Mi, *Analyst*, 2021, **146**, 5102–5114.
460 R. Wang, J. Wu, X. He, P. Zhou and Z. Shen, *Micromachines*, 2021, **12**, 263.
461 Z. Yu, W. Lyu, M. Yu, Q. Wang, H. Qu, R. F. Ismagilov, X. Han, D. Lai and F. Shen, *Biosens. Bioelectron.*, 2020, **155**, 112107.
462 A. Y. Trick, J. H. Melendez, F.-E. Chen, L. Chen, A. Onzia, A. Zawedde, E. Nakku-Joloba, P. Kyambadde, E. Mande, J. Matovu, M. Atuheirwe, R. Kwizera, E. A. Gilliams, Y.-H. Hsieh, C. A. Gaydos, Y. C. Manabe, M. M. Hamill and T.-H. Wang, *Sci. Transl. Med.*, 2021, **13**, eabf6356.
463 X. Ye, Y. Li, L. Wang, X. Fang and J. Kong, *Talanta*, 2021, **221**, 121462.
464 A. L. Horst, J. M. Rosenbohm, N. Kolluri, J. Hardick, C. A. Gaydos, M. Cabodi, C. M. Klapperich and J. C. Linnes, *Biomed. Microdevices*, 2018, **20**, 35.
465 J. Hoffman, J. van Griensven, R. Colebunders and M. McKellar, *HIV Ther.*, 2010, **4**, 27–39.
466 M. Stone, J. Bainbridge, A. M. Sanchez, S. M. Keating, A. Pappas, W. Rountree, C. Todd, S. Bakkour, M. Manak, S. A. Peel, R. W. Coombs, E. M. Ramos, M. K. Shriver, P. Contestable, S. V. Nair, D. H. Wilson, M. Stengelin, G. Murphy, I. Hewlett, T. N. Denny and M. P. Busch, *J. Clin. Microbiol.*, 2018, **56**, e02045-17.
467 D. J. Shin, P. Athamanolap, L. Chen, J. Hardick, M. Lewis, Y. H. Hsieh, R. E. Rothman, C. A. Gaydos and T. H. Wang, *Sci. Rep.*, 2017, **7**, 4495.
468 D. J. Shin, A. Y. Trick, Y.-H. Hsieh, D. L. Thomas and T.-H. Wang, *Sci. Rep.*, 2018, **8**, 9793.
469 F. Li, Y. Zheng, J. Wu, L. Zhao, L. Shui, Q. Pu and S. Liu, *Talanta*, 2019, **203**, 83–89.
470 J. Song, C. Liu, M. G. Mauk, J. Peng, T. Schoenfeld and H. H. Bau, *Anal. Chem.*, 2018, **90**, 1209–1216.
471 W. Ouyang and J. Han, *Proc. Natl. Acad. Sci. U. S. A.*, 2019, **116**, 16240–16249.
472 K. Kadimisetty, K. Yin, A. M. Roche, Y. Yi, F. D. Bushman, R. G. Collman, R. Gross, L. Feng and C. Liu, *Analyst*, 2021, **146**, 3234–3241.
473 H. J. Goux, B. Raja, K. Kourentzi, J. R. C. Trabuco, B. V. Vu, A. S. Paterson, A. Kirkpatrick, B. Townsend, M. Lee, V. T. T. Truong, C. Pedroza and R. C. Willson, *PLoS One*, 2019, **14**, e0225365.
474 B. Shu, L. Lin, B. Wu, E. Huang, Y. Wang, Z. Li, H. He, X. Lei, B. Xu and D. Liu, *Biosens. Bioelectron.*, 2021, **181**, 113145.
475 WHO Vector-borne diseases, **https://www.who.int/news-room/fact-sheets/detail/vector-borne-diseases**, (accessed 7 January 2024).
476 WHO Global vector control response 2017–2030, **https://www.who.int/publications-detail-redirect/9789241512978**, (accessed 7 January 2024).
477 A. L. Wilson, O. Courtenay, L. A. Kelly-Hope, T. W. Scott, W. Takken, S. J. Torr and S. W. Lindsay, *PLoS Neglected Trop. Dis.*, 2020, **14**, e0007831.
478 L. H. V. Franklinos, K. E. Jones, D. W. Redding and I. Abubakar, *Lancet Infect. Dis.*, 2019, **19**, e302–e312.
479 J. Rocklöv and R. Dubrow, *Nat. Immunol.*, 2020, **21**, 479–483.
480 A. C. Steere, F. Strle, G. P. Wormser, L. T. Hu, J. A. Branda, J. W. R. Hovius, X. Li and P. S. Mead, *Nat. Rev. Dis. Primers*, 2016, **2**, 16090.
481 S. Li, L. Gilbert, S. O. Vanwambeke, J. Yu, B. V. Purse and P. A. Harrison, *Environ. Health Perspect.*, 2019, **127**, 067010.
482 R. Bellini, A. Michaelakis, D. Petrić, F. Schaffner, B. Alten, P. Angelini, C. Aranda, N. Becker, M. Carrieri, M. Di Luca, E. Fălcuță, E. Flacio, A. Klobučar, C. Lagneau, E. Merdić, O. Mikov, I. Pajovic, D. Papachristos, C. A. Sousa, A. Stroo, L. Toma, M. I. Vasquez, E. Velo, C. Venturelli and M. Zgomba, *Travel Med. Infect. Dis.*, 2020, **35**, 101691.
483 M. G. Guzman and E. Harris, *Lancet*, 2015, **385**, 453–465.
484 A. Wilder-Smith, E.-E. Ooi, O. Horstick and B. Wills, *Lancet*, 2019, **393**, 350–363.
485 WHO Dengue and severe dengue, **https://www.who.int/news-room/fact-sheets/detail/dengue-and-severe-dengue**, (accessed 7 January 2024).
486 X. Yang, M. B. M. Quam, T. Zhang and S. Sang, *J. Travel Med.*, 2021, **28**, taab146.
487 M. G. Guzmán and G. Kourí, *Int. J. Infect. Dis.*, 2004, **8**, 69–80.
488 R. Eivazzadeh-Keihan, P. Pashazadeh-Panahi, T. Mahmoudi, K. K. Chenab, B. Baradaran, M. Hashemzaei, F. Radinekiyan, A. Mokhtarzadeh and A. Maleki, *Microchim. Acta*, 2019, **186**, 329.
489 N. T. Darwish, S. D. Sekaran and S. M. Khor, *Sens. Actuators, B*, 2018, **255**, 3316–3331.
490 Y. Yao, N. Zhao, W. Jing, Q. Liu, H. Lu, W. Zhao, W. Zhao, Z. Yuan, H. Xia and G. Sui, *Sens. Actuators, B*, 2021, **333**, 129521.
491 W. Lee, H. Kim, P. K. Bae, S. Lee, S. Yang and J. Kim, *Biosens. Bioelectron.*, 2021, **190**, 113388.
492 A. M. Jankelow, H. Lee, W. Wang, T.-H. Hoang, A. Bacon, F. Sun, S. Chae, V. Kindratenko, K. Koprowski, R. A. Stavins, D. D. Ceriani, Z. W. Engelder, W. P. King, M. N. Do, R. Bashir, E. Valera and B. T. Cunningham, *Analyst*, 2022, **147**, 3838–3853.
493 S. Sharma, M. A. Kabir and W. Asghar, *Arch. Pathol. Lab. Med.*, 2020, **144**, 1335–1343.
494 P. Biswas, G. N. Mukunthan Sulochana, T. N. Banuprasad, P. Goyal, D. Modak, A. K. Ghosh and S. Chakraborty, *ACS Sens.*, 2022, **7**, 3720–3729.

495 Y. Seok, B. S. Batule and M.-G. Kim, *Biosens. Bioelectron.*, 2020, **165**, 112400.
496 G. Theillet, G. Grard, M. Galla, C. Maisse, M. Enguehard, M. Cresson, P. Dalbon, I. L. Leparc-Goffart and F. Bedin, *J. Med. Virol.*, 2019, **91**, 899–910.
497 E. Chou, E. Lasek-Nesselquist, B. Taubner, A. Pilar, E. Guignon, W. Page, Y.-P. Lin and N. C. Cady, *PLoS One*, 2020, **15**, e0228772.
498 H.-A. Joung, Z. S. Ballard, A. Ma, D. K. Tseng, H. Teshome, S. Burakowski, O. B. Garner, D. D. Carlo and A. Ozcan, *Lab Chip*, 2019, **19**, 1027–1034.
499 H.-A. Joung, Z. S. Ballard, J. Wu, D. K. Tseng, H. Teshome, L. Zhang, E. J. Horn, P. M. Arnaboldi, R. J. Dattwyler, O. B. Garner, D. Di Carlo and A. Ozcan, *ACS Nano*, 2020, **14**, 229–240.
500 S. Arumugam, S. Nayak, T. Williams, F. S. D. S. Maria, M. S. Guedes, R. C. Chaves, V. Linder, A. R. Marques, E. J. Horn, S. J. Wong, S. K. Sia and M. Gomes-Solecki, *J. Clin. Microbiol.*, 2019, **57**, e01142-19.
501 W. F. Wright and P. G. Auwaerter, *Open Forum Infect. Dis.*, 2020, **7**, ofaa132.
502 J. Elven, P. Dahal, E. A. Ashley, N. V. Thomas, P. Shrestha, K. Stepniewska, J. A. Crump, P. N. Newton, D. Bell, H. Reyburn, H. Hopkins and P. J. Guérin, *BMC Med.*, 2020, **18**, 279.
503 J. J. L. Tan, M. Capozzoli, M. Sato, W. Watthanaworawit, C. L. Ling, M. Mauduit, B. Malleret, A.-C. Grüner, R. Tan, F. H. Nosten, G. Snounou, L. Rénia and L. F. P. Ng, *PLoS Neglected Trop. Dis.*, 2014, **8**, e3043.
504 S. Hin, D. Baumgartner, M. Specht, J. Lüddecke, E. M. Arjmand, B. Johannsen, L. Schiedel, M. Rombach, N. Paust, F. von Stetten, R. Zengerle, N. Wipf, P. Müller, K. Mavridis, J. Vontas and K. Mitsakakis, *Processes*, 2020, **8**, 1677.
505 S. Moutailler, L. Yousfi, L. Mousson, E. Devillers, M. Vazeille, A. Vega-Rúa, Y. Perrin, F. Jourdain, F. Chandre, A. Cannet, S. Chantilly, J. Restrepo, A. Guidez, I. Dusfour, F. V. S. De Abreu, T. P. Dos Santos, D. Jiolle, T. M. Visser, C. J. M. Koenraadt, M. Wongsokarijo, M. Diallo, D. Diallo, A. Gaye, S. Boyer, V. Duong, G. Piorkowski, C. Paupy, R. L. De Oliveira, X. De Lamballerie and A.-B. Failloux, *Viruses*, 2019, **11**, 904.
506 T. Liao, X. Wang, M. Donolato, E. Harris, M. M. Cruz, A. Balmaseda and R. Y. L. Wang, *Diagnostics*, 2020, **10**, 372.
507 I. Alejo-Cancho, J. Navero-Castillejos, A. Peiró-Mestres, R. Albarracín, J. Barrachina, A. Navarro, V. Gonzalo, V. Pastor, J. Muñoz and M. J. Martínez, *PLoS Neglected Trop. Dis.*, 2020, **14**, e0008082.
508 A. Ganguli, A. Ornob, H. Yu, G. L. Damhorst, W. Chen, F. Sun, A. Bhuiya, B. T. Cunningham and R. Bashir, *Biomed. Microdevices*, 2017, **19**, 73.
509 R. R. G. Soares, A. Pettke, A. Robles-Remacho, S. Zeebaree, S. Ciftci, M. Tampere, A. Russom, M.-R. Puumalainen, M. Nilsson and N. Madaboosi, *Sens. Actuators, B*, 2021, **336**, 129723.
510 X. Zhu, J. Zhao, A. Hu, J. Pan, G. Deng, C. Hua, C. Zhu, Y. Liu, K. Yang and L. Zhu, *Micromachines*, 2020, **11**, 186.
511 S. Pal, A. L. Dauner, I. Mitra, B. M. Forshey, P. Garcia, A. C. Morrison, E. S. Halsey, T. J. Kochel and S.-J. L. Wu, *PLoS One*, 2014, **9**, e113411.
512 R. Luo, N. Fongwen, C. Kelly-Cirino, E. Harris, A. Wilder-Smith and R. W. Peeling, *Clin. Microbiol. Infect.*, 2019, **25**, 659–666.
513 M. Kikuti, J. S. Cruz, M. S. Rodrigues, A. S. Tavares, I. A. D. Paploski, M. M. O. Silva, P. M. Santana, L. B. Tauro, G. A. O. F. Silva, G. S. Campos, J. M. G. Araújo, U. Kitron, M. G. Reis and G. S. Ribeiro, *PLoS One*, 2019, **14**, e0213301.
514 K. Kaarj, P. Akarapipad and J.-Y. Yoon, *Sci. Rep.*, 2018, **8**, 12438.
515 M. Shehata Draz, M. Venkataramani, H. Lakshminarayanan, E. Saygili, M. Moazeni, A. Vasan, Y. Li, X. Sun, S. Hua, X. G. Yu and H. Shafiee, *Nanoscale*, 2018, **10**, 11841–11849.
516 K. Arias-Alpízar, A. Sánchez-Cano, J. Prat-Trunas, E. de la Serna Serna, O. Alonso, E. Sulleiro, A. Sánchez-Montalvá, A. Diéguez and E. Baldrich, *Biosens. Bioelectron.*, 2022, **215**, 114513.
517 X. Guo, M. A. Khalid, I. Domingos, A. L. Michala, M. Adriko, C. Rowel, D. Ajambo, A. Garrett, S. Kar, X. Yan, J. Reboud, E. M. Tukahebwa and J. M. Cooper, *Nat. Electron.*, 2021, **4**, 615–624.
518 C. Flynn and A. Ignaszak, *Biosensors*, 2020, **10**, 137.
519 S. Nayak, A. Sridhara, R. Melo, L. Richer, N. H. Chee, J. Kim, V. Linder, D. Steinmiller, S. K. Sia and M. Gomes-Solecki, *Sci. Rep.*, 2016, **6**, 35069.
520 P. Banović, E. Piloto-Sardiñas, D. Mijatović, A. Foucault-Simonin, V. Simin, I. Bogdan, D. Obregón, L. Mateos-Hernández, S. Moutailler and A. Cabezas-Cruz, *Acta Trop.*, 2023, **238**, 106756.
521 R. Amino, S. Thiberge, B. Martin, S. Celli, S. Shorte, F. Frischknecht and R. Ménard, *Nat. Med.*, 2006, **12**, 220–224.
522 M. Prudêncio, A. Rodriguez and M. M. Mota, *Nat. Rev. Microbiol.*, 2006, **4**, 849–856.
523 T. F. de Koning-Ward, M. W. A. Dixon, L. Tilley and P. R. Gilson, *Nat. Rev. Microbiol.*, 2016, **14**, 494–507.
524 R. N. Price, R. J. Commons, K. E. Battle, K. Thriemer and K. Mendis, *Trends Parasitol.*, 2020, **36**, 560–570.
525 World malaria report 2022, **https://www.who.int/publications-detail-redirect/9789240064898**, (accessed 7 January 2024).
526 T. Bousema, L. Okell, I. Felger and C. Drakeley, *Nat. Rev. Microbiol.*, 2014, **12**, 833–840.
527 K. Elfving, D. Shakely, M. Andersson, K. Baltzell, A. S. Ali, M. Bachelard, K. I. Falk, A. Ljung, M. I. Msellem, R. S. Omar, P. Parola, W. Xu, M. Petzold, B. Trollfors, A. Björkman, M. Lindh and A. Mårtensson, *PLoS One*, 2016, **11**, e0146054.
528 B. A. Mathison and B. S. Pritt, *J. Clin. Microbiol.*, 2017, **55**, 2009–2017.
529 A. Mbanefo and N. Kumar, *Trop. Med. Infect. Dis.*, 2020, **5**, 102.
530 N. M. Pham, W. Karlen, H.-P. Beck and E. Delamarche, *Malar. J.*, 2018, **17**, 260.

531 M. S. Cordray and R. R. Richards-Kortum, *Am. J. Trop. Med. Hyg.*, 2012, **87**, 223–230.
532 S. Britton, Q. Cheng and J. S. McCarthy, *Malar. J.*, 2016, **15**, 88.
533 S. Sharma, J. Singh, A. Sen and A. R. Anvikar, *J. Vector Borne Dis.*, 2022, **59**, 29–36.
534 C. B. Nair, J. Manjula, P. A. Subramani, P. B. Nagendrappa, M. N. Manoj, S. Malpani, P. K. Pullela, P. V. Subbarao, S. Ramamoorthy and S. K. Ghosh, *PLoS One*, 2016, **11**, e0146961.
535 J. C. Mouatcho and J. P. D. Goldring, *J. Med. Microbiol.*, 2013, **62**, 1491–1505.
536 A. N. Mukkala, J. Kwan, R. Lau, D. Harris, D. Kain and A. K. Boggild, *Curr. Infect. Dis. Rep.*, 2018, **20**, 49.
537 A. Jimenez, R. R. Rees-Channer, R. Perera, D. Gamboa, P. L. Chiodini, I. J. González, A. Mayor and X. C. Ding, *Malar. J.*, 2017, **16**, 128.
538 L. Marquart, A. Butterworth, J. S. McCarthy and M. L. Gatton, *Malar. J.*, 2012, **11**, 74.
539 N. Thorne, L. Flores-Olazo, R. Egoávil-Espejo, E. A. Vela, J. Noel, J. Valdivia-Silva and D. van Noort, *Micromachines*, 2021, **12**, 1245.
540 N. Kolluri, C. M. Klapperich and M. Cabodi, *Lab Chip*, 2018, **18**, 75–94.
541 K. V. Ragavan, S. Kumar, S. Swaraj and S. Neethirajan, *Biosens. Bioelectron.*, 2018, **105**, 188–210.
542 K. Mitsakakis, S. Hin, P. Müller, N. Wipf, E. Thomsen, M. Coleman, R. Zengerle, J. Vontas and K. Mavridis, *Int. J. Environ. Res. Public Health*, 2018, **15**, 259.
543 M. Depond, B. Henry, P. Buffet and P. A. Ndour, *Front. Physiol.*, 2020, **10**, 1613.
544 S. Jackson, S. Lee and A. K. Badu-Tawiah, *Anal. Chem.*, 2022, **94**, 5132–5139.
545 A. M. Ogunmolasuyi, R. Fogel, H. Hoppe, D. Goldring and J. Limson, *Malar. J.*, 2022, **21**, 174.
546 S. Ghosh and C. H. Ahn, *Analyst*, 2019, **144**, 2109–2119.
547 N. M. Pham, S. Rusch, Y. Temiz, H.-P. Beck, W. Karlen and E. Delamarche, *Biomed. Microdevices*, 2019, **21**, 24.
548 J. Choi, S.-J. Cho, Y. T. Kim and H. Shin, *Biomed. Microdevices*, 2019, **21**, 86.
549 J. Reboud, G. Xu, A. Garrett, M. Adriko, Z. Yang, E. M. Tukahebwa, C. Rowell and J. M. Cooper, *Proc. Natl. Acad. Sci. U. S. A.*, 2019, **116**, 4834–4842.
550 G. Choi, T. Prince, J. Miao, L. Cui and W. Guan, *Biosens. Bioelectron.*, 2018, **115**, 83–90.
551 A. J. Colbert, K. Co, G. Lima-Cooper, D. H. Lee, K. N. Clayton, S. T. Wereley, C. C. John, J. C. Linnes and T. L. Kinzer-Ursem, *Malar. J.*, 2021, **20**, 380.
552 G. Ruiz-Vega, K. Arias-Alpízar, E. de la Serna, L. N. Borgheti-Cardoso, E. Sulleiro, I. Molina, X. Fernàndez-Busquets, A. Sánchez-Montalvá, F. J. del Campo and E. Baldrich, *Biosens. Bioelectron.*, 2020, **150**, 111925.
553 N. K. Singh, P. Jain, S. Das and P. Goswami, *Anal. Chem.*, 2019, **91**, 4213–4221.
554 S. Ghosh, K. Aggarwal, T. U. Vinitha, T. Nguyen, J. Han and C. H. Ahn, *Microsyst. Nanoeng.*, 2020, **6**, 5.
555 R. Clément, A. Bienvenu, A. Lavoignat, G. Bonnot, B. Doumèche and S. Picot, *Talanta*, 2023, **252**, 123839.
556 K. Malpartida-Cardenas, N. Miscourides, J. Rodriguez-Manzano, L.-S. Yu, N. Moser, J. Baum and P. Georgiou, *Biosens. Bioelectron.*, 2019, **145**, 111678.